UHF SATELLITE COMMUNICATION DURING SCINTILLATION

Edward A. Bucher

Massachusetts Institute of Technology

Prepared for:

Electronic Systems Division
Naval Electronic Systems Command

5 August 1975

UNCLASSIFIED

SECURITY CLASSIFICATION OF THIS PAGE *(When Data Entered)*

REPORT DOCUMENTATION PAGE		READ INSTRUCTIONS BEFORE COMPLETING FORM
1. REPORT NUMBER ESD-TR-75-242	2. GOVT ACCESSION NO.	3. RECIPIENT'S CATALOG NUMBER
4. TITLE *(and Subtitle)* UHF Satellite Communication During Scintillation		5. TYPE OF REPORT & PERIOD COVERED Technical Note 6. PERFORMING ORG. REPORT NUMBER Technical Note 1975-10
7. AUTHOR(s) Bucher, Edward A.		8. CONTRACT OR GRANT NUMBER(s) F19628-76-C-0002
9. PERFORMING ORGANIZATION NAME AND ADDRESS Lincoln Laboratory, M.I.T. P.O. Box 73 Lexington, MA 02173		10. PROGRAM ELEMENT, PROJECT, TASK AREA & WORK UNIT NUMBERS Project No. 3279
11. CONTROLLING OFFICE NAME AND ADDRESS Naval Electronic Systems Command Department of the Navy Washington, DC 20360		12. REPORT DATE 5 August 1975 13. NUMBER OF PAGES 103
14. MONITORING AGENCY NAME & ADDRESS *(if different from Controlling Office)* Electronic Systems Division Hanscom AFB Bedford, MA 01731		15. SECURITY CLASS. *(of this report)* Unclassified 15a. DECLASSIFICATION DOWNGRADING SCHEDULE

16. DISTRIBUTION STATEMENT *(of this Report)*

Approved for public release; distribution unlimited.

17. DISTRIBUTION STATEMENT *(of the abstract entered in Block 20, if different from Report)*

18. SUPPLEMENTARY NOTES

None

19. KEY WORDS *(Continue on reverse side if necessary and identify by block number)*

satellite communication
scintillation phenomenology
time diversity modulation
UHF
threshold processing

20. ABSTRACT *(Continue on reverse side if necessary and identify by block number)*

The effects of ionospheric UHF scintillation on satellite communications are described in terms of relatively simple fading channel models. Two methods of countering the effects of scintillation induced fading on satellite communications are presented and analyzed. First, threshold testing techniques which effectively erase "faded" data are discussed. These techniques are most easily applied to add scintillation protection to an operating communication system which handles segments or blocks of data. Second, time diversity modulation techniques which can counter scintillation and other channel problems such as RFI and excess noise in the same operation are discussed. These time diversity modulation techniques offer somewhat better performance than the threshold techniques at the cost of a somewhat more complex interface between the basic receiver and the anti-scintillation processor.

DD FORM 1 JAN 73 1473 EDITION OF 1 NOV 65 IS OBSOLETE

UNCLASSIFIED

SECURITY CLASSIFICATION OF THIS PAGE *(When Data Entered)*

MASSACHUSETTS INSTITUTE OF TECHNOLOGY
LINCOLN LABORATORY

UHF SATELLITE COMMUNICATION DURING SCINTILLATION

E. A. BUCHER
Group 67

TECHNICAL NOTE 1975-10

5 AUGUST 1975

LEXINGTON MASSACHUSETTS

ABSTRACT

The effects of ionospheric UHF scintillation on satellite communications are described in terms of relatively simple fading channel models. Two methods of countering the effects of scintillation induced fading on satellite communications are presented and analyzed. First, threshold testing techniques which effectively erase "faded" data are discussed. These techniques are most easily applied to add scintillation protection to an operating communication system which handles segments or blocks of data. Second, time diversity modulation techniques which can counter scintillation and other channel problems such as RFI and excess noise in the same operation are discussed. These time diversity modulation techniques offer somewhat better performance than the threshold techniques at the cost of a somewhat more complex interface between the basic receiver and the anti-scintillation processor.

CONTENTS

I. INTRODUCTION

Satellite communication systems involving large numbers of mobile users such as Naval vessels often operate in the 225-400 MHz band because the communication link can be established with relatively inexpensive terminals with low-gain antennas which do not require pointing. These UHF satellite communication systems are most often designed assuming a free-space propagation model which is usually adequate to model link performance. However, electron density fluctuations in the ionosphere can substantially alter the propagation model and the resulting signal scintillation can cause the disruption of operating satellite communication links. This signal scintillation produces signal fading at rates which are quite variable but on the order of a fade every ten seconds. Section II discusses the phenomenology of scintillation in the UHF band and introduces models of the fading which can be used to develop and evaluate means of preventing the scintillation from disrupting communications.

The basic scintillation phenomena is such that only time diversity can be implemented in a mobile terminal which desires continued communication during scintillation. Neither frequency nor polarization diversity are available because of the basic characteristics of scintillation. Antenna diversity or spatial diversity is available at fixed installations where site separations on the order of kilometers are possible but not on ships and airplanes.

Implementing a time diversity system implies an essential processing delay because the diversity system must effectively either wait-out or average-out the scintillation induced fading. For all terminals except those on aircraft, the fading rates are such that this processing delay is on the order of tens of seconds which is too long to allow for meaningful two-way voice conversation but which should still permit timely record communication.

For a reasonably conservative propagation model, theoretical arguments indicate that a communication system with fixed average transmitter power but unlimited peak transmitter power and unlimited bandwidth can be designed in a way that is unaffected by scintillation fading. If the unrealistic conditions

of unlimited peak power and unlimited bandwidth are replaced by constant transmitter power and constant bandwidth; theoretical models show that a communication link can be designed which requires only 4.34 dB (a factor of e) more transmitter average power to counter the onset of severe scintillation. Two different classes of time diversity system implementations discussed in Sections III and IV below come close to this performance under certain conditions.

Using the threshold approach detailed in Section III, time diversity processing first divides the message into segments somewhat shorter than a "fade" but perhaps many bits long. The quality of each received segment is compared to a threshold to determine the segment's "acceptability". Disregarding "unacceptable" segments, the receiver has a copy of the message with gaps in it which may be filled by either 1) piecing together several copies of the same message or, 2) requesting repeats of missing sections or, 3) using an erasure filling code. Section III develops models to predict the performance of these threshold techniques. Generally, the segment techniques are best implemented in a communication system in which buffering, acceptability checking and data block manipulation are readily accommodated. The more easily implemented and controlled threshold techniques base the anti-scintillation processing on relatively long data segments containing many bits. Unfortunately, processing to counter bursts of errors is not necessarily effective against randomly occurring errors which may be due to other link degradations such as RFI, excess noise, etc. Thus, a threshold system using relatively long data segments offers primarily a means of adding scintillation protection to a communication system which already operates satisfactorily except for scintillation.

Time diversity modulation techniques discussed in Section IV combine different pieces of the received signal, account for the "reliability" of each channel symbol (or "chip"), and then make a final decision on the received message bits. Since the time diversity modulation technique operates on the basic received signal in individual chips, the basic processing used to counter scintillation can be easily extended to counter other received signal problems such as RFI increased noise, etc. Since time diversity modulation operates at the level

of the received signal rather than received bit blocks, the interface between the internal circuits of the demodulator modem and the anti-scintillation processor is considerably more complicated for time diversity modulation than for a thresholding technique using long data segments. However, this extra complication allows the anti-scintillation processing also to be effective against other more common channel problems. Section IV discusses time diversity modulation processing applied to scintillation fading and describes the basic issues involved in implementing such an approach.

Both Sections III and IV implicitly consider scintillation as occurring only on either the uplink to the satellite or on the downlink from the satellite but not both. In a satellite communication system where the communications to mobile terminals are channeled through a few large fixed installations, this assumption is reasonable because either 1) the ground stations can be situated outside regions where scintillation is likely to occur on the fixed installation/satellite path or, 2) the fixed stations in regions where scintillation is encountered can be modified to counter the scintillation between that station and the satellite by a combination of antenna diversity and increases of 10 dB or so in transmitting power. If mobile-to-mobile UHF satellite communication is desired when the paths from both users to the satellite are scintillating, satellite processing could be used to effectively separate the two links and solve the scintillation problem on the uplink and downlink separately. If satellite processing is not available, scintillation protection for mobile-to-mobile communications with both uplink and downlink scintillation could be obtained by end-to-end use of the techniques discussed in Sections III and IV with degraded performance; however, the extent of this degradation has not been considered here.

Section V describes a means of adding time diversity to a particular UHF satellite broadcast system. The system has a compatibility feature which allows specially modified receivers to receive the message with full time diversity scintillation protection while unmodified receivers may still receive the message in the absence of scintillation. This basic approach is being

implemented in an experimental unit which Lincoln Laboratory is building for use with an AN/SSR-1 receiver in a scintillation experiment using a Navy UHF channel of the MARISAT satellite. This experimental add-on also contains additional circuitry to test several other anti-scintillation codes which have the potential of allowing higher effective scintillation protected data rates if the compatibility feature is not required. The experimental hardware and the results of the experiments will be discussed in detail separately in later documents.

II. SCINTILLATION PHENOMENOLOGY

A. Overview

This section describes the phenomena of UHF scintillation to the extent necessary to develop a model to describe the aspects of UHF scintillation which degrade UHF satellite communication. Given this model, the effectiveness of various counter scintillation processing techniques may be evaluated. Crane's report[2-1] provides a much more detailed description and reference list of the whole phenomena of ionospheric scintillation.

Turbulent electron-density fluctuations in the ionosphere cause diffraction of electromagnetic waves propagating through the ionosphere. This diffraction causes both constructive and destructive interference in the radio waves propagating across the ionosphere and thus induces fluctutions in the received power from these links. This fluctuation or scintillation particularly affects satellite communications links in the military UHF band (225-400 MHz) and at lower frequencies. Scintillation is a probabilistic event occurring most frequently near the geomagnetic poles and the geomagnetic equator. Figure 2-1 shows the regions within 20° of the geomagnetic equator and 30° of the geomagnetic poles where scintillation is commonly observed. The intensity of the signal level fluctuations caused by scintillation is frequency dependent with fades of only one or two dB observed at radio frequencies above a few Gigahertz and of ten or more dB at frequencies below several hundred Megahertz.

Communications systems usually counter the effects of deep fading by using several diversity paths with hopefully independent fading to reduce the probability of the link's being completely faded out. The diversity paths are obtained by establishing radio links sufficiently separated to obtain independent samples of the fading process. Depending upon the physics of the fading process, the separation may be obtained by using different frequencies, polarizations, terminal sites or transmission times. Crane[2-1] indicates that polarization diversity is not available to counter the scintillation induced fading. Very wide frequency separations of many tens of Megahertz are required[2-1,2-2] to obtain frequency diversity against scintillation in the UHF band. Frequency

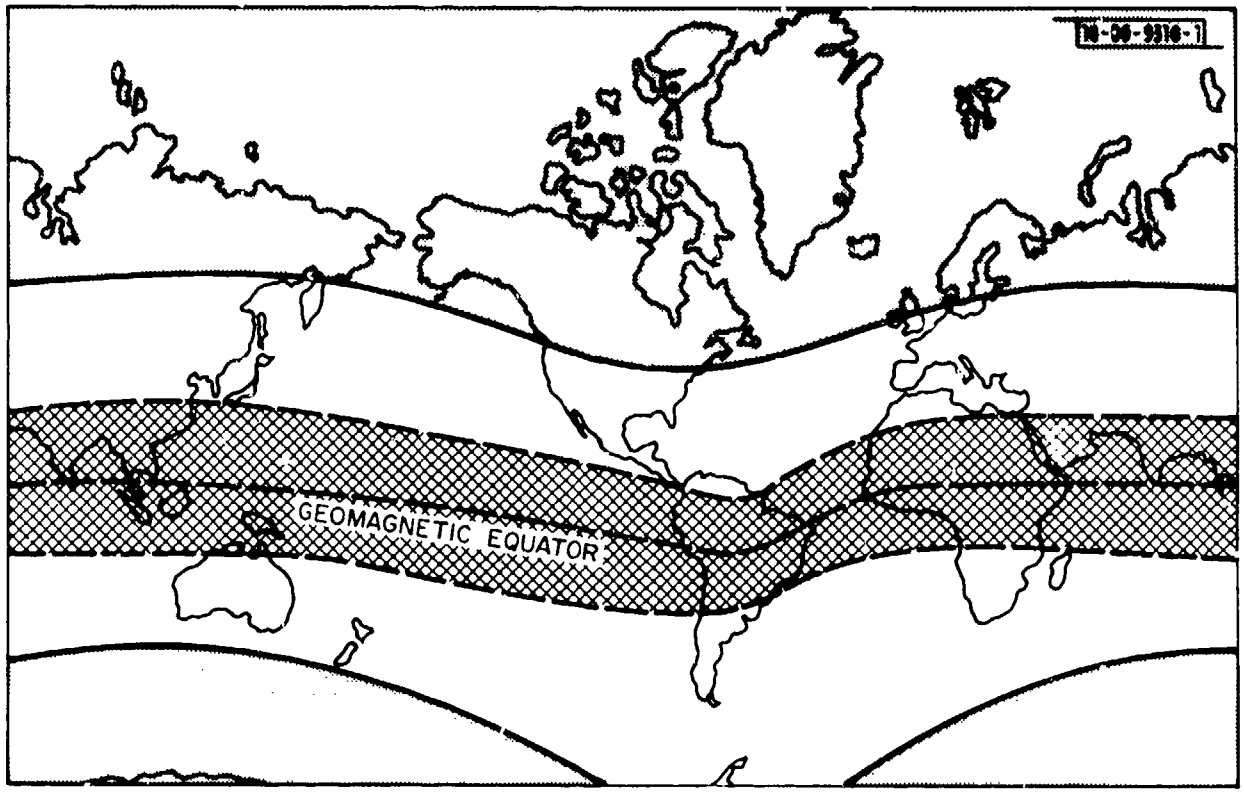

Fig. 2-1. Map showing the geomagnetic equator and those regions within 20° of the geomagnetic equator and 30° of the geomagnetic poles where scintillation is most likely to occur.

diversity is not practically available in UHF satellite communications systems because both frequency allocation problems and satellite design problems preclude the separation necessary to obtain diversity. Paulson and Hopkin's[2-2] experiments indicate that site separations of a kilometer or so are required to implement spatial diversity against UHF scintillation. Thus, only time diversity is available on mobile platforms such as ships or airplanes to counter UHF scintillation. Both the fade depth and fade rate statistics must be characterized before designing a time diversity system to counter scintillation.

B. Fade Depth Statistics

Crane[2-1] and Whitney et al.[2-3] find that the Nakagami-m probability distribution closely approximates the received signal amplitude distribution during UHF scintillation. The shape of the Nakagami-m distribution is completely specified by the parameter m which may be any positive number 1/2 or greater. For the Nakagami-m distribution, the probability density function given by

$$p(v) = \frac{2\, m^m\, (v)^{2m-1}}{\Gamma(m)\ \Omega^m}\ e^{-mv^2/\Omega} \qquad (2\text{-}1)$$

where v is the received signal amplitude and Ω = Avg. (v^2). Since v^2 is proportional to the received power level P_r, a change of variables produces the probability density

$$p(P_r) = \frac{m^m\ (P_r/P_o)^{m-1}}{\Gamma(m)}\ e^{-m(P_r/P_o)} \qquad (2\text{-}2)$$

where P_o is the average received power. Figure 2-2 shows the probability or fraction of time, that the received power is below a specified threshold T for integer and half integer values of m. It can be shown that the variance of the relative received power (P_r/P_o) is 1/m.

Figure 2-2 shows that the signal level fluctuations become more extreme as the value of m decreases. Briggs and Parkin's analysis[2-4] and Crane's observations[2-1] both indicate that the m-value saturates at m=1. This saturation of m-value was also observed when the author examined Hopkin's data

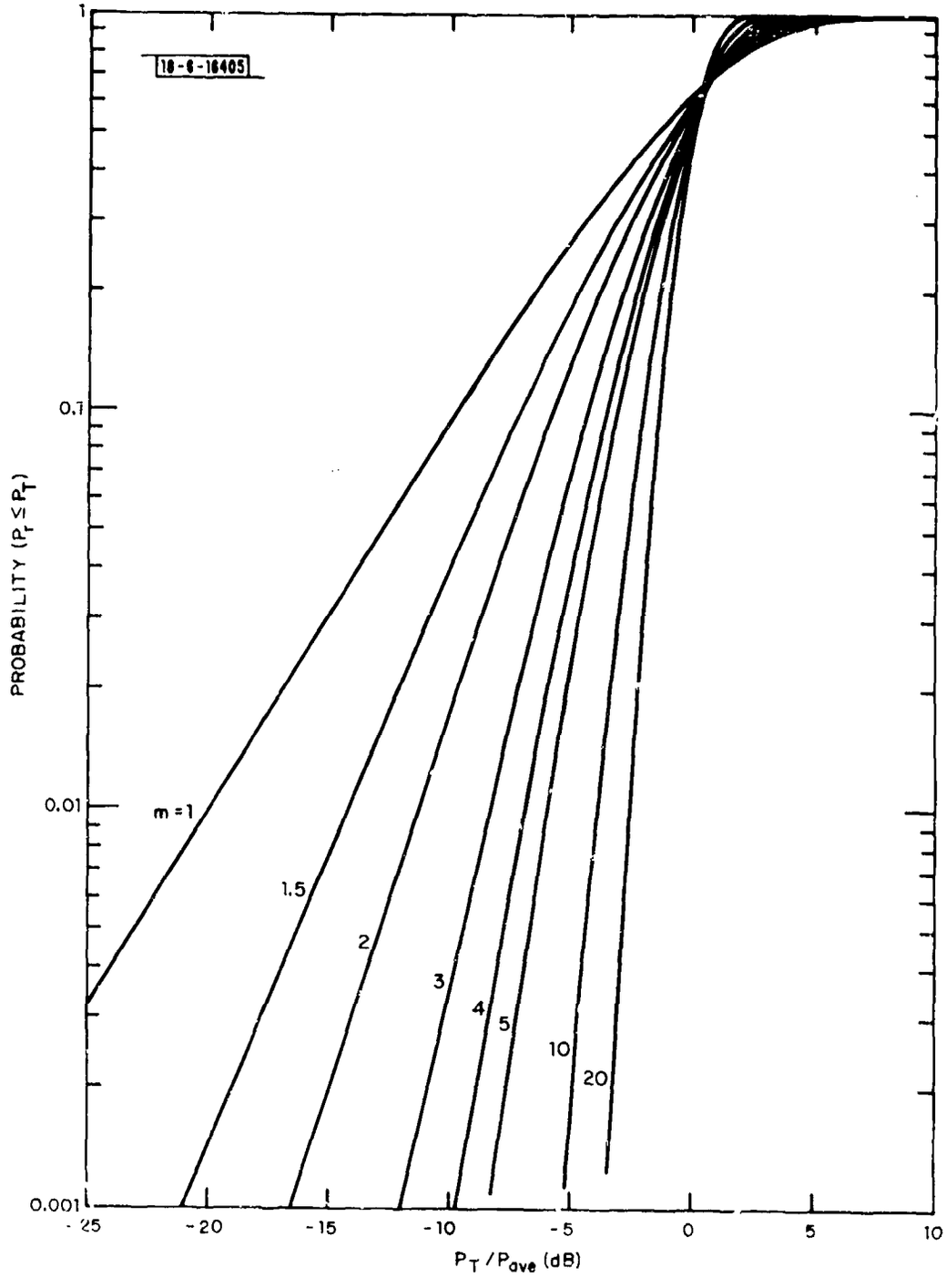

Fig. 2-2. Probability of fade depth for Nakagami-m fading.

in the fade rate analysis discussed below. At the saturation value m=1, the Nakagami-m distribution reduces to the Rayleigh distribution commonly encountered in fading communications channels.[2-5] Since both theory and experimental observations indicate that the saturation value m=1 characterizes the most intense signal level fluctuations caused by UHF scintillation, it is reasonable to require that any anti-scintillation processing must work in the presence of this m=1 or Rayleigh fading. Furthermore, since this worst case is also frequently observed, it is also a good engineering design point. Crane's study of UHF scintillation morphology[2-1] indicates that there is a large probability that the UHF scintillation will be nearly saturated and characterized by a Rayleigh fading distribution if there is any significant scintillation at all. Nichol's data[2-6] on the occurrence of UHF scintillation at Kwajalein indicates that UHF scintillation so intense as to be nearly saturated (Rayleigh) occurred for an average of 2-1/2 to 3 hours per night during the summer months when scintillation occurred for an average of 3-1/2 to 4 hours per night.

C. Fading Rate Statistics

Fourier techniques producing frequency spectra and time correlation functions and level-crossing techniques producing statistical descriptions of the duration and separation of fades may both be used to characterize the fading rate. Recording and measurement limitations restrict the accuracy of both methods. For example, measurement accuracy, time resolution and recorder bandwidth all limit the time-level resolution for level-crossing studies and the overall resolution of frequency spectra. Since the basic physical situation producing UHF scintillation is random and slowly time varying, the accuracy of any characterization of fading rate is also limited by the available sample size of any given sample of "the same" scintillation event.

UHF scintillation propagation data taken by Hopkins and Paulson of the Naval Electronics Laboratory center was analyzed using both Fourier and level-crossing techniques. The data was taken at Guam from 29 September 1972 to 8 October 1972 by recording the received beacon signal level from the TACSAT satellite. The data was recorded on analog magnetic tape. The playback signal

was low-pass filtered, sampled at a 50/sec rate and digitized for subsequent processing. The 3-Hz 4-pole low-pass filter was inserted to prevent high frequency tape noise from aliasing down into the "signal" band during sampling. Using a half inverse bandwidth rule, the time resolution limit imposed by the filter is approximately 1/6 sec.

The recorded signal levels were first divided into twenty-second records and the mean and variance of both $P_r(t)$ and $\log P_r(t)$ was calculated for each record. Time plots of these means and variances were used to [illegible] manually those records containing UHF scintillation. During UHF scinti[illegible], both the record means and variances of $P_r(t)$ and $\log P_r(t)$ showed increased variability from record to record. The received log-power variance was especially sensitive to scintillation and was used to determine the boundaries of groups of records containing the same "type" of UHF scintillation.

Five and one-half minute segments of data manually selected to have "the same type and rate" scintillation were Fourier transformed to estimate the power spectrum of received power fluctuations. These estimated power spectra were inverse Fourier transformed to estimate the magnitude of the correlation function $\rho_s(\tau)$ of the received signal power level fluctuations. The correlation function for this case is defined as

$$\rho_s(\tau) = \text{Avg} \frac{[P_r(t+\tau)-P_o]\ [P_r(t)-P_o]}{P_o^2}$$

where $P_t(t)$ is the received signal power and P_o is the average received power. These estimated power spectra were then used to refine the boundaries of incidents of "the same" scintillation event.

Figures 2-3 to 2-6 show the range of power spectra shapes observed for the received power fluctuations during incidents of relatively severe UHF scintillation. The power spectrum in Fig. 2-3 is typical of those observed for some of the slightly less severe incidents of UHF scintillation characterized by the Nakagami-m distribution with an m-value between 1.5 and 2. Figures

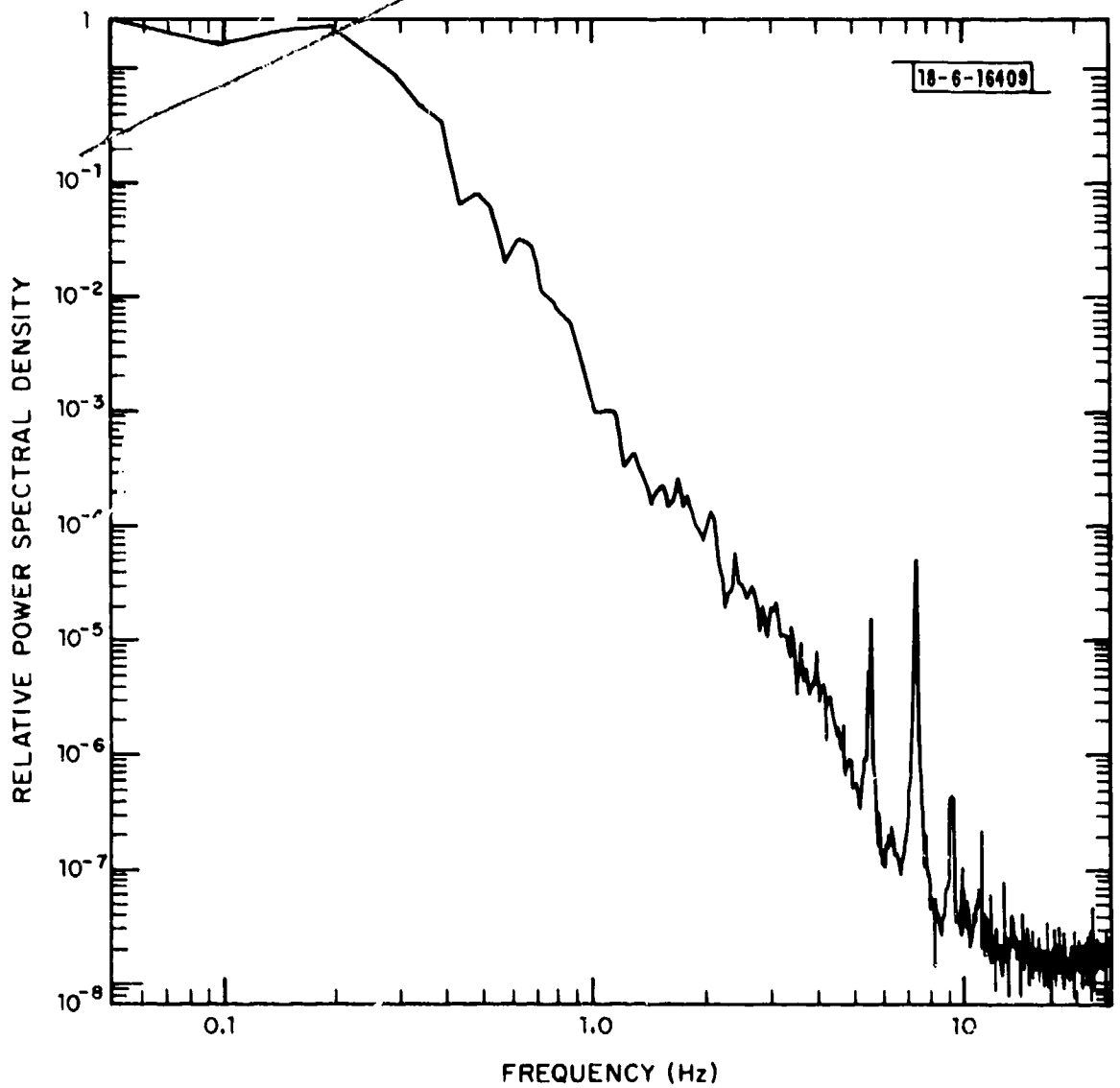

Fig. 2-3. Power spectral density of received signal power fluctuations during UHF scintillation, example 1. Less severe scintillation.

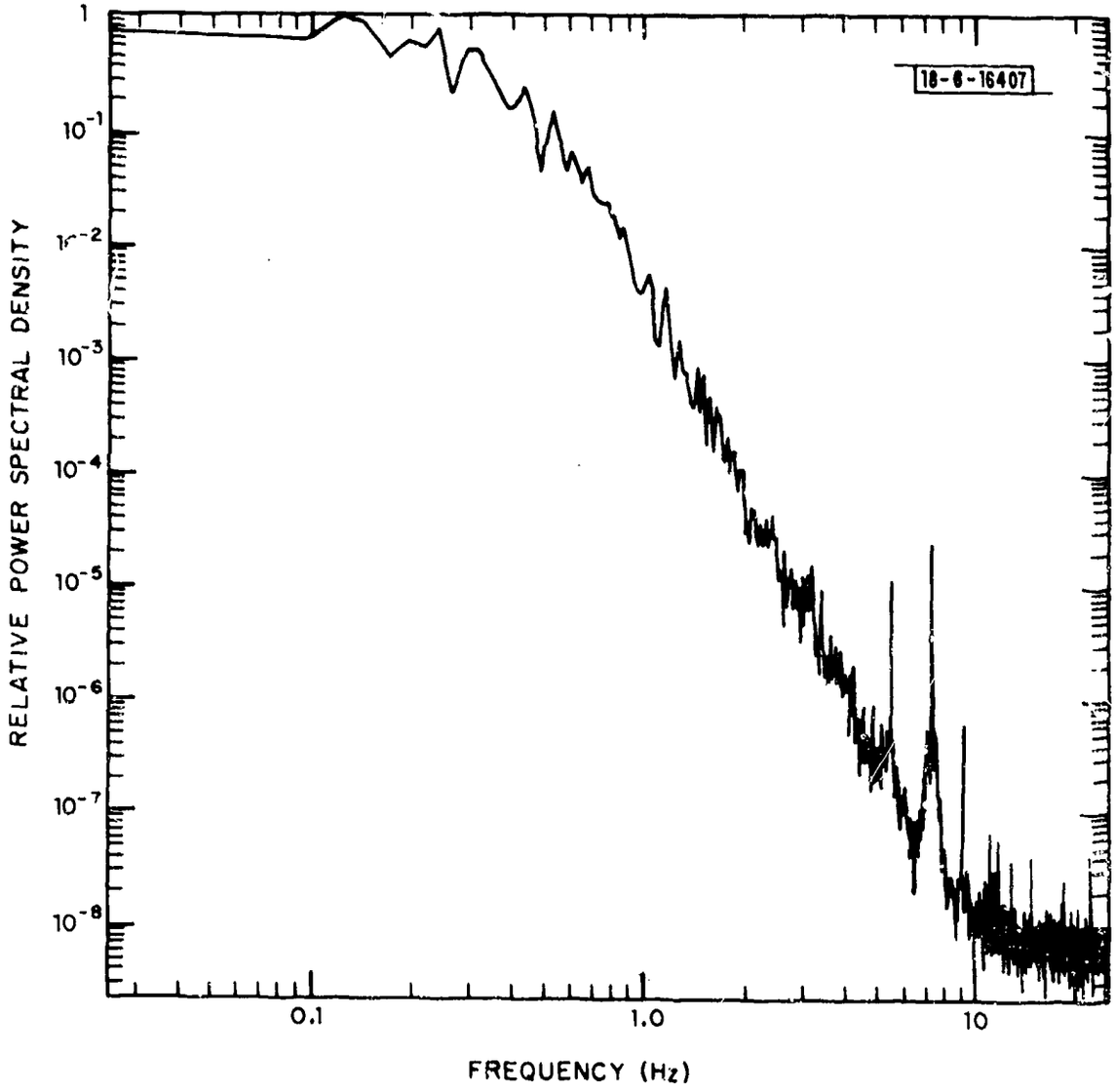

Fig. 2-4. Power spectral density of received signal power fluctuations during UHF scintillation, example 2. Nearly saturated scintillation.

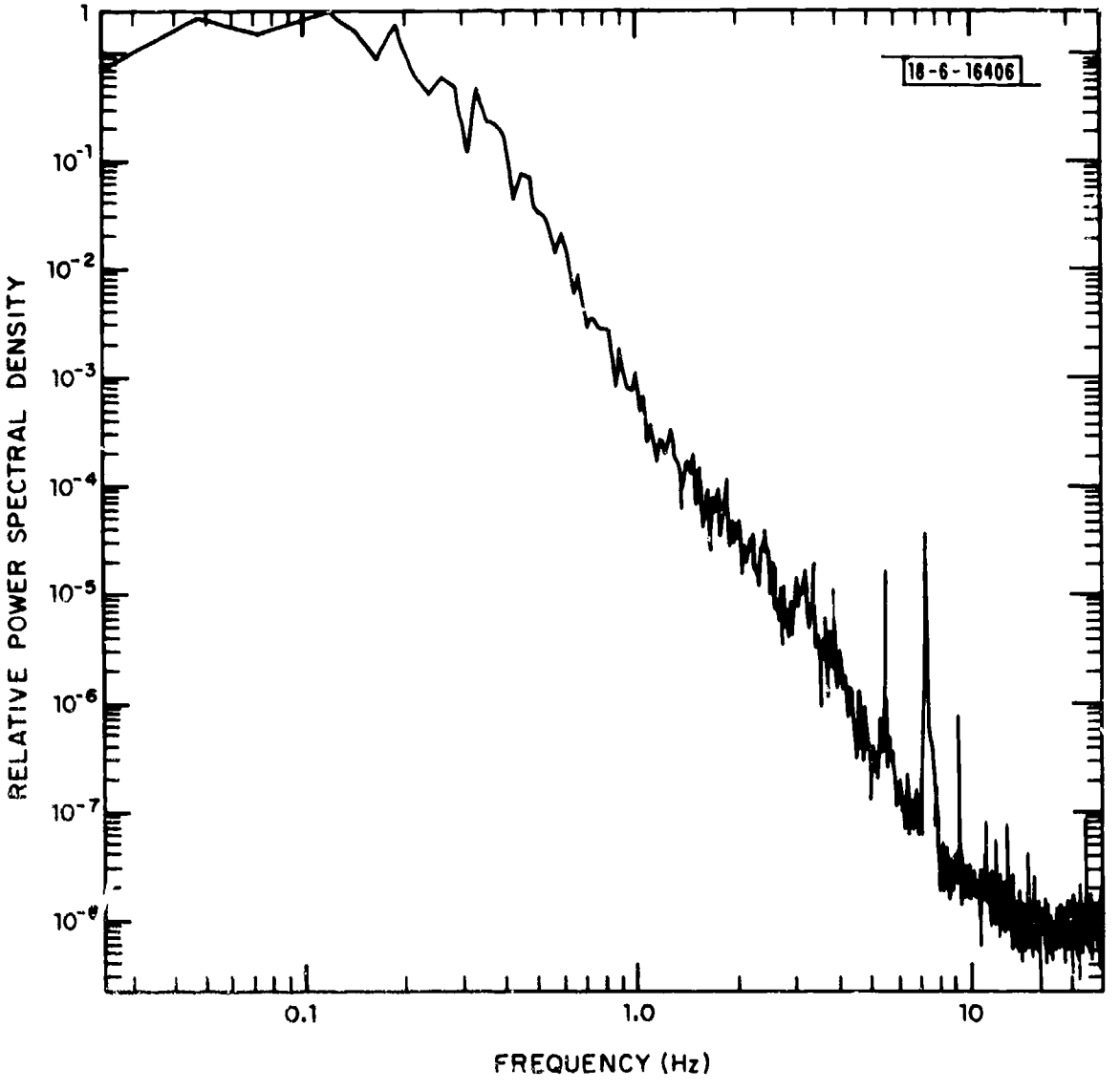

Fig. 7-5. Power spectral density of received signal power fluctuations during UHF scintillation, example 3. Nearly saturated scintillation.

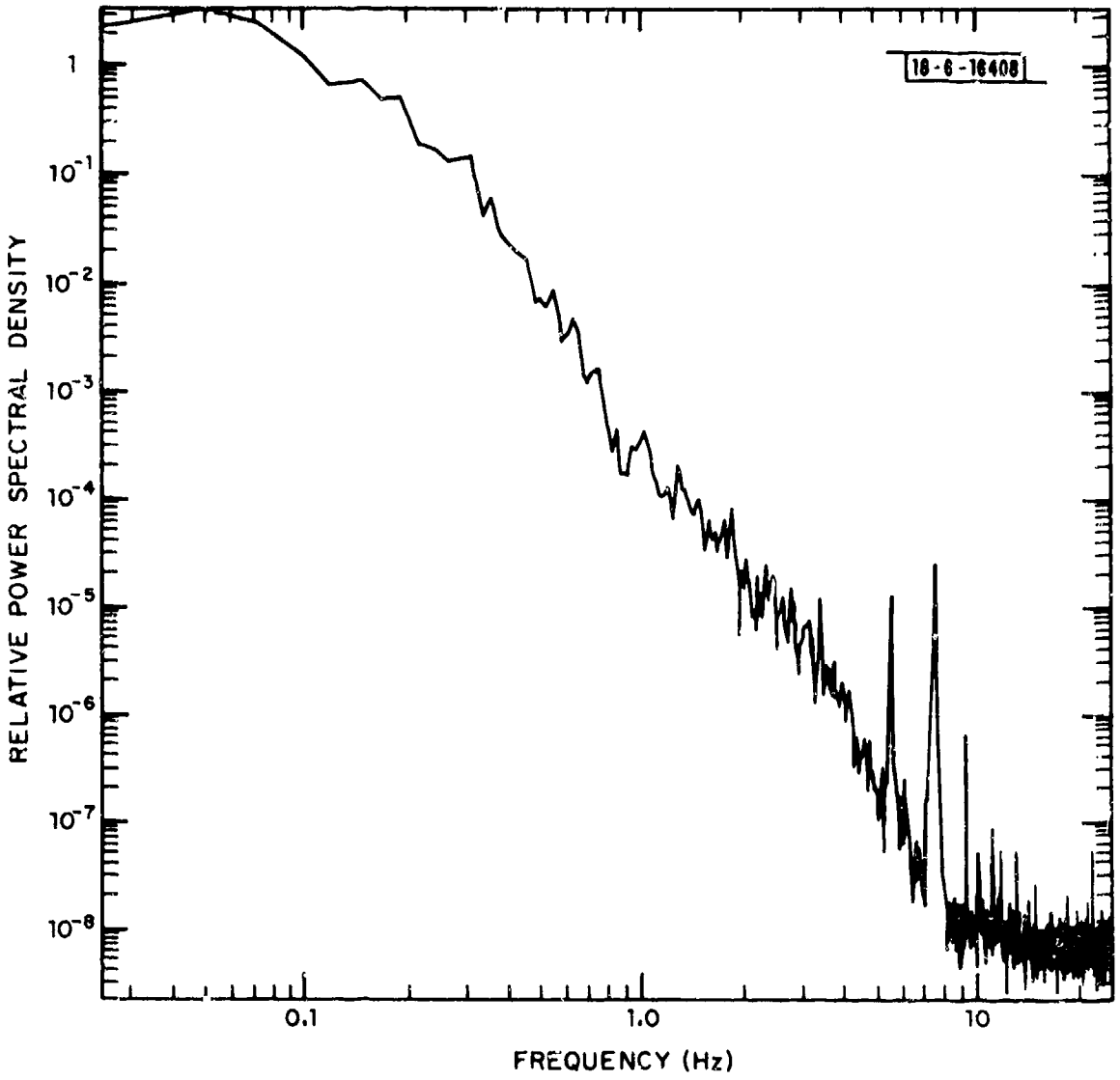

Fig. 2-6. Power spectral density of received signal power fluctuations during UHF scintillation, example 4. Nearly saturated scintillation.

2-4 through 2-6 illustrate the types of spectra most frequently observed during the most severe incidents of UHF scintillation which would be characterized by m-values between 1.3 and the saturation value m=1 characterizing Rayleigh fading. As noted above, Crane's morphology study[2-1] indicates that many of the occurrences of UHF scintillation are characterized as near or at the Rayleigh limit. No single spectral shape can characterize all the power spectra; however, a flat low frequency spectrum with a f^{-4} roll-off above some cut-off frequency is a good description of many of the spectra such as those in Figs. 2-3 and 2-5. A less rapid transition between baseband and the high frequency cut-off is needed to match the continuously steepening roll-off in some of the spectra such as those in Figs. 2-4 and 2-6. The spectra in Figs. 2-3, 2-5 and 2-6 all appear to have a slight shifting-over in the high-frequency asymptote when the power spectrum is three to four orders of magnitudes below its peak value. Crane[2-7] has observed similar shifts in other scintillation data; as far as the author knows, there is no theoretical model explaining this shift. The slight spikes in the spectra in the vicinity of 5.6 Hz and 7.4 Hz are believed to be produced by the measurement system and the satellite rather than the scintillation.

The "cut-off" frequency in the power spectra is a means of characterizing the rate of the scintillation fading process. There is some degree of arbitrariness in any fitting of this type. The less abrupt transitions between low frequency band and the high frequency roll-off band such as those in Fig. 2-4 and 2-6 illustrate the problems of "fitting". Some of this difficulty can be avoided by arbitrarily defining the cut-off frequency as the frequency below which there is 80% of the total energy in the power spectra. With this characterization, the cut-off frequencies ranged from 0.09 Hz to 0.54 Hz with all but 5-10% of the observed data having cut-offs in the range from 0.12 Hz to 0.4 Hz.

Figures 2-7 through 2-10 show the magnitude of the correlation functions corresponding to the power spectra in Figs. 2-3 through 2-7. None of the data sections analyzed produced correlation functions with any secondary peaks of magnitude greater than 0.3. Since the power spectra and the correlation

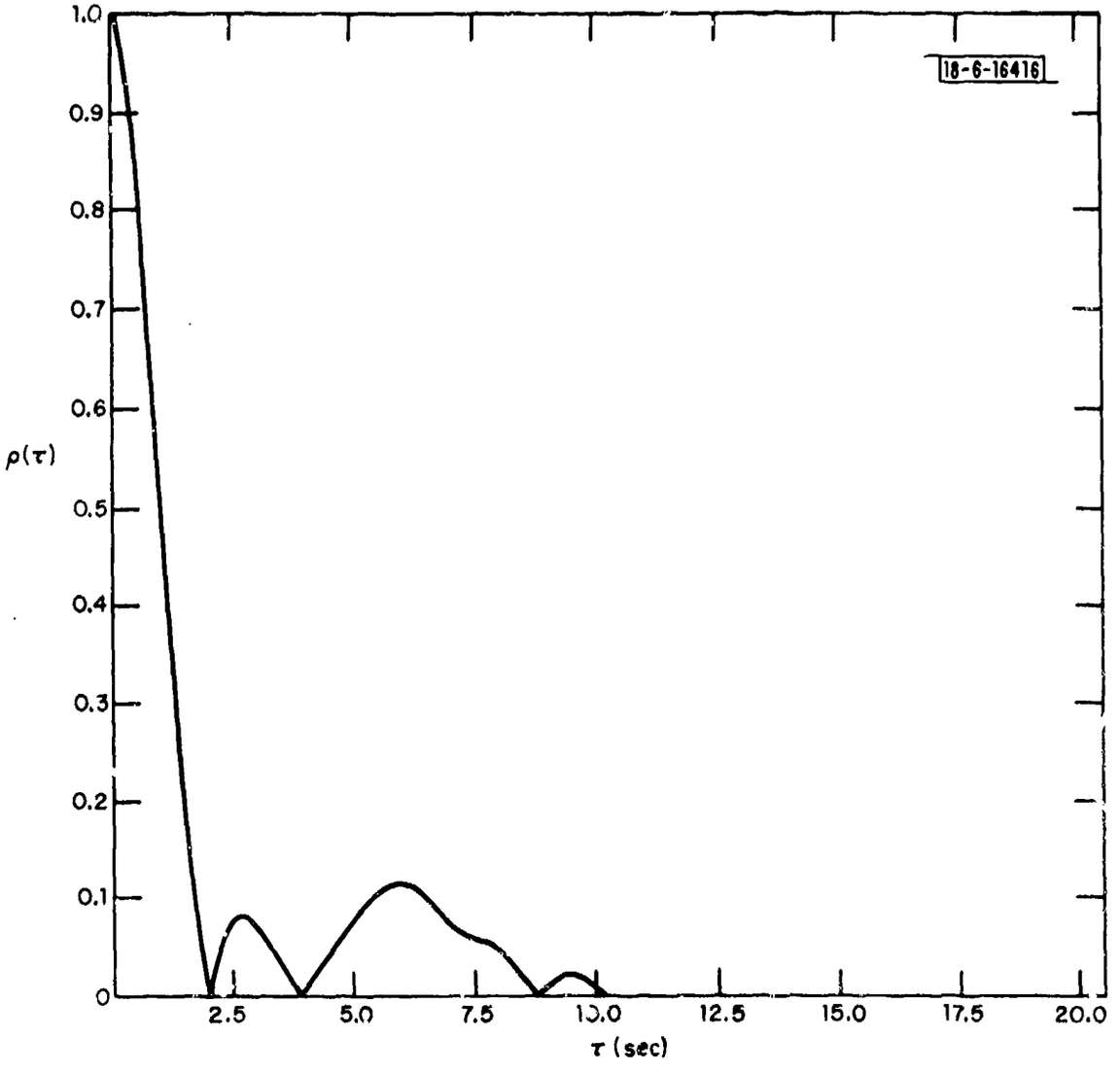

Fig. 2-7. Correlation function of received signal power fluctuations during UHF scintillation, example 1. The correlation estimate does not extend beyond 10 sec because of data segment length limitations.

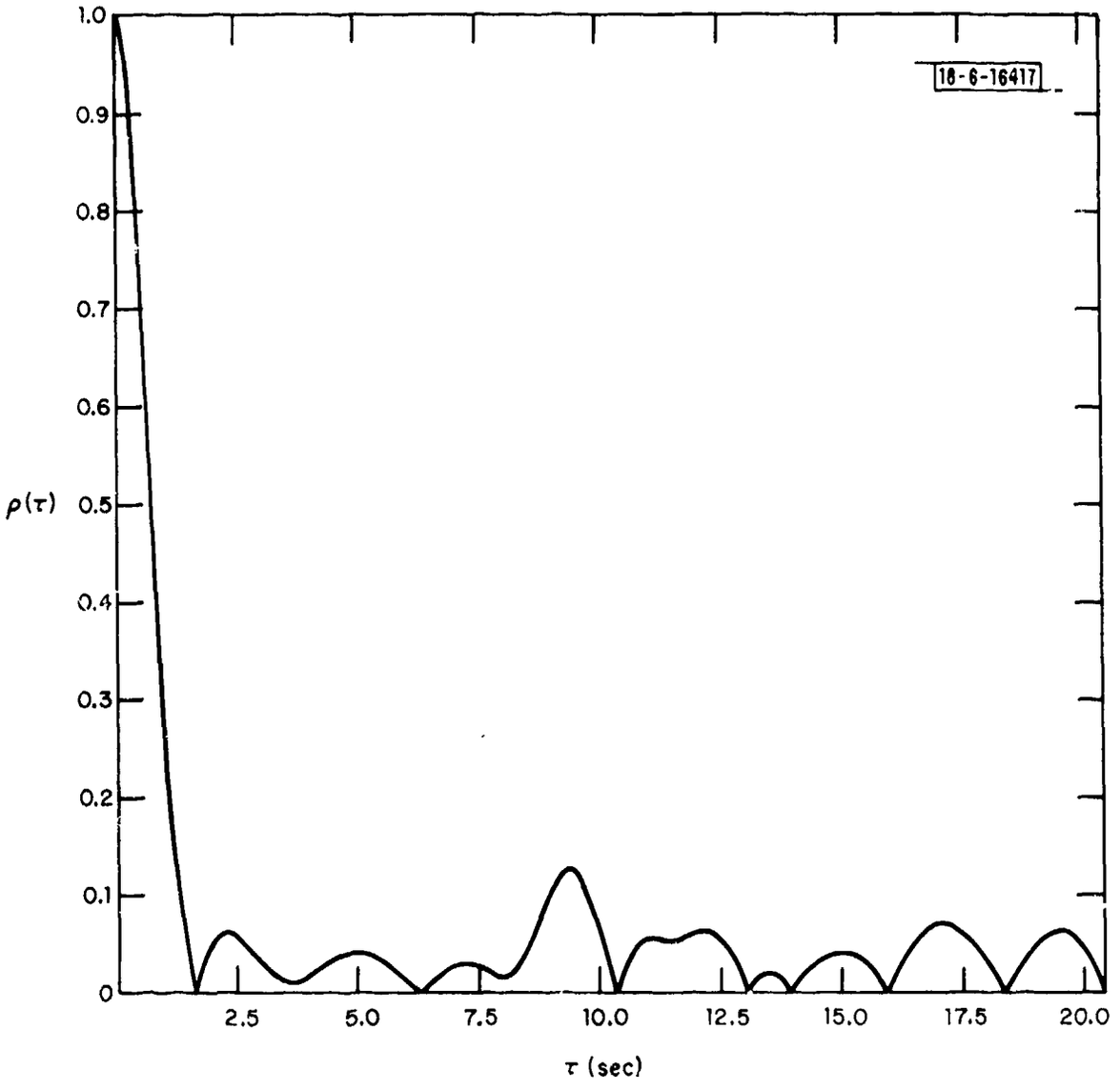

Fig. 2-8. Correlation function of received signal power fluctuations during UHF scintillation, example 2.

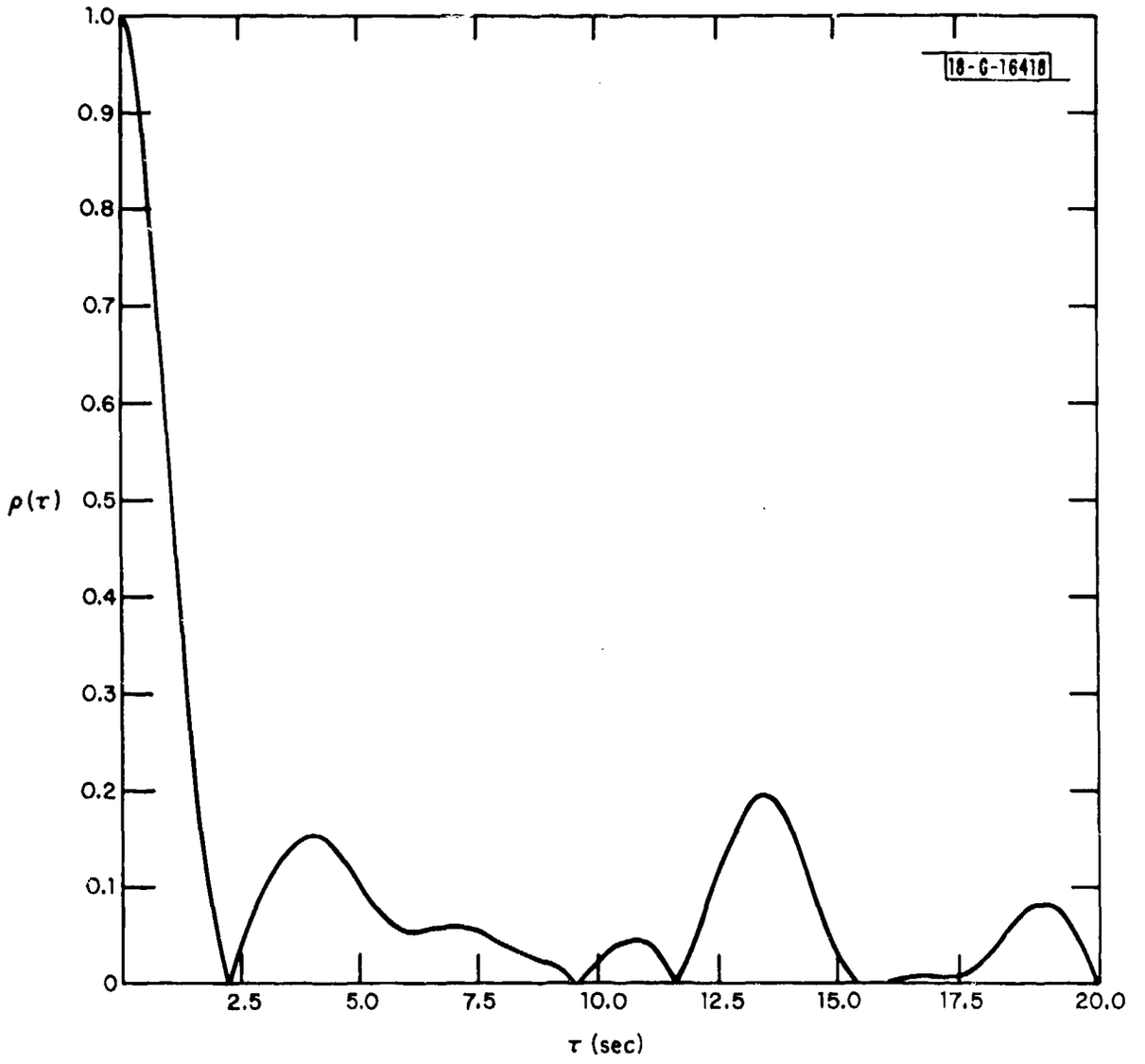

Fig. 2-9. Correlation function of received signal power fluctuations during UHF scintillation, example 3.

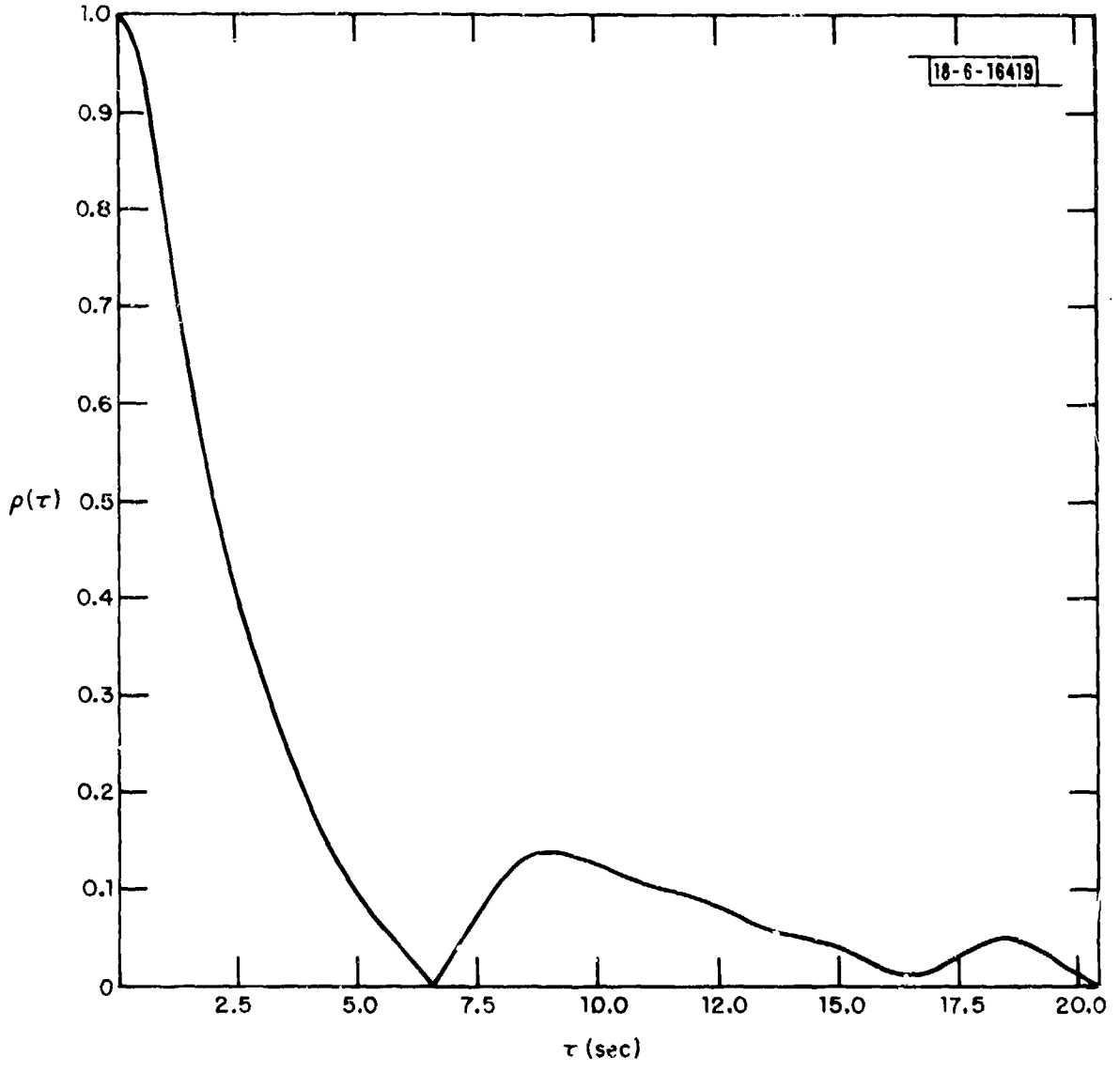

Fig. 2-10. Correlation function of received signal power fluctuations during UHF scintillation, example 4.

function are a Fourier transform pair, the width of the correlation function is inversely proportional to the "bandwidth" of the power spectrum. For the scintillation data analyzed, the τ for which the correlation function was 0.7, 0.5 and 0.3 were very close to $0.16/f_{cut\text{-}off}$, $0.24/f_{cut\text{-}off}$ and $0.32/f_{cut\text{-}off}$, respectively, with $f_{cut\text{-}off}$ defined as above.

Crane[2-7] has developed a theoretical expression for the variation in the cut-off frequency as various parameters of the ionosphere change. Crane's basic equation is

$$f_c = a \frac{v_d}{2\pi\lambda h_{eff}} \qquad (2\text{-}4)$$

where v_d is the ionospheric drift velocity, λ is the free-space wavelength of the electromagnetic energy being scattered, h_{eff} is the effective distance to the ionosphere from the earth-based terminal, and a is a constant of proportionality. A first-order approximation to h_{eff} is

$$h_{eff} \simeq \sqrt{R^2 \sin^2\theta + 2hR + h^2} - R\sin\theta \qquad (2\text{-}5)$$

where θ is the elevation angle to the satellite from the terminal, R is the effective earth radius and h is the altitude of the lowest effective scattering layer in the ionosphere. In equatorial regions,[2-7] the ionospheric drift rate v_d normally varies from approximately 40 m/sec to approximately 200 m/sec and the height of the lowest scattering layer in the ionosphere may vary from approximately 240 km to approximately 450 km. The range in variations of $f_{cut\text{-}off}$ predicted by Crane's equations closely matches the range in $f_{cut\text{-}off}$ in the analyzed data assuming that almost the full range of variations in v_d and h were observed. For the definition of $f_{cut\text{-}off}$ used here, the constant of proportionality a in Eq. (2-1) is in the vicinity of 2.5 to 5 depending upon the term matched.

The fading signal level fluxtuations can easily be simulated in a digital computer or in the laboratory for a power spectra falling off above $f_{cut\text{-}off}$ as f^{-4}

for all integer values of m in the Nakagami-m distribution. Figure 2-11 sketches the process of simulating the fluctuations for m=1. Two independent Gaussian random processes are used as the input signals to two independent two-pole low-pass filters with a cut-off frequency $f_{cut\text{-}off}$. The outputs of both filters are both narrow-band Gaussian processes. Taking the square root of the sum of the squares of these two Gaussians gives a number proportional to the amplitude (intensity) fluctuations with a Rayleigh distribution and a power spectra falling off as f^{-4} above $f_{cut\text{-}off}$. A number proportional to the power fluctuations can be obtained by deleting the square-root operation. Figure 2-12 shows the power spectrum of the received power fluctuations simulated using a two-pole low-pass filter with both poles real and located at 0.1 Hz.

To estimate the time distributions of both fades below a threshold and inter-fade separations, one must analyze a data sample long enough to obtain good estimates but short enough a sample to avoid large changes in the underlying physical process. To observe enough fades to estimate accurately the distributions, one may need an hour's data; however, the basic conditions in the ionosphere which cause the scintillation may change on time scales shorter than an hour. With these stationarity problems, one must carefully select data sections which characterize a long run of "the same kind of" fading. Sections of data for use in estimating the time distributions of fades and inter-fade intervals were selected by grouping together those consecutive records having comparable received power fluctuation spectra.

Each section selected as being a continuous run of the "same" type scintillation was analyzed with a number of fade thresholds at varying levels below the average signal. The average signal level was chosen as the reference level because there are theoretical arguments[2-1] that the average level during scintillation is approximately the received power level which would have been observed were there no scintillation. Figures 2-13 and 2-14 show examples of typical cumulative distributions of the fade durations and inter-fade separations observed during periods of relatively intense UHF scintillation characterized by m-values between approximately 1.3 and the limiting m=1. The fade threshold T used in compiling Figs. 2-13 and 2-14 was -6 dB relative to the average

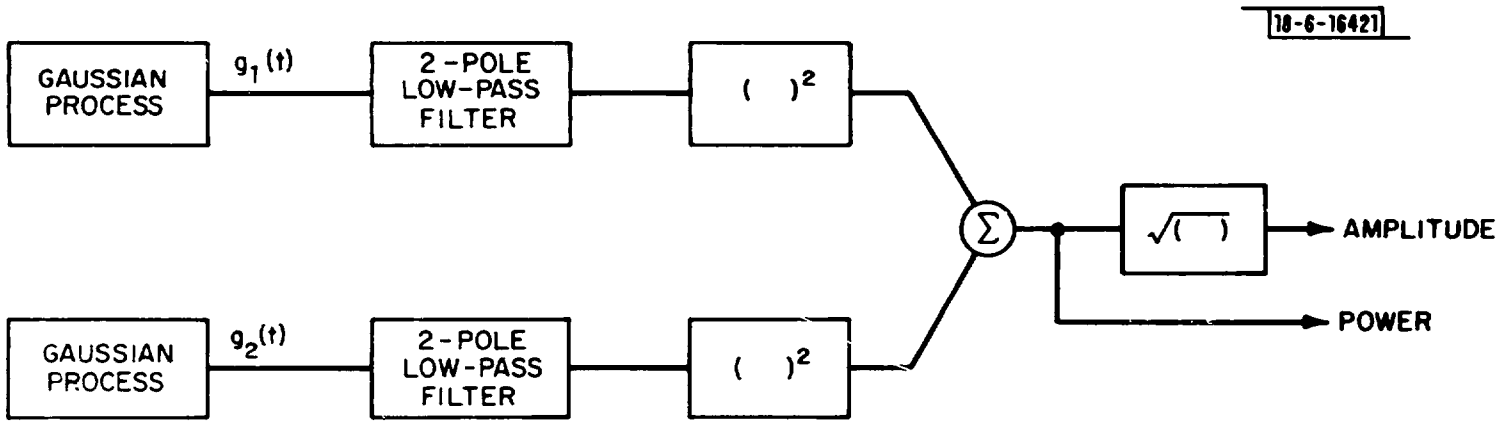

Fig. 2-11. Circuit for simulating UHF scintillation fading.

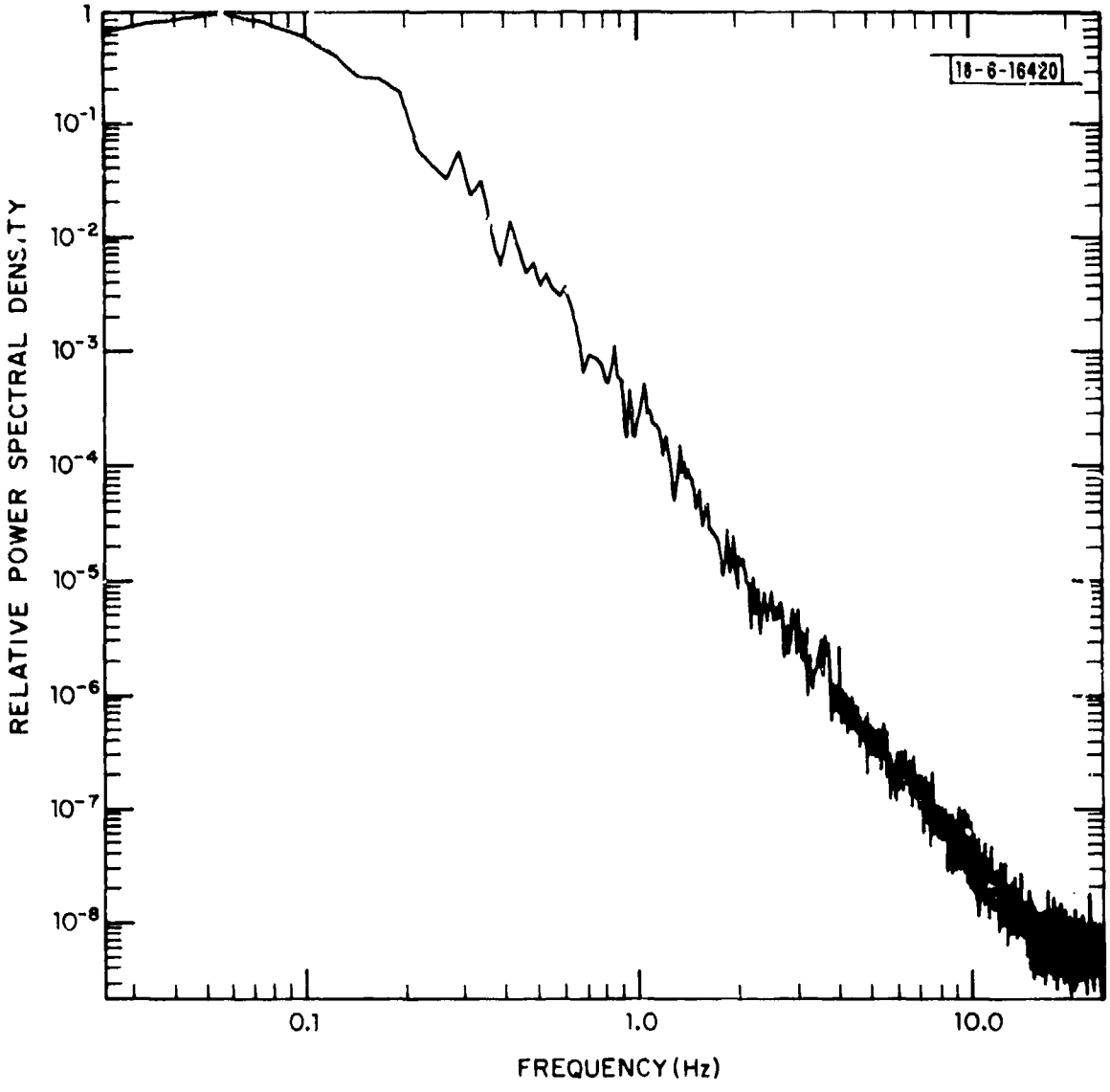

Fig. 2-12. Power spectral density of received signal power with simulated UHF scintillation.

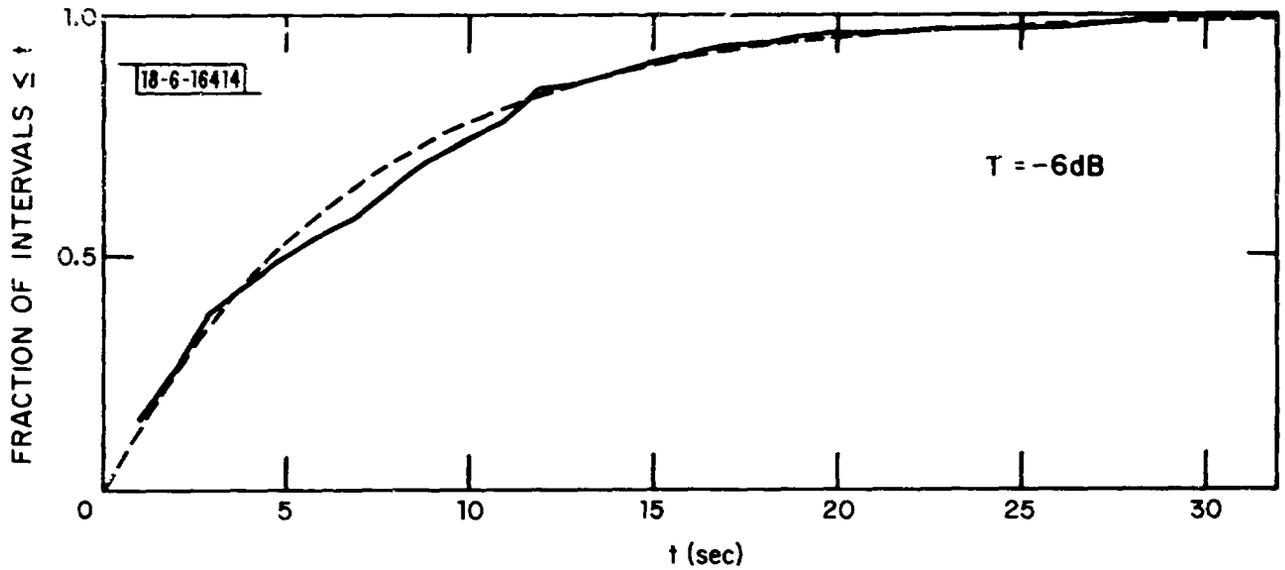

Fig. 2-13. Cumulative distribution of the length of intervals between successive fades for fade threshold T 6 dB below average received power.

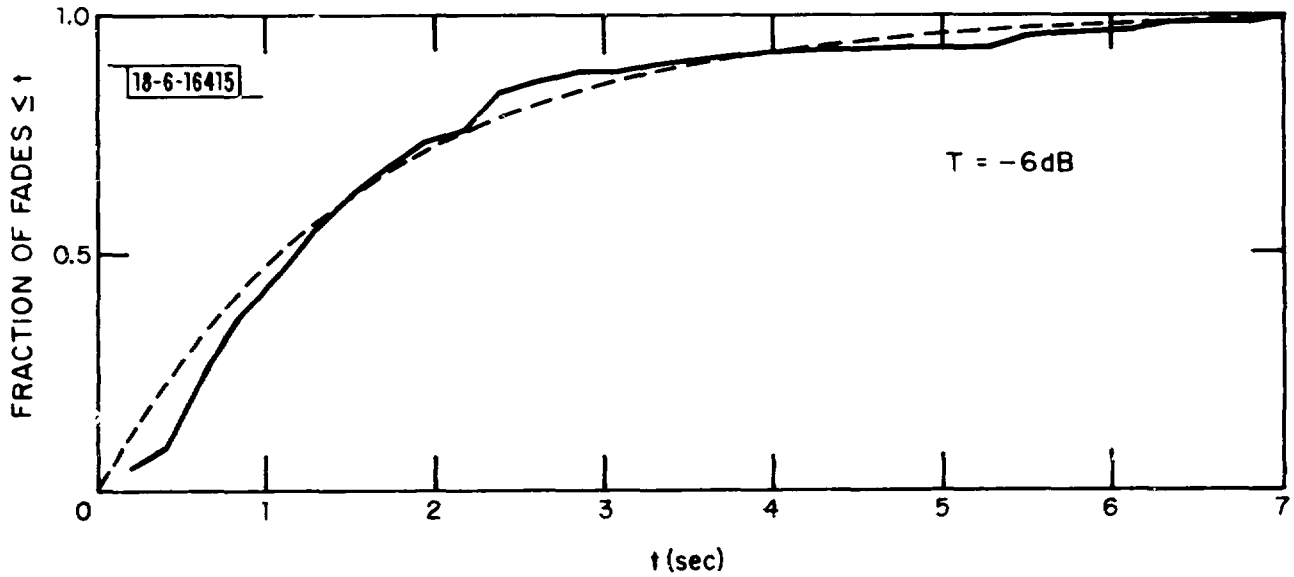

Fig. 2-14. Cumulative distribution of the length of fades below a threshold 6 dB below average received power.

received power P_o. Figures 2-15 and 2-16 show the result of changing T/P_o to -8 dB. Comparably shaped cumulative distributions were observed for T/P_o ranging from -2 dB to -12 dB. Although the time scale of the distributions changed with threshold T and $f_{cut-off}$ the basic shape remained relatively constant. The data which produced Figs. 2-13 to 2-16 contained the segment which produced the power-spectra correlation-function pair in Figs. 2-6 and 2-10.

There are no known theoretical expressions for the distributions of the duration of fades and inter-fade intervals during UHF scintillation. Thus, any analytic form for these distributions must be fitted on an ad hoc basis. The smooth lines in Figs. 2-13 through 2-16 are the cumulative distributions which would have been observed were the actual distribution an exponential probability distribution in which the probability of an event of duration between t_0 and t_1 is given by

$$\int_{t_0}^{t_1} \frac{1}{<T>} e^{-t/<T>} dt \qquad (2-5)$$

where <T> is the average duration of an event. Subjectively, the hypothesized exponential distribution offers a good, but certainly not perfect, fit to the experimentally observed distributions. In the same subjective sense, hypothesized distributions of the form $\sqrt{t}\ e^{-t}$ and te^{-t} offer less good fits to the experimental data. In assessing the goodness of any fit between an analytical form and the experimentally observed distributions of fade durations, one must remember that the accuracy of the experimental data is limited both by the finite bandwidth and noise in the measurement and recording process and by the unknown dynamic response of the radio receiver. At the very best, one would expect that the 3-Hz filter in the recorder playback would tend to blur and suppress events shorter than 1/6 second giving less resolution in resolving short deep fades.

Although the exponential distribution is not a perfect fit to the experimentally observed distributions of fade and inter-fade durations, it gives a sufficiently good fit to allow evaluation of the performance of communi-

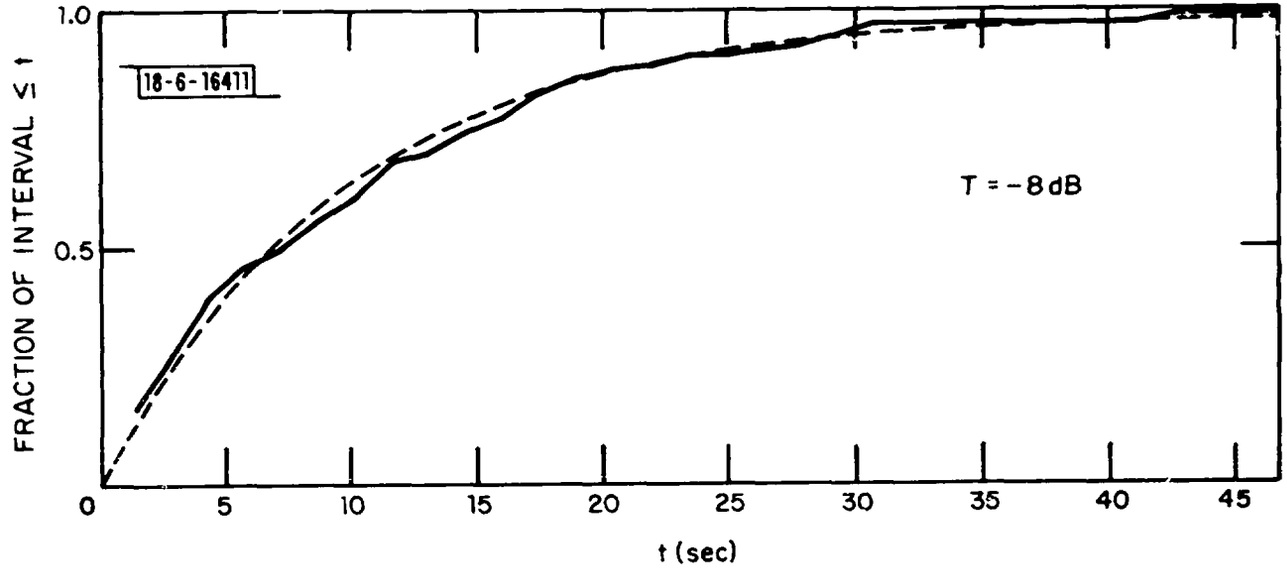

Fig. 2-15. Cumulative distribution of the length of intervals between successive fades for fade threshold T 8 dB below average received power.

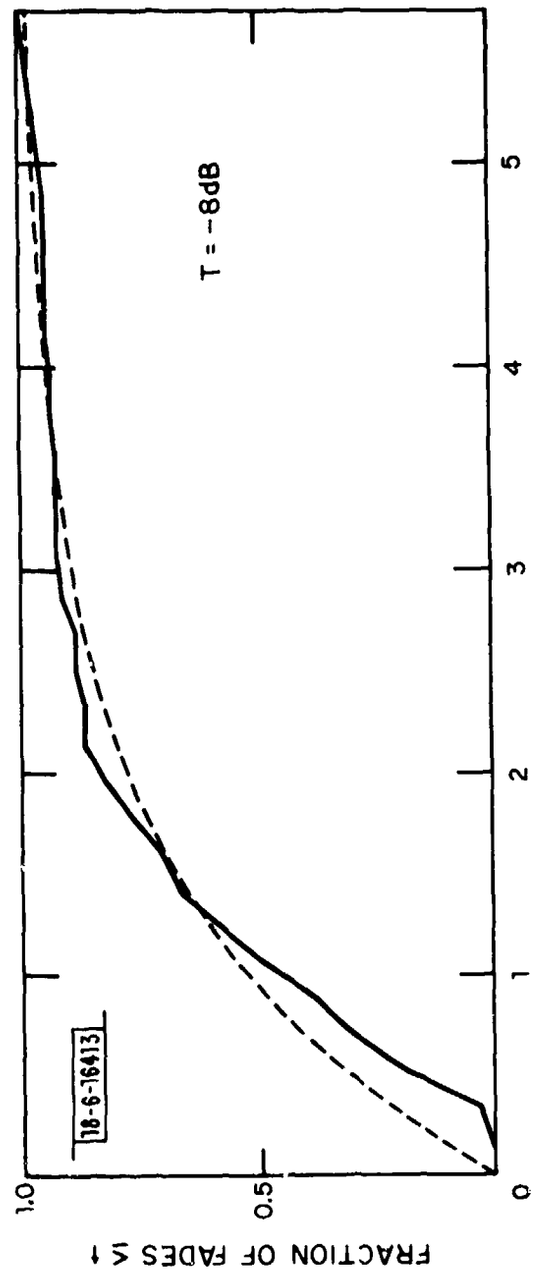

Fig. 2-16. Cumulative distribution of the length of fades below a threshold 8 dB below average received power.

cations systems during UHF scintillation. Much of this crudeness should be tolerable because a communication system capable of operating during UHF scintillation must be sufficiently robust to counter a wide range of fading rates having different distributions of fade durations. The exponential distribution for fade duration and inter-fade separation has the additional advantage of permitting a simpler analysis.

The exponential density is a one parameter distribution which is completely specified by the average. Thus, for a given fading threshold T, the model for the duration of fades and inter-fade intervals is specified by two numbers $\langle t_i \rangle$ the average duration of an inter-fade interval and $\langle t_f \rangle$ the average duration of a fade below the threshold T. The numbers $\langle t_i \rangle$ and $\langle t_f \rangle$ are functions both of the threshold T and of the fading rate which was characterized by $f_{\text{cut-off}}$ above. For a specific incident of UHF scintillation with a relatively constant fading rate, the variations of $\langle t_i \rangle$ and $\langle t_f \rangle$ with threshold T are reasonably well matched by power law formulas.

$$\langle t_i \rangle = \langle t_{io} \rangle \left(\frac{T}{P_o}\right)^{-\eta} \tag{2-6}$$

$$\langle t_f \rangle = \langle t_{fo} \rangle \left(\frac{T}{P_o}\right)^{+\lambda} \tag{2-7}$$

where $\langle t_{io} \rangle$ and $\langle t_{fo} \rangle$ are constants and η and λ are positive numbers. Figures 2-17 and 2-18 show plots of experimentally observed $\langle t_i \rangle$ and $\langle t_f \rangle$ and the power-law fitted curves for the same data as in Figs. 2-13 to 2-16 and 2-6 and 2-10. It should be noted in passing that Eqs. (2-6) and (2-7) together predict the fraction of time the signal is below T. This prediction is not functionally identical to the same quantity derived from Eq. (2-2). This inconsistency is judged not to be significant for the purposes addressed here. The approximation is close enough over an interesting and important range to yield useful results.

The values of $\langle t_{io} \rangle$ and $\langle t_{fo} \rangle$ are obviously dependent on the fading rate however defined. For rather frequently observed conditions of intense UHF scintillation characterized by m-values close to 1, the values of $\langle t_{io} \rangle$ ranged

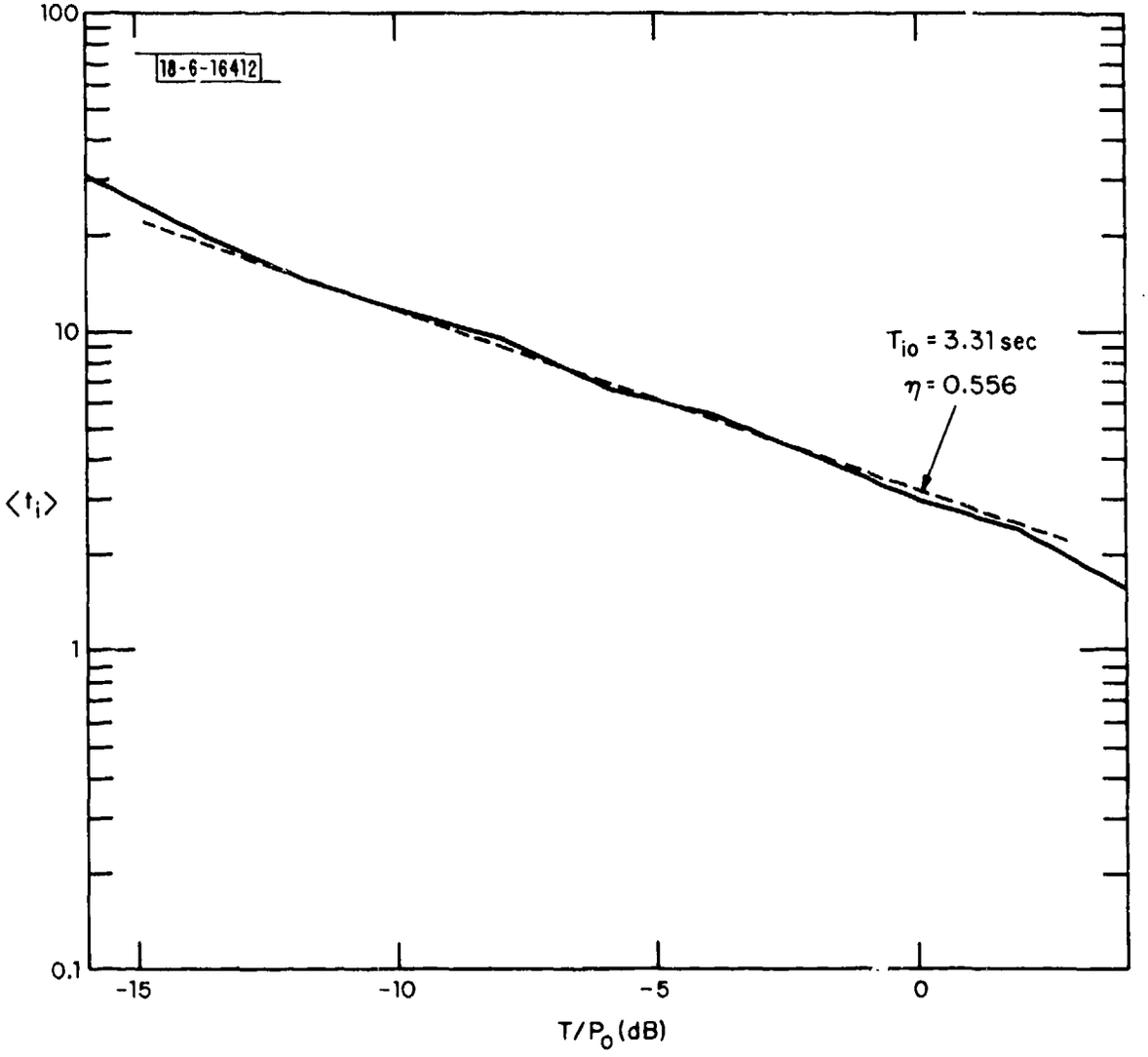

Fig. 2-17. Variation of the average time interval between successive fades below T as a function of threshold level T. Scintillation data same as in example 4.

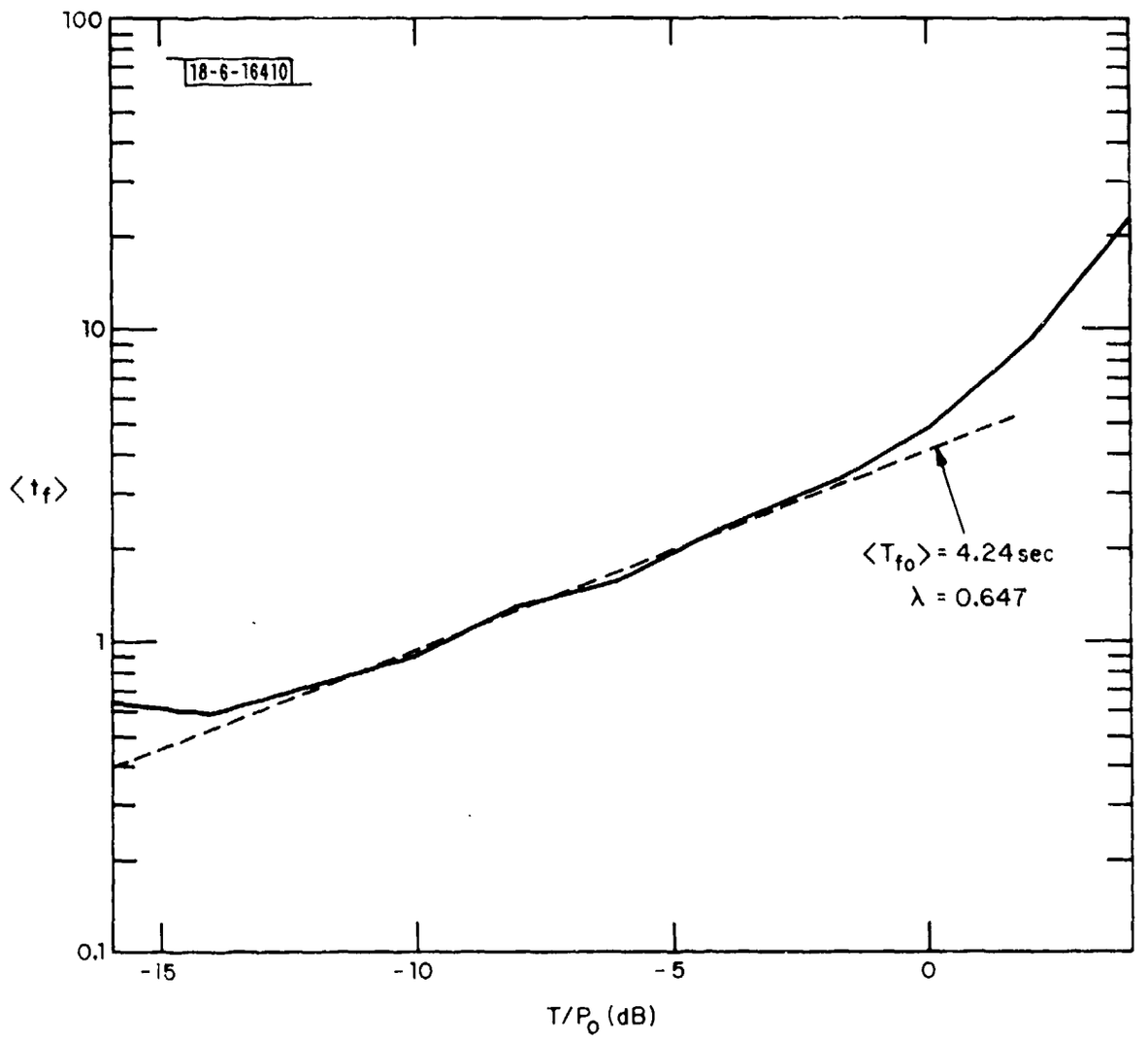

Fig. 2-18. Variation of the average fade duration as a function of fade threshold T. Scintillation data same as in example 4.

from approximately 1 sec to approximately 5 sec with η values ranging from .5 to .8 with larger values tending to be more common as the m-value became closer to 1.3 or so; the $\langle t_{fo} \rangle$ values ranged from approximately 1 sec to 5 sec and the λ values ranged from .6 to .9 again with the larger values becoming more likely as the m-value came closer to 1.3. For less intense UHF scintillation with m-values near 2, the η values ranged from .9 to 1.3 while the λ values ranged from .4 to .7; this less intense scintillation was observed so infrequently that there is little basis upon which to give any meaningful estimates of the ranges of rate parameters except to note that the observed rate parameters were within the range observed for the more intense scintillation. In some qualitative sense, the values of $\eta + \lambda$ tended to show less variation that the two individual variables themselves. The present data base is too small to attempt to quantify this observation.

Simulating the scintillating signal level with the filtered Gaussian technique described above, the fade duration and inter-fade interval distributions were somewhat closer to the exponential distribution than the experimental observations. Since the time resolution of the simulation was greater than that of the experiment and since there was also no noise in the simulation, this simulation lends some plausibility to the conjecture of exponential distributions for fade and inter-fade durations. The variations of $\langle t_{io} \rangle$ and $\langle t_{fo} \rangle$ with T also followed the power law forms.

D. Received Phase Variations During Scintillation

Comparatively little data has been taken on phase fluctuations in signals received during scintillation. Crane's work[2-7] involving both theoretical models and measured data indicates that the phase fluctuations are dominated by very low frequency terms substantially below $f_{cut\text{-}off}$ in the characterization of received-power level flucutations. In a communications system operation context, large but very slow fluctuations in received phase may be irrelevant to a receiver having a phase lock loop for tracking oscillator instabilities, Doppler shift, etc. Thus, the practical communications system impact of received phase fluctuations during scintillation is somewhat receiver dependent.

It may be that a receiver's phase lock loop/oscillator tracking circuit can follow the received phase fluctuations well enough to permit coherent detection. On the other hand, some of these scintillation induced fluctuations may be too fast to be tracked. The question of received phase stability can be circumvented if the chip modulation is selected to require only differential coherence or no coherence. DPSK and FSK are examples of modulation techniques which do not require a receiver phase reference. At this point in time, the issue of receiver coherence or non-coherence cannot be resolved without more experimental work with real scintillation and real receivers.

E. Limitations Imposed by Fading

Theoretically, fading need not decrease the ultimate capacity of a given communications channel; however, it may greatly increase the difficulty of obtaining a given performance. Figure 2-19 compares the error probability as a function of bit energy to noise ratio E_b/N_o for incoherent DPSK modulation with Rayleigh fading and without. Since Rayleigh fading is a reasonable but conservative model of UHF scintillation fading, the results of Fig. 2-19 are indicative of the effects of scintillation as well. The much worse error probability performance in the presence of fading occurs because the deep fades essentially disrupt the transmission of some of the bits while others are received cleanly.

Cavers[2-8] has shown that the imposition of Rayleigh fading on an established channel need not decrease the average data rate or the bit error probability if the user adjusts the instantaneous data rate to a level proportional to the received signal level. This data rate adjustment implies both an unlimited bandwidth and a feedback link from the receiver to the transmitter. Information theory[2-9] shows that this feedback link cannot increase the capacity of the channel. Thus, the feedback link can be disregarded when looking for ultimate performance limits at the cost of finding limits which may be much more difficult to reach without feedback than with. Imposing a maximum instantaneous data rate limit R_{max} on Cavers results forces a degradation due to fading. Constraining the instanteous data rate adjustments to be steps of ΔR rather infinitesimal increments imposes further penalties on Cavers technique. If R_o is the maximum data rate which the channel will support in the absence of scintillation, the average data rate which can be supported during Rayleigh fading is

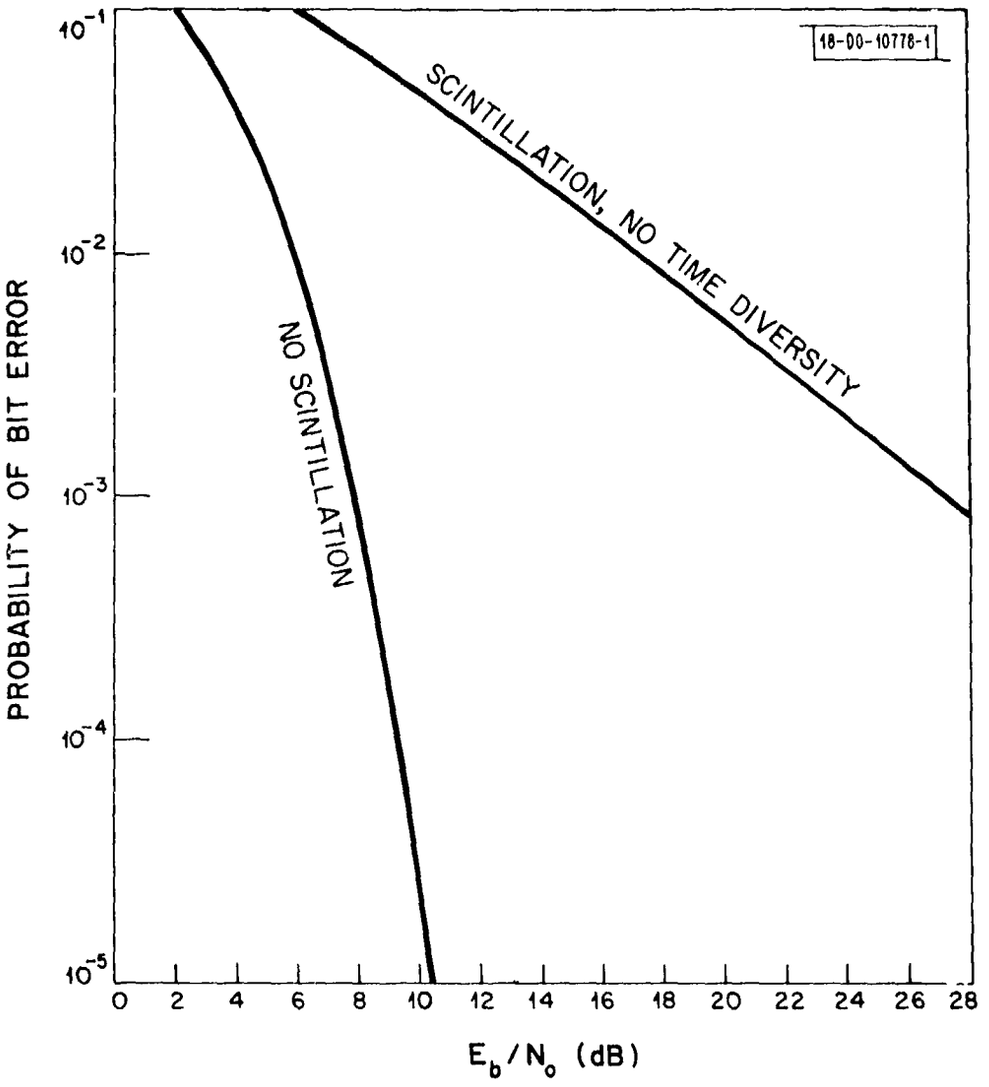

Fig. 2-19. Error probability for binary DPSK signaling with no fading and with Rayleigh fading and no time diversity.

$$[1-e^{-R_{max}/R_o}] \quad [\frac{e^{-\Delta R/R_o}}{1-e^{-\Delta R/R_o}}] \; R_o \; .$$

Eliminating any rate expansion beyond R_o and requiring a fixed transmission rate imposes a degradation of 4.34 dB to counter Rayleigh fading. In theory, an increase of 4.34 dB in transmitter power or a decrease of 4.34 dB in data rate is sufficient to counter Rayleigh fading without a feedback channel; however, the processing may be much greater than that required to support the maximum data rate without fading. Under certain circumstances, the techniques discussed in Sections III and IV will come close to this performance limit for "simple" systems.

In summary, UHF scintillation produces a broadband fading which can only be countered on mobile platforms by time diversity. This fading is theoretically no worse than Rayleigh and is frequently observed to be nearly Rayleigh. Thus, a Rayleigh fading model is a reasonable and conservative basis to use in evaluating techniques for countering the scintillation induced fading. In the frequency domain, the power spectra of this fading process has most of its energy below 0.5 Hz at the highest with the spectrum rolling of as f^{-4} at higher frequencies. The passages of the signal level across a fixed threshold T and the distribution of the lengths of these passages above and below can be approximated by three parameters--the m-value and the average duration of the passages above and below. The distribution of the passage lengths can be approximated by an exponential distribution. These three parameters are interdependent--two of them specifying the third.

III. THRESHOLD PROCESSING

A. Introduction

One method of implementing time diversity combining to counter scintillation induced fading is to divide the message into segments and accept only those segments which are reliable. The reliability of each received segment can be estimated either from received power levels or from an error control code. After rejecting the unreliable segments, the receiver must combine the remaining segments to obtain the full message. This combining could be as simple as piecing together the acceptable segments of several repeated copies of the message. It might be as complicated as using an erasure filling algebraic code with special redundant characters inserted in the transmitted message to allow the receiver to reconstruct the message text from some subset of the message segments. If there is a feedback channel from the receiver to the transmitter, the combining could also take the form of combining specifically requested repeats of unacceptable segments with the already received segments of the message.

Some acceptance/rejection threshold T must be established to test the received segments. This threshold is best specified as a level of instantaneous received power P_r referred to P_o the time average received power during scintillation. The threshold operation essentially assumes that any data received when P_r/P_o is greater than T is reliable. If this is to be the case, the channel must operate satisfactorily in the absence of scintillation with a margin of 1/T. Thus, there is an implicit assumption that the basic communications system has successfully dealt with other channel problems such as RFI, multipath, path irregularities, etc.

B. Threshold Crossing Statistics Models

A statistical model for the passages of the normalized received signal power P_r/P_o across the threshold T is necessary to analyze the performance of the segment thresholding. Section II contains the basis for such a model; however, time must be considered as a segmented rather than continuous variable as in Section II. The threshold crossing description in Section II models the

durations of the scintillating signal's passages across the threshold as exponentially distributed random variables. The two states "above" and "below" and the exponentially distributed holding times which describe the threshold crossings of P_r/P_o during intense UHF scintillation are also the properties of a two-state continuous-time Markov process. Since there has been extensive research into the properties of Markov processes, there are a number of results which can be readily applied to the special case of threshold crossings of the scintillating signal. A fundamental property of Markov processes is that all the information conveyed about future event probabilities by past events is contained within the present state. In this sense, Markov processes are memoryless.

Figure 3-1 shows the two states and the time incremental transition probabilities for the two-state Markov process modelling the threshold crossings of the scintillating signal. The Markov model state A corresponds to normalized signal levels above T; state B, below T. If the process is in state A at time t_o, it will enter state B before time $t_o + \Delta t$ with probability $\Delta t/\langle t_i \rangle$ for incrementally small Δt and remain in state A otherwise. The quantity $\langle t_i \rangle$ is the average duration of an interval between fades or of a passage into state A. Similar probabilities apply to state B except that the time parameter is $\langle t_f \rangle$ the average fade duration. The differential equations implied by these incremental relationships can be solved to give general expressions for the probability that the process is in a given state at t given the state at t_o:

$$P_A(t) = p_A + [P_A(t_o)-p_A]\, e^{-(t-t_o)/\tau} \qquad (3\text{-}1)$$

$$P_B(t) = p_B + [P_B(t_o)-p_B]\, e^{-(t-t_o)/\tau} \qquad (3\text{-}2)$$

where the process time constant τ is defined as

$$\frac{1}{\tau} = \frac{1}{\langle t_i \rangle} + \frac{1}{\langle t_f \rangle} \qquad (3\text{-}3)$$

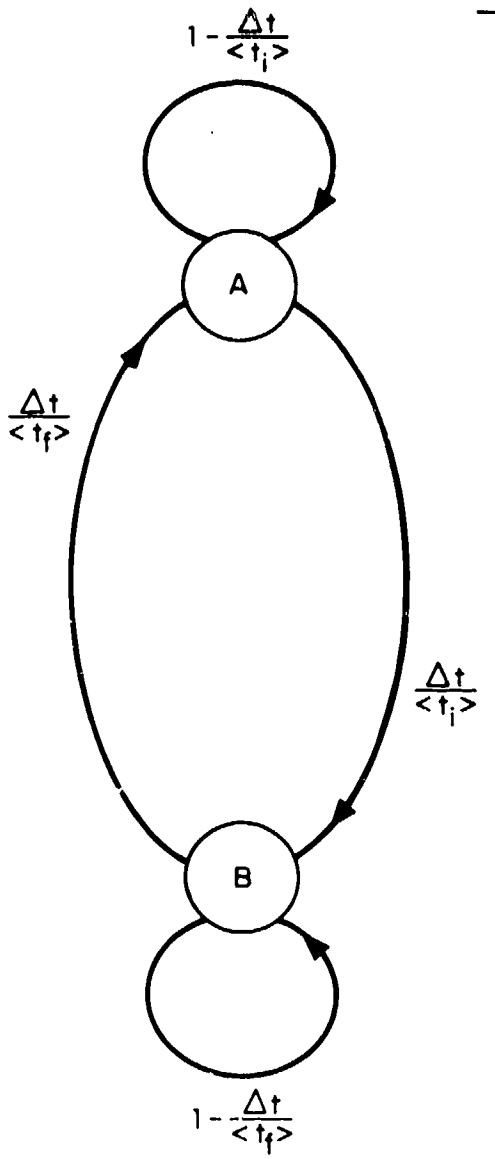

Fig. 3-1. Two-state time-continuous Markov model characterizing passages of a scintillating signal above and below a threshold.

and where the long-term average probabilities

$$p_A = \frac{\langle t_i \rangle}{\langle t_i \rangle + \langle t_f \rangle} \tag{3-4}$$

and

$$p_B = \frac{\langle t_f \rangle}{\langle t_i \rangle + \langle t_f \rangle} \quad . \tag{3-5}$$

Replacing state A by two states permits counting the acceptable segments. For a data segment t_s seconds long to be acceptable, every piece of the segment must be reliable. Thus, we assume that it is acceptable if and only if the normalized received power never dips below T while the segment is being received. Since future event probabilities of a Markov process are dependent only upon the present state, we need only know the state of the Markov process at the end of each segment in order to develop the probabilities for its state at the end of future segments. The ending state of each segment is preserved if state A is divided into states A* and A- in which A* is a Markov state corresponding to a segment ending with the channel in state A and during which the channel was never in state B and in which A- is a Markov state corresponding to a segment ending with the channel in state A but during which the channel was in state B at some time and if state B is defined as corresponding to a segment ending with the channel in state B. With these three state definitions, A*, A- and B, the statistics of acceptable segments are those of occupancies of state A* since the channel must have been in state A for an entire segment for that segment to be acceptable.

Figure 3-? shows the transition probabilities for the 3-state discrete-time Markov process modeling the statistics of acceptable channel segments. Equation (3-2) gives the probability of the two-state channel model being in state B at any subsequent time given its initial state. Thus, Eq. (3-2) gives the probability of all transitions into B from A*, A- and from B. Since an acceptable segment corresponding to a transition to A* must begin with the two-state channel model

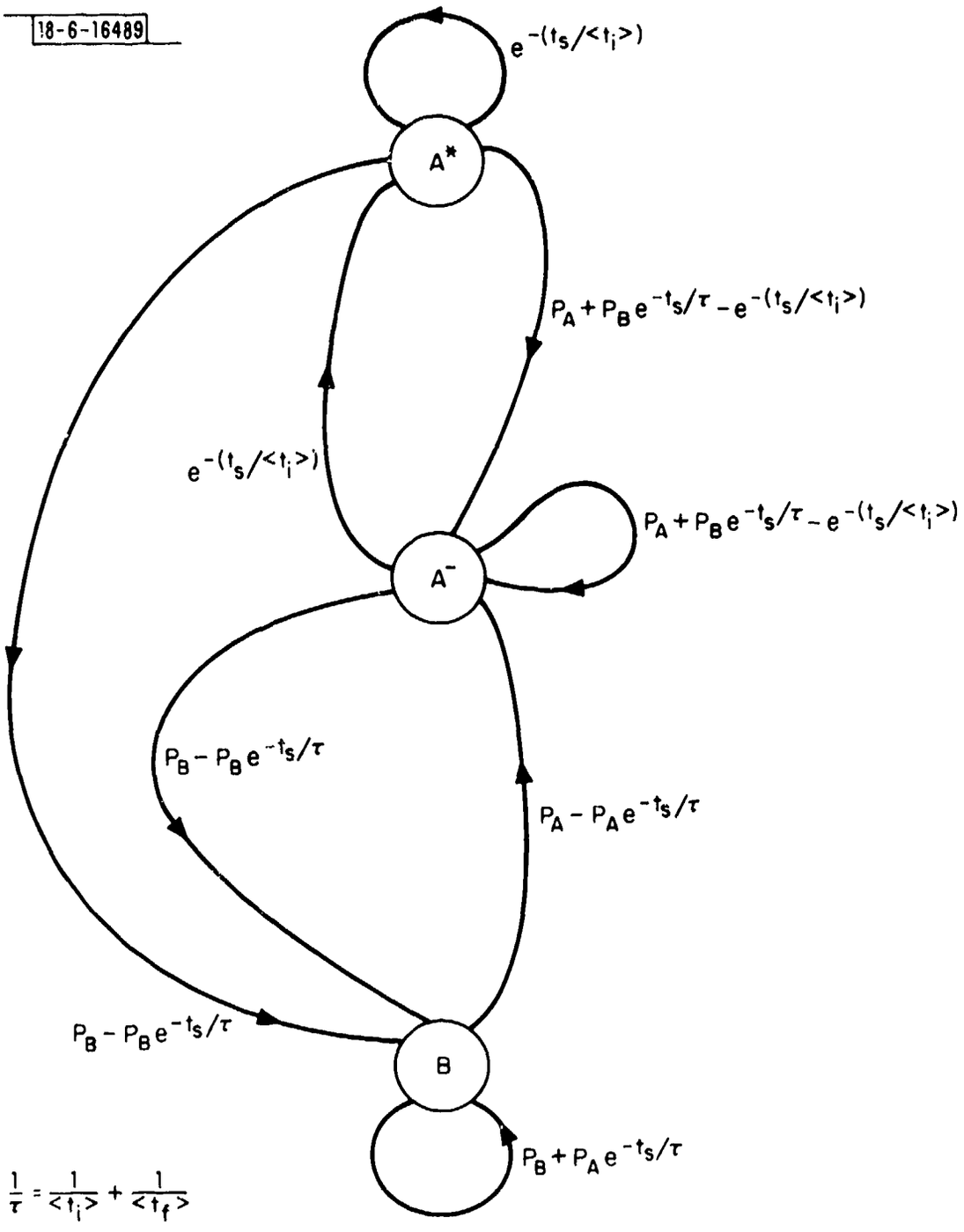

Fig. 3-2. Three-state discrete-time Markov model for the statistics of acceptable data segments during UHF scintillation.

in state A, there can be no transitions from B to A* (probability 0) and Eq. (3-1) can be used directly to determine the transition probability from B to A-. For a transition from either A- or A* into A* to occur, the two-state channel model starting in state A must not leave state A for t_s seconds, this occurs with probability $e^{-t_s/\langle t_i \rangle}$ for the exponential density. Substracting $e^{-t_s/\langle t_i \rangle}$ from the probability of the two-state channel model's being state A in t_s seconds given that it started in state A gives the transition probabilities from A* or A- into A-.

Given the transition probabilities for the 3-state Markov process, the statistics of state A* which represents the occurrence of acceptable segments can be determined from the results derived for Markov chains. Feller[3-1] uses linear algebra and canonic decomposition of matrices to develop expressions for both the average probability of occurrence for every state and the probability of a given state's occurring n transitions later given the present state. For the 3-state process which gives the statistics of acceptable segments, these average occurrence probabilities are:

$$P(A^*) = p_A \, e^{-t_s/\langle t_i \rangle} \tag{3-6}$$

$$P(A-) = p_A \, (1-e^{-t_s/\langle t_i \rangle}) \tag{3-7}$$

$$P(B) = p_B \tag{3-8}$$

The second-order transition probabilities which give the probability of a specific state N transitions after the occurrence of a given state, are all that is required to calculate the variance σ^2 of the number of acceptable segments occurring in a block of N consecutive segments. The general expression for this variance is dependent upon both the initial state and N. Assuming that N is sufficiently large to negate the effects of the starting state and taking the expectation of the variance over all starting states,

$$\sigma^2 \simeq N P_A \left[e^{-t_s/\langle t_i \rangle}\right]\left[1-P_A e^{-t_s/\langle t_i \rangle} + \frac{2P_B e^{-t_s/\langle t_i \rangle}}{1-e^{-t_s/\tau}}\right]$$

$$= NP(A^*)[1-P(A^*) + 2P(B)\frac{e^{-t_s/\langle t_i \rangle}}{1-e^{-t_s/\tau}}] \qquad (3\text{-}9)$$

Covariance techniques presented in Kemeny and Snell[3-3] produce this asymptotic variance in a simpler but less direct way. If the segments of interest to a particular user are interleaved with other traffic in such a way that the user effectively sees only every k^{th} segment received from the fading channel, the average occurrence probabilities in Eqs.(3-5) to (3-7) are unchanged but the variance becomes

$$\sigma^2 \simeq N\, P(A^*)[1-P(A^*) + 2P(B)\frac{e^{-t_s/\, t_i}\; e^{-(k-1)t_s/\tau}}{1-e^{-kt_s/\tau}}] \qquad (3\text{-}10)$$

As k increases, the asymptotic variance decreases because the increased separation between consecutive segments in the message effectively increases the number of "independent" samples of fading observed in N observations. These statistical characterizations can be used to estimate the performance of various methods of dealing with the gaps in received messages remaining once the faded segments have been rejected.

C. Repeated Segment Transmissi

One method of filling these gaps in acceptable traffic is to repeat the whole message several times and have the receiver attempt to piece the whole message together from acceptable fragments. If a message one segment long is transmitted c times, the receiver will fail to get the message if, and only if, it fails to receive an acceptable copy in all c trials. If the c copies are transmitted far enough apart in time to assume that statistically independent scintillation fading occurred during every repeat,

$$P(\text{received}) = 1 - [1-P(A^*)]^c \qquad (3\text{-}11)$$

If the repeats are not sufficiently separated to occur during essentially

independent samples of the fading, the number of effective repeats is reduced to c_{eff}. If the message is longer than a single segment, every segment must be received in order to receive the message. For segments closely spaced in time, the acceptability of consecutive segments may be strongly correlated and the number of effectively independent message blocks b_{eff} may be substantially less than the number of segments. If there are b_{eff} independent message blocks

$$P(\text{receive}) = \left\{1 - [1-P(A^*)]^{c_{eff}}\right\}^{b_{eff}} \qquad (3\text{-}12)$$

Equation (3-10) may be used to estimate the separation required between effectively independent repeats and the duration of effectively dependent blocks. The last term in the sum in brackets on the right-hand side of Eq. (3-10) is the only term in the asymptotic variance dependent upon segment separation. If the separation is sufficiently large to make this term negligible, that separation should produce effective independence. Separations of two or three time constants should be sufficient to produce effectively independent trials. An effectively dependent block of data might be one-half to one time constant long.

As an example, let us consider a case typical of the slower fading rates seen in the 1972 Guam data. A close approximation to these conditions uses Eq. (2-6) to determine $\langle t_i \rangle$ with $\langle t_{io} \rangle$ 2.5 sec and η=0.5. For the saturation limit of m=1, this set of numbers implies an average fade duration of 2.86 sec with an average fade separation of 10 sec for a fade threshold T/P_o = -6 dB. With a -6 dB threshold, the time constant is 2.22 sec and 2.78 sec for -3dB and 1.5 sec with a threshold of -10 dB. For a fade threshold of -6 dB, Eq. (3-11) implies that a minimum of five repeats are required to produce 0.999 message receipt probability for t_s much shorter than an average fade; this minimum number of repeats will suffice only if the repeats are sufficiently separated in time to be effected by statistically independent fading.

If a feedback channel to the transmitter is available, the receiver could greatly decrease the number of transmitted repeats by specifically requesting

repeats of only those segments rejected because of low reliability. Conceptually, a repeat request may be either a specific request or a failure to acknowledge. If the segments are many bits long, the repeat requests for missing segments could be communicated over a channel with a much lower data rate than the forward channel. The number of times a segment is repeated is a random variable in any repeat request system. Exactly n transmissions of a message segment will be required if, and only if, the first n-1 transmissions are not accepted and the n^{th} transmission is accepted. Thus, the probability that exactly n transmissions are needed to communicate a segment to one intended receiver is

$$P(n \text{ trans}) = [1-P(A^*)]^{n-1} P(A^*) \qquad (3\text{-}13)$$

The expectation of n, $\langle n \rangle$ or the average number of transmissions required to communicate one segment to one intended receiver can be found from (3-13)

$$\langle n \rangle = 1/P(A^*) \qquad (3\text{-}14)$$

Continuing the above example, a -6 dB threshold implies that an average of 1.29 transmissions are required to transmit one segment and that a -3 dB threshold implies 1.65 transmissions and that -10 dB implies 1.1 transmissions. That is, an increase in margin increases the probability that a segment will be received and thus decreases the number of repeats required. In each case, the use of a feedback channel to guide the repeating increases the message segment throughput of the channel by a factor of two or more over using multiple repeats alone as a technique of countering scintillation induced fading.

If there is more than one intended receiver as in a broadcast, the repeat request handling becomes more complex as repeat requests from several receivers must be simultaneously fed back and processed. The repeat request processing is simpler if the repeats for each intended receiver are handled separately; however, the total number of repeats transmitted is smaller if all repeated segments are available to all receivers. Since the several intended receivers will usually

observe different scintillation rates and have different link margins, analytic expressions for the distribution of the total number of repeats needed to service two or more receivers are rather tedious for the general case. However, repeated applications of equations similar to Eq. (3-13) can develop expressions for the average number of transmissions to service multiple receivers for any particular control strategy.

D. Erasure Filling Codes

An erasure filling code allows the receiver to use a mathematical process to recover the whole message text whenever $N-d_{min}+1$ or more of the N codeword segments have been correctly received. The encoder accepts a block of K message segments and mathematically generates N, (N>K), segments for transmission. The minimum distance, d_{min}, of the erasure filling code is a basic parameter of all error control codes.[3-4,3-5] The erasure filling code can be used to fill the erasures caused by rejecting the scintillation faded segments if enough segments of the codeword have been accepted to permit decoding. To reliably communicate in the presence of scintillation fading, the parameters N, K and implicitly d_{min} must be chosen to permit decoding with a sufficiently high probability. On the average, the number of acceptable codeword segments will be N times the probability of accepting a specific segment P(A*). There will be statistical fluctuations around the average number of acceptable segments NP(A*) and the code must be designed to operate during these fluctuations below and above average.

Approximating the number of acceptable segments in a block of N received segments by a normal distribution, the number of received segments which can be assumed acceptable with a given probability can be estimated by moving the right number of standard deviations from the mean. With a normal distribution, 99% reliability can be obtained by operating 2.33 standard deviations below the mean and 99.9% reliability at 3.08. With this approximation, the code must be selected in such a way that the minimum number of acceptable segments permitting decoding

$$N-d_{min} + 1 = NP(A^*) - k\sigma$$

$$= NP(A^*) - k\,NP(A^*)[1-P(A^*) + 2P(B)\,\frac{e^{-t_s/\langle t_i\rangle}\,e^{-(k-t_s)}}{1-e^{kt_s/T}}] \qquad (3\text{-}15)$$

where k is the number of standard deviations below average required to obtain the desired reliability. Comparing estimates of the number of acceptable segments in a block of N made with the Gaussian approximation with results obtained from the Guam data shows some discrepancies which must be attributed to the Gaussian model. Simulations using the three-state Markov model produce more accurate estimates.

The code parameters N, K and d_{min} are interrelated by the structure of the particular algebraic code used. Any error control code[3-4,3-5] can be applied to the problem of filling erasures. Reed-Solomon codes are a very flexible member of the class of "maximum distance separable codes" which are especially useful for this type problem. For any maximum distance separable code d_{min} = N-K+1 which is the maximum possible for the particular combination of N and K. A Reed-Solomon code with codewords N segments long exists for all N less than 2^b where b is the number of bits in a segment and any K less than N. The decoder will be able to recover the message as soon as K presumably correct segments have been accepted. The decoder could also be designed to correct errors in the accepted segments at the cost of being able to fill in two fewer erasures for every error corrected. If desired, the segments of the Reed-Solomon code could be made shorter than the segment lengths implied by the scintillation rate and the codewords could be interleaved if the shorter segment length simplified the decoder processing. Crude estimates of the decoder complexity indicate that real time decoding of a 2400 bit/sec scintillation protected data stream would require a processor comparable to a small mini-computer.

E. Performance Estimates

Figure 3-3 shows the fraction of the data rate available in the absence of scintillation which can be used to carry scintillation protected data for each of the three strategies as a function of the erasure threshold to average power ratio T/P_o. The erasure filling code was assumed to be a Reed-Solomon code with the N, K and d_{min} parameters selected to permit the highest data rate for the required message reliability. Messages 30 seconds long at the clear channel data rate were assumed in drawing Fig. 3-3. Fig. 3-4 shows the additional transmitter power required to counter scintillation if it is desired to hold the same data rate when both the power for the fade margin and the power to increase the signaling rate are charged to the cost of countering scintillation. With longer messages, the performance of the erasure filling code improves while the performance of the unguided repeat scheme decreases. The performance of the repeat request strategy is independent of message length.

F. Implementation Users

Each of the three techniques for handling the gaps caused by rejecting unacceptable faded segments presents a different point in the cost-performance trade-off. Piecing together the acceptable segments of multiple copies of the whole message is the conceptually simplest technique and requires only block data editing capabilities at the receiver. However, the transmission of these multiple copies is inefficient in terms of the required power and bandwidth. On the other hand, specifically requested repeats are the most efficient method of communicating a message to one intended receiver in the presence of scintillation. However, there must be an operating communication link from the receiver back to the transmitter to relay the requests. Moreover, accommodating another intended receiver within the system changes the efficiency and control operations for the requested repeat system but implies no changes either in the multiple unguided repeat technique or in the erasure filling code approach. The receiver processing for the erasure filling code technique is much more complex than the processing for either repeat technique because the decoder must process data in addition to moving it. Of the three techniques, only the requested repeat

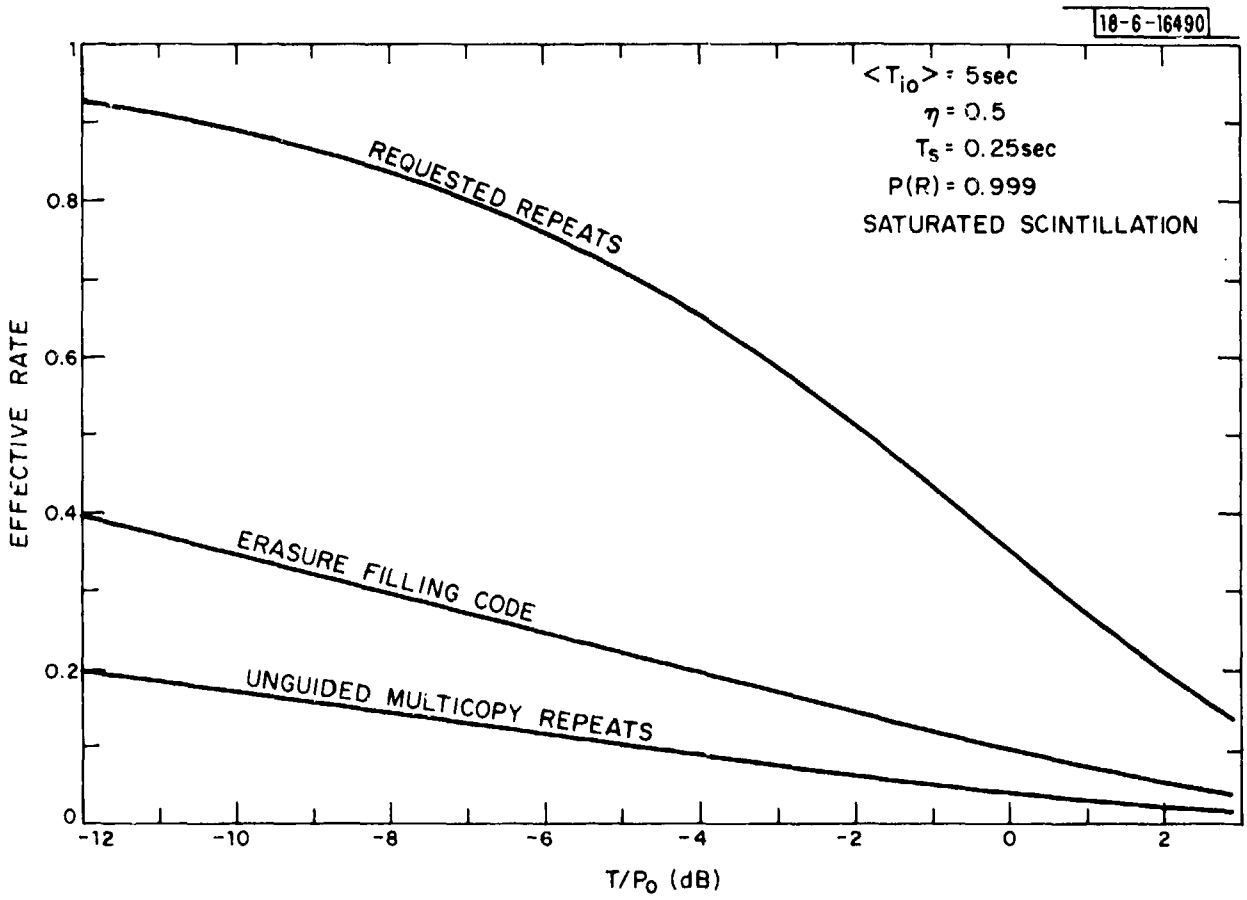

Fig. 3-3. Effective data rate available during scintillation for various hole-filling techniques.

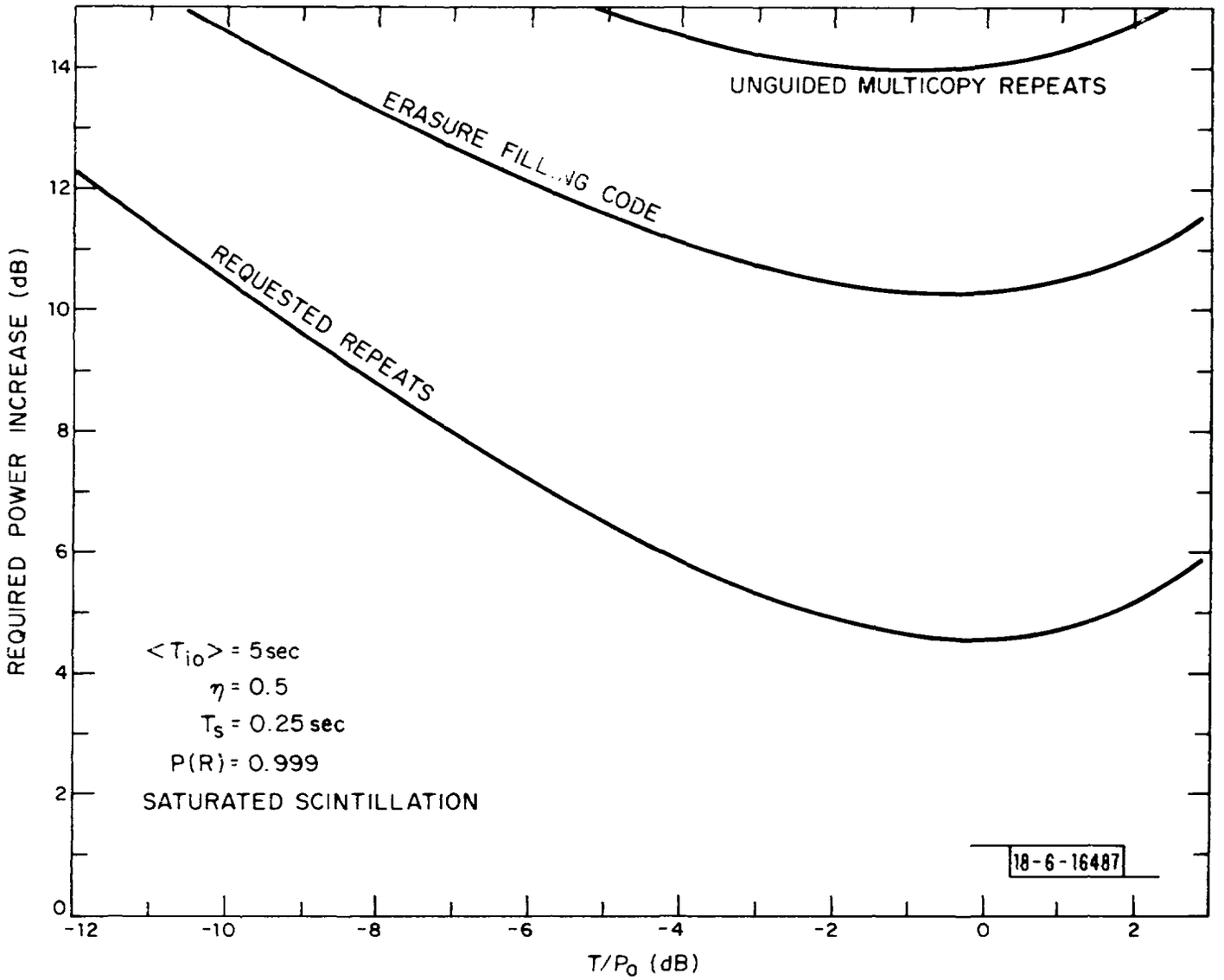

Fig. 3-4. Extra link power required to counter the onset of saturated scintillation with a threshold testing technique using various hole-filling techniques.

technique can be used to be sure that short burst messages are eventually received. The performance of all three techniques is dependent on the fading rate; however, the requested repeat strategy is by comparison quite robust in the face of large changes in the fading rate; unless the fading rate becomes so fast that almost all segments contain some faded data. For particular applications, combinations of these three approaches could also be used such as using an erasure filling code to fill in a few gaps after multiple repeats were used. Combinations of techniques could also be used with the same system with the basic communication being done with a repeat request strategy and the repeats requested via a repeated copies technique.

In implementing any of these segmented approaches to countering scintillation fading, there are a number of practical issues to be faced. First, the receiver has been assumed to be ready to receive whenever the received signal level is acceptable; however, if the receiver acquisition circuits start a new frequency or bit-time search during the fade, this will probably not be the case. If the receiver phase and/or frequency tracking circuits drift too far during a fade, some provision must be made to reacquire quickly when an acceptable signal returns. At all but very low data rates, the carrier power available at the edges of fades should be sufficient to permit fine tuning of tracking loops before the acceptable communication signal returns. Second, operating communications systems often have to handle messages of several "values". The more valuable messages may be either especially important to the communicator or essential to the operation of the system. For these special messages some extra measure of reliability will have to be provided and failure modes more carefully studied. For example, in a time division multiplex system, the order-wire messages controlling "what terminal transmits when" are essential to the communications of all users. A "transmit upon positive authorization" control algorithm for such a system would be resilient to terminals missing order-wire messages because of scintillation while a "transmit until further notice" algorithm would be more vulnerable to lost messages. Third, there remains the assumption made in the beginning that the communication system operated well in the absence of scintillation. If there are some system degradations in fact, the use of margin

and the error control techniques designed for countering scintillation induced fading is probably not the best or even a reasonable approach to handle degradations due to RFI, excess link losses, etc. This division of margin between scintillation and other losses can be avoided if the scintillation protection is developed in the same way as the protection against increased noise, multipath, etc.

IV. TIME DIVERSITY MODULATION SYSTEMS

A. Coded Modulation

Time diversity modulation signal structures counter the effects of scintillation induced fades at the basic modulation signal level where interference (RFI) and other equipment/link degradations can also be countered. This combined approach increases system flexibility in that the receiver processor directs whatever margin is available against whatever is degrading communications at the time. For example, this approach permits whatever link margin would be used to counter scintillation to be used effectively against RFI if there is no scintillation and vice versa. Coded modulation signal structures can be implemented with any size signal alphabet; however, since binary is least complicated and illustrates the basic principles it will be used exclusively in this report.

In a binary coded modulation system, every k message bits produce n (n>k) binary chips which are transmitted in some convenient format, such as PSK, DPSK, FSK or MFSK. The receiver compares the relative likelihood of each alternative estimated on the basis of several received chips to make the final decision on a specific message bit. The likelihood estimates are calculated as sums of numbers which approximate the incremental contributions to the total likelihood estimates provided by each received chip. Figure 4-1 sketches the optimum receiver processing structure for coded modulation with statistically independent fading in each received chip. The receiver matched filter outputs are multiplied by a weighting factor proportional to the instantaneous voltage transmission factor (square root of power transmission) of the channel. The weighted matched filter outputs then pass through a generally non-linear shaping factor f( ), dependent on the chip modulation format, to a receiver storage buffer. The demodulator decoder then selects and adds together various weighted filter outputs stored in the buffer to compare the various possible hypotheses for a given message bit. If the receiver has any information indicating that some of the received chips may be very unreliable because of RFI, setting the weighting factor to zero incorporates that information into the processing. If the fading

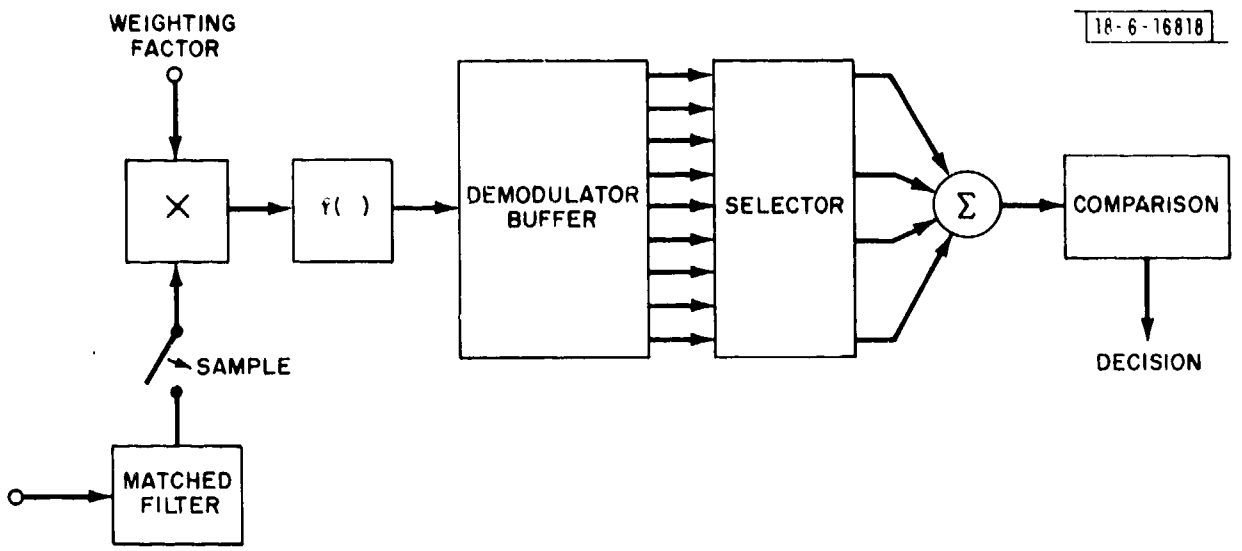

Fig. 4-1. Block diagram of the optimum receiver for a fading channel with statistically independent fades from chip-to-chip.

signal level is not known (measured) at the receiver, all the weights must be identical but the form of f( ) changes.

In a practical implementation, the whole receiver processing would usually be done digitally. This digital calculation implies quantizing the matched filter outputs, the weighting factors and the shaping function f( ). The number of quantization levels must be selected in a design compromise between accuracy and better performance on one hand and simplicity and lower hardware cost on the other. At one extreme, each received chip would be hard quantized; that is, the likelihood calculations would be performed with a single bit indication of whether each received chip indicated that a binary zero or one was most likely transmitted. Increasing the number of quantization levels allows the receiver to include some information on the certainty of the one/zero decision. The simplest weighting is a simple acceptance/rejection test, like that in Section III, in which arithmetic zero and one are the only admissible weights.

B. Error Performance Estimates

The error rate performance of a coded modulation system with full analog resolution in the demodulator decoder is the best performance attainable and provides a reference for determining the effects of different quantization strategies. For a few special cases, the performance of this unquantized receiver can be calculated easily; however, the calculations often become quite tedious and are circumvented by a digital computer simulation of the channel and decoder. The analytic calculations can be done for a coherent PSK channel with statistically independent known (level) Rayleigh fading on each chip. This model would represent the conditions observed during the commonly observed saturated scintillation if: 1) the chips used in a given decoder decision are sufficiently separated by interleaving to produce essentially independent fading, 2) the receiver knows the relative received power level, and 3) the receiver has maintained a phase reference. The first condition can be met if the interleavers are long enough; the question of how long will be discussed later. The second condition should be easily satisfied for the slow process of scintillation because the receiver will have many received bit times to average over and thus should be able to make a good estimate of received signal level.

In a real receiver, the received signal level might be estimated from the AGC circuit with some averaging. The third condition of the receiver having a phase reference might be met either by a very stable local oscillator if the scintillation process causes no phase shifts or by a receiver with a phase lock loop which is sufficiently fast to recover lock quickly after dropping out during a deep fade. Whether these three conditions can all be met simultaneously during real UHF scintillation can only be resolved by experiment; however, the performance of a PSK modulation system under these circumstances would be an indication of the best performance available during scintillation even if all the questionable items were resolved in a manner favoring good communications. At the other extreme, a model of statistically independent unknown Rayleigh fading from chip to chip on an incoherent channel implies neither a fade depth measurement nor a phase reference and represents the conditions during saturated scintillation if the questionable matters are all resolved in a manner not conducive to good communications. Fortunately, the analytic equations for this case are also tractible. Thus, there are convenient analytic expressions for the performance of coded modulation systems during scintillation under the two extremes of having good phase and signal level estimates and of having neither.

The probability of error $P_2(E,d)$ in determining which of two possible chip sequences differing in d chips was actually transmitted forms the basis for the union bound estimate of performance for a coded modulation system. The appendix shows that with PSK modulation and statistically independent known (at the receiver) Rayleigh fading from chip to chip,

$$P_2(E,d) = \frac{1}{2^d} \sum_{i=0}^{d-1} \binom{d+i-1}{i} \frac{1}{2^i (E_s/N_o + 1)^i} \left[1 - \frac{\sqrt{E_s/N_o}}{\sqrt{E_s/N_o + 1}} \right]^{d-i} \qquad (4\text{-}1)$$

where E_s is the signal chip energy, $N_o/2$ is the noise spectral density and the large parenthesis indicate binomial coefficients. The appendix also shows that an upper bound for the right-hand side of Eq. (4-1) is

$$P_2(E,d) \leq \frac{1}{2} \sqrt{\frac{E_s/N_o + 1}{E_s/N_o}} \frac{1}{\sqrt{\pi(d-1)}} \frac{1}{(E_s/N_o + 1)^d} \qquad (4\text{-}2)$$

For DPSK modulation with incoherent detection and statistically independent unknown Rayleigh fading from chip to chip weighting at the receiver cannot be done and the shaping function $f(x) = x^2$ and[4-1]

$$P_2(E,d) = \frac{1}{2d(E_s/N_o + 1)^d} \sum_{i=o}^{d-1} \binom{d+i-1}{i} \left[1 - \frac{1}{2(E_s/N_o + 1)}\right]^i \qquad (4\text{-}3)$$

with an upper bound of

$$P_s(E,d) \leq \frac{1}{2} \left(\frac{E_s/N_o + 1}{E_s/N_o}\right) \frac{1}{\sqrt{\pi(d-1)}} \left[\frac{1 + 2E_s/N_o}{(1 + E_s/N_o)^2}\right]^d \qquad (4\text{-}4)$$

The chips for transmission are generated from the input message bits by encoding those bits in some error control code to produce the signal sequence. Figures 4-2 and 4-3 show the upper bound on the bit error probability P(E) obtained by using the expressions in Eqs. (4-2) and (4-4) in the union bounds[4-1] for the (8,4) Hamming and the (24,12) Golay block codes and for some systematic and non-systematic convolutional codes of encoder memory length K=5 and 7 with Viterbi decoding. For the convolutional codes with Viterbi decoding, the union bound upper bounds on P(E) were calculated using the combinatorial generating function approach of Viterbi.[4-2] The P(E) curves are plotted as a function of E_b/N_o the bit energy to noise ratio. These codes are typical of the codes used in coded modulation systems which allow weighting or more than one-bit chip quantization of the matched filter outputs. For both coherent PSK with known fading and incoherent DPSK with unknown fading, the convolutional codes with Viterbi decoding generally offer better error-rate performance than the block codes. Since the design and implementation of K=5 and K=7 Viterbi decoders is well within the state-of-the-art, this report will only give further consideration to convolutional codes with Viterbi decoding.

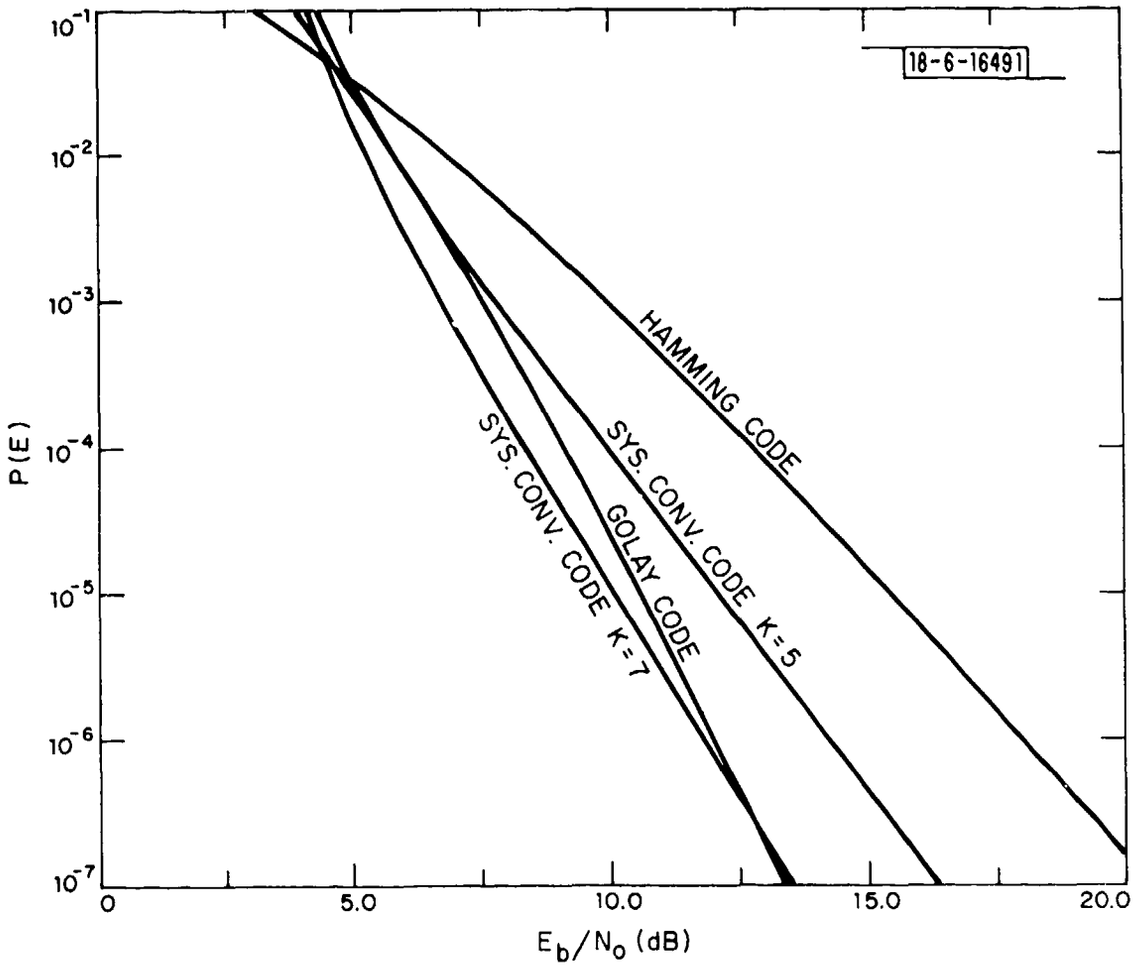

Fig. 4-2. Bit error probability upper bounds for the Hamming and Golay block codes and systematic convolutional codes with optimum receiver and statistically independent Rayleigh fading from chip-to-chip with PSK chip modulation.

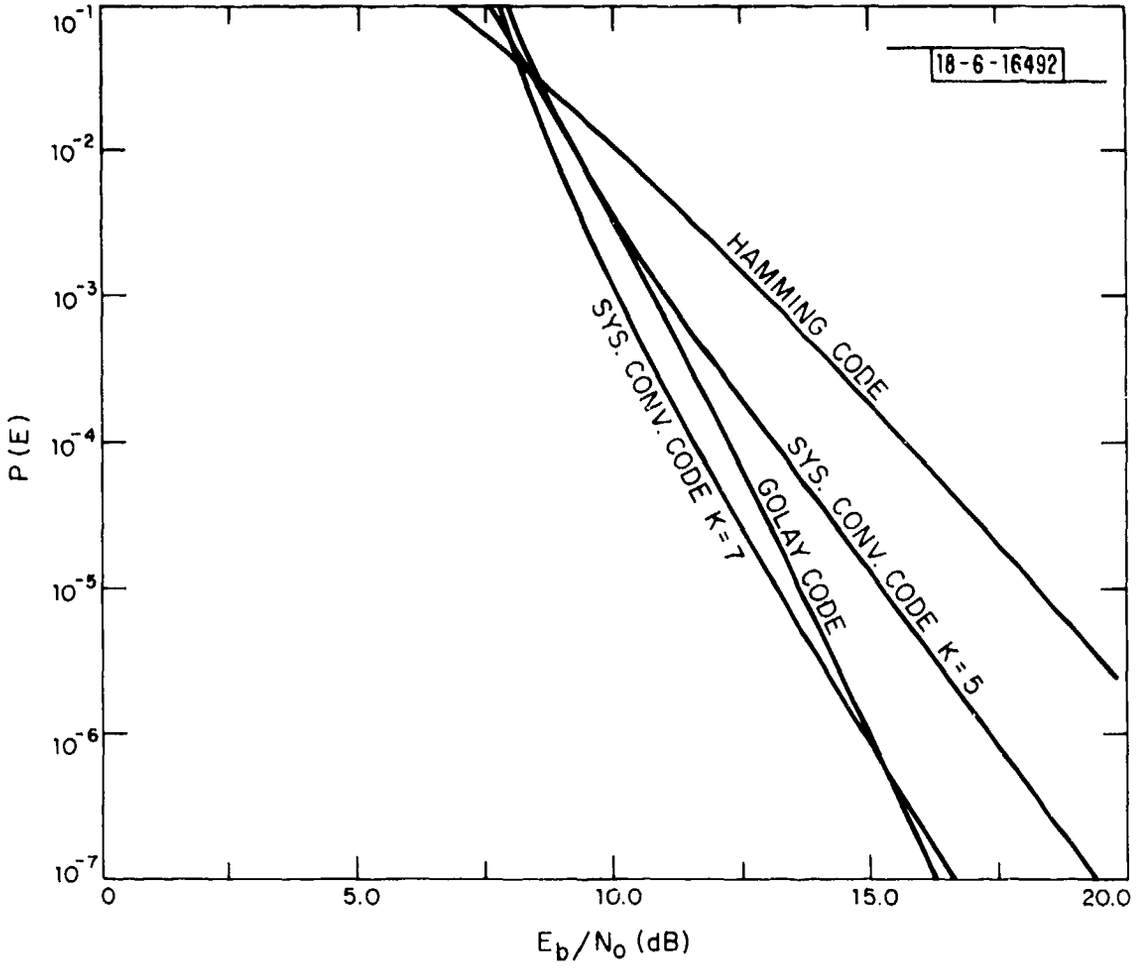

Fig. 4-3. Code performance comparison with DPSK chip modulation.

C. Convolutional Codes and Viterbi Decoding

Although convolutional codes and the Viterbi decoding algorithm are detailed in the literature,[4-2] a brief description of the codes and the decoder is necessary before discussing some of the issues arising when implementing Viterbi decoding of convolutional codes in actual hardware. Figure 4-4 sketches a convolutional encoder. A K-stage encoder memory shift register receives the message bits to be encoded. At the end of each encoder cycle, n binary chips are generated by taking the modulo 2 sum (finding the parity) of n different combinations of the K message bits in the encoder shift register. In a rate 1/n convolutional code which produces n chips to be transmitted for every message bit encoded, the encoder shift register is shifted once bringing in one new message bit at the start of each encoder cycle. During the shift, the oldest message bit in the encoder shift register drops off the end and no longer influences the encoder output. To transmit more information at a fixed channel transmission rate, the encoder shift register memory may be shifted k times ($k < n$) per encoder cycle to produce a rate k/n convolutional code. In each encoder cycle, k new information bits enter the encoder and n binary chips are produced for transmission. Since the encoder shift register is K bits long, any specific information bit is in the decoder for K/k cycles and the "oldest" k bits in the encoder are dropped during the start of the next cycle.

Viterbi decoding proceeds in cycles analogous to those of the encoder and decodes k bits per decoder cycle. During each cycle, the decoder determines the most likely sequence of past information bits, or "path history", for every possible combination of the K-k information bits in the encoder which will be carried over to the next cycle. The calculations to select the most likely path history use the information in the n received chips and can be performed iteratively with a fixed number of operations per cycle. There are 2^{K-k} possible hypotheses for the information bits carried over in the encoder and thus 2^{K-k} possible path histories to maintain. In can be shown[4-2] that all these path histories must eventually merge together as the decoder progresses along. In practice[4-2] the path histories have merged to a sufficient extent after 3K/k or 4K/k decoder cycles to permit a final decoding decision to be

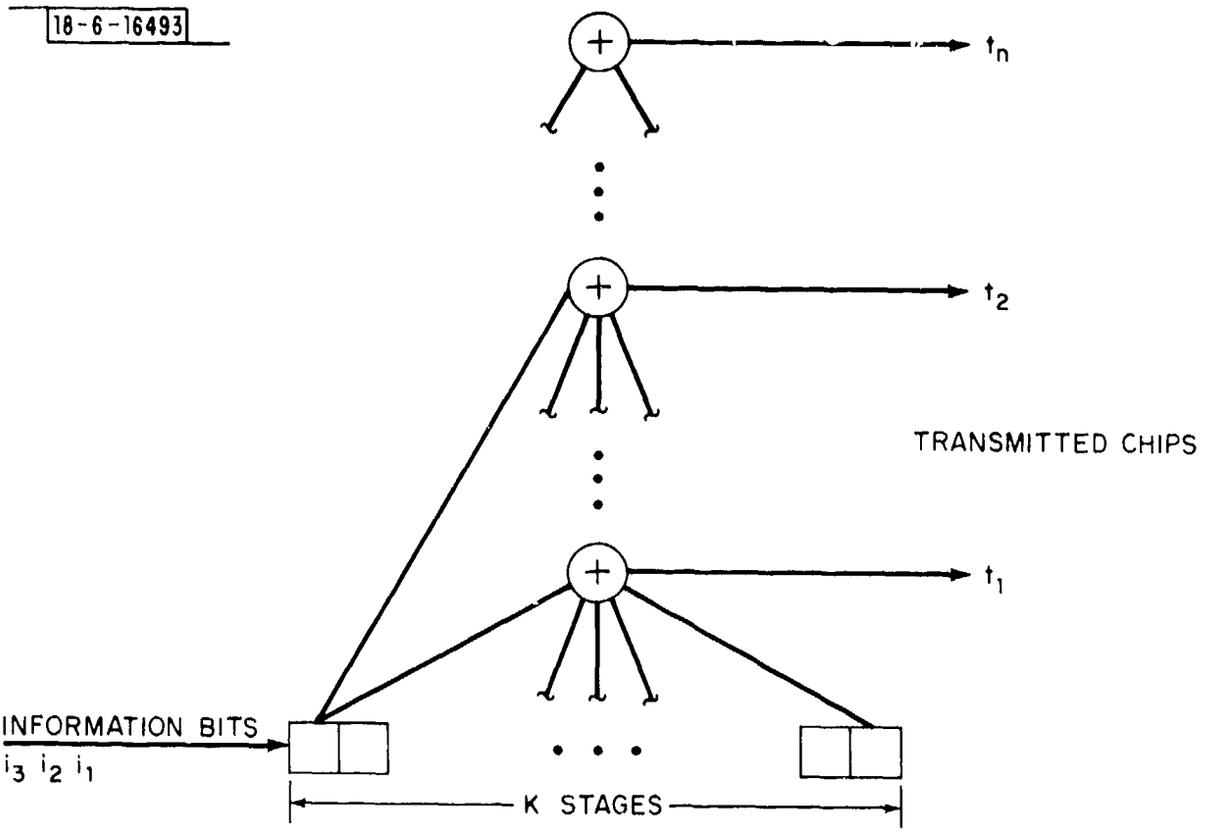

Fig. 4-4. Block diagram of a convolutional encoder.

made. The path history memories have a finite length L. The k information bits decoded for the user during each decoder cycle are selected as the oldest bits in the path memory associated with the K-k bit hypothesis presently having the highest likelihood rating. This decision on the most likely path history can be made from calculations done as part of the path history selection procedure. The simulations reported here all made the final decision by selecting the most likely path after a path memory (exclusive of the K-k bits in the decoder hypothesis) of 4(K-1) bits. Since there are 2^{K-k} possible hypotheses tested per decoder cycle, each of which requires a path memory and each of which requires 2^k-fold comparison, both the memory requirements and the decoder calculation increase as 2^K. Thus implementation of a Viterbi decoder becomes much more difficult and expensive as K increases. The present state-of-the-art in Viterbi decoder implementation[4-4] is such that K's in the range of 7 to 9 are reasonable but near the limits of practicality.

The n sets of information symbols used in calculating the n parities which are transmitted determine the code and hence the error probability obtained when using that code on a given channel. In "systematic" convolutional codes, each information bit entering the encoder is sent unaltered as one of the n chips transmitted per encoder cycle; thus, a systematic rate k/n convolutional code transmits k information symbols and n-k parity combinations per encoder cycle. In a "non-systematic" convolutional code, every one of the n transmitted chips is generated by a parity combination. Intuitively, the best systematic convolutional code of a fixed rate and encoder register length should be less powerful than the best non-systematic convolutional code of the same rate and encoder register length because a specific message bit can affect few transmitted chips with a systematic convolutional code than with a non-systematic convolutional code. The degradation in performance in changing from a non-systematic convolutional code to a systematic convolutional code is significant and has been analyzed.[4-3] On the other hand, a receiver without a decoder is still able to read the original message only with a systematic code. If only some of the broadcast receivers are effected by the degradation which

necessitated the use of coded modulation, the ability to accommodate uneffected receivers without decoders in the same broadcast by using a systematic code may make the decreased performance of the systematic convolutional code acceptable. Figures 4-5, 4-6, and 4-7 show the error probability upper bounds for both systematic and non-systematic convolutional codes of rate 1/2, 2/3 and 3/4 with PSK modulation and known statistically independent Rayleigh fading from chip to chip with K=7, 8 and 9, respectively. The range of K's used in the figures was chosen because the Viterbi decoders for the three rates all require the same encoder memory and can be implemented in a common structure. For example, if an E_b/N_o of 15 dB is available on the channel and a 10^{-4} error rate is required, the rate 3/4 systematic code is unusable while the non-systematic code meets with requirement 1.5 dB of margin. For rate 2/3 codes, the systematic code will function with only 0.4 dB margin while the non-systematic code will function with 3.2 dB margin. For this example, one can choose between two and three scintillation protected information streams. In the two-stream case, unmodified receivers without decoders will be able to read the message whenever they see no scintillation. However, in the three-stream case, unmodified receivers will not be able to read the message even when there is no scintillation.

D. Decoder Implementation and Design

Some compromises from the optimum processing must be made in implementing the actual decoder/demodulator. At the very least, the analog matched filter output must be digitized before being stored in the decoder buffer. Often the whole weighting and shaping function f( ) will be implemented digitally. Precision is lost in these quantizations and the error probability performance decreases as fewer and fewer quantization levels or bits of resolution are used. Further compromises from the optimum processing may also be made in a deliberate attempt to further simplify the processing to reduce cost and complexity. For example, at high data rates, the memory required for the interleavers is quite large and could be substantially reduced by making only a "hard" decision of whether 1 or 0 was most likely transmitted given the received chip while keeping

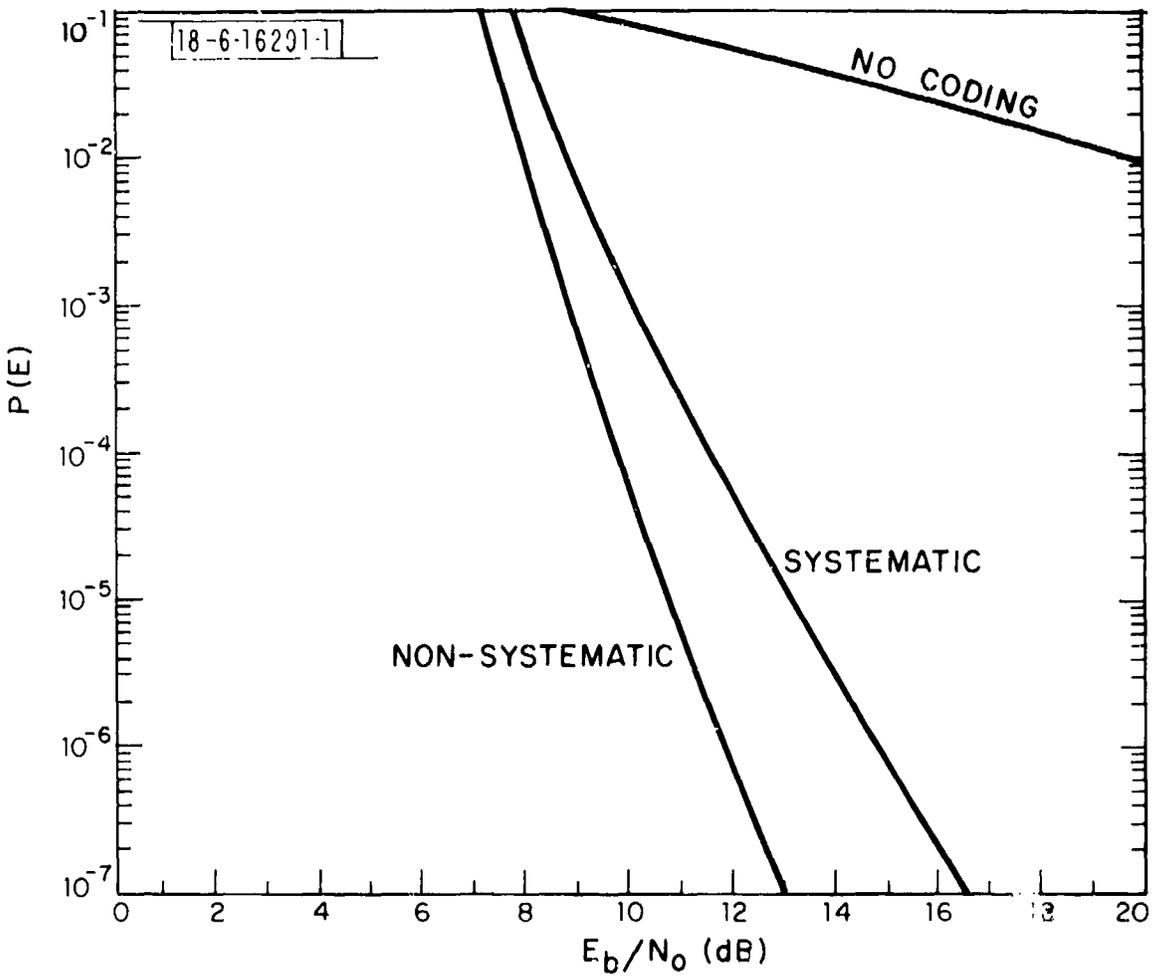

Fig. 4-5. Bit error probability upper bounds for rate 1/2 K=7 systematic and non-systematic convolutional codes with Viterbi decoding and PSK chip modulation with statistically independent Rayleigh fading from chip-to-chip.

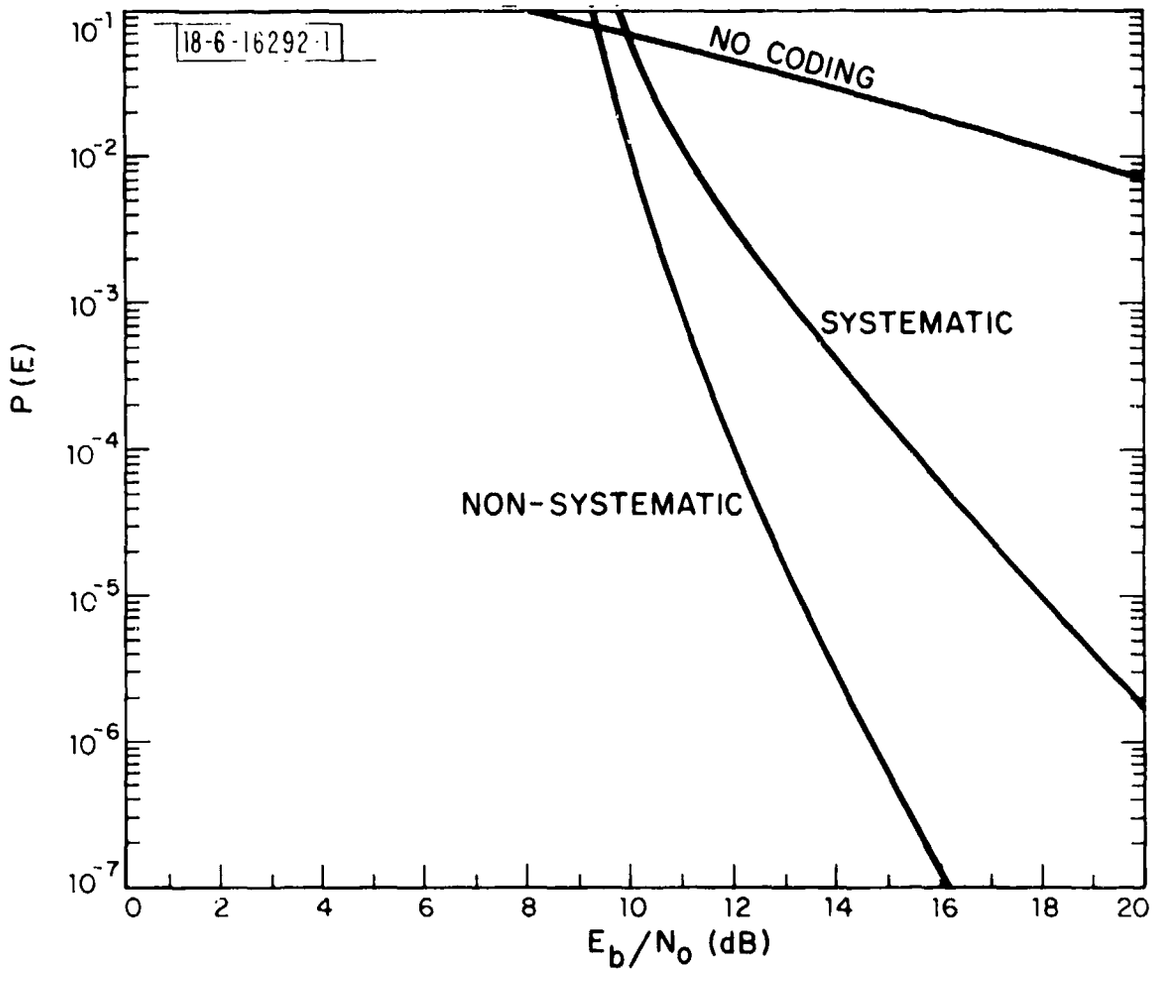

Fig. 4-6. Bit error probability upper bounds for rate 2/3 K=8 systematic and non-systematic convolutional codes with Viterbi decoding and PSK chip modulation with statistically independent Rayleigh fading from chip-to-chip.

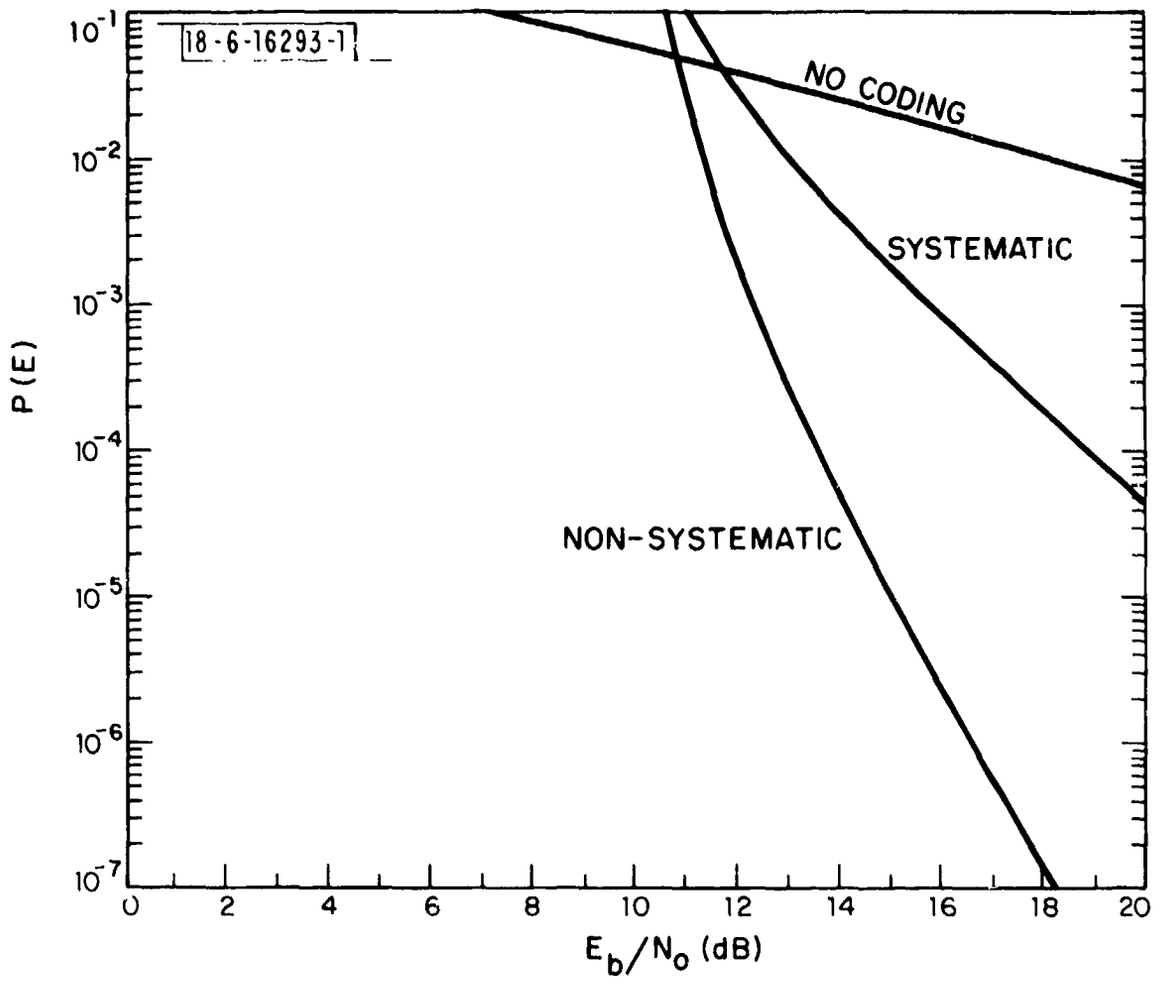

Fig. 4-7. Bit error probability upper bounds for rate 3/4 K=9 systematic and non-systematic convolutional codes with Viterbi decoding and PSK chip modulation with statistically independent Rayleigh fading from chip-to-chip.

more resolution in the weighting which varies much more slowly during scintillation than the bit rate. Also, with DPSK modulation, the shaping functions f( ) are logarithms of hyperbolic cosines and I_o Bessel functions for coherent and incoherent detection, respectively. Some simplifications can be made by replacing these rather complicated functions by either linear or square law approximations. Another possible simplification would be to eliminate the weighting operation, i.e., not estimate the fluctuations in the received power level, and attempt to decode with just matched filter outputs and shaping. For DPSK modulation with incoherent detection and unknown Rayleigh fading, the optimum receiver uses a square law shaping function f( ) (and no weighting). The performance degradation imposed by any combination of quantization techniques and receiver simplifications is best determined by computer simulation except for a very few special cases. Figure 4-8 compares the analytically calculable error probability upper bounds of the optimum receiver for PSK modulation with known statistically independent Rayleigh fading from chip-to-chip and of a receiver which hard quantizes the received chips and does not estimate the received signal level. The substantially worse performance in the second case shows the degrading effects of the receiver's losing all information about the location of deep fades in the received signal.

The computation required to estimate by simulation the performance of a convolutional code with Viterbi decoding and a specific modulation and receiver quantization grows as 2^K where K is the encoder memory length.. This exponential growth of computation with increasing constraint length forces a compromise between economy of simulation and code constraint length particularly when several independent parameters must be varied. The author's approach was to perform most of the simulations to evaluate various weighting and quantization strategies at K=5 and then use these results to extrapolate to longer K's with consistency check at K=7.

Figure 4-9 compares the upper-bound calculated for the case of coherent PSK modulation with independent known Rayleigh fading from chip to chip and optimum receiver processing with the simulated performance and shows very close agreement (to within 0.2 dB) for error probabilities below .003. Figure 4-10 shows the simulated error probability for the optimum receiver processing

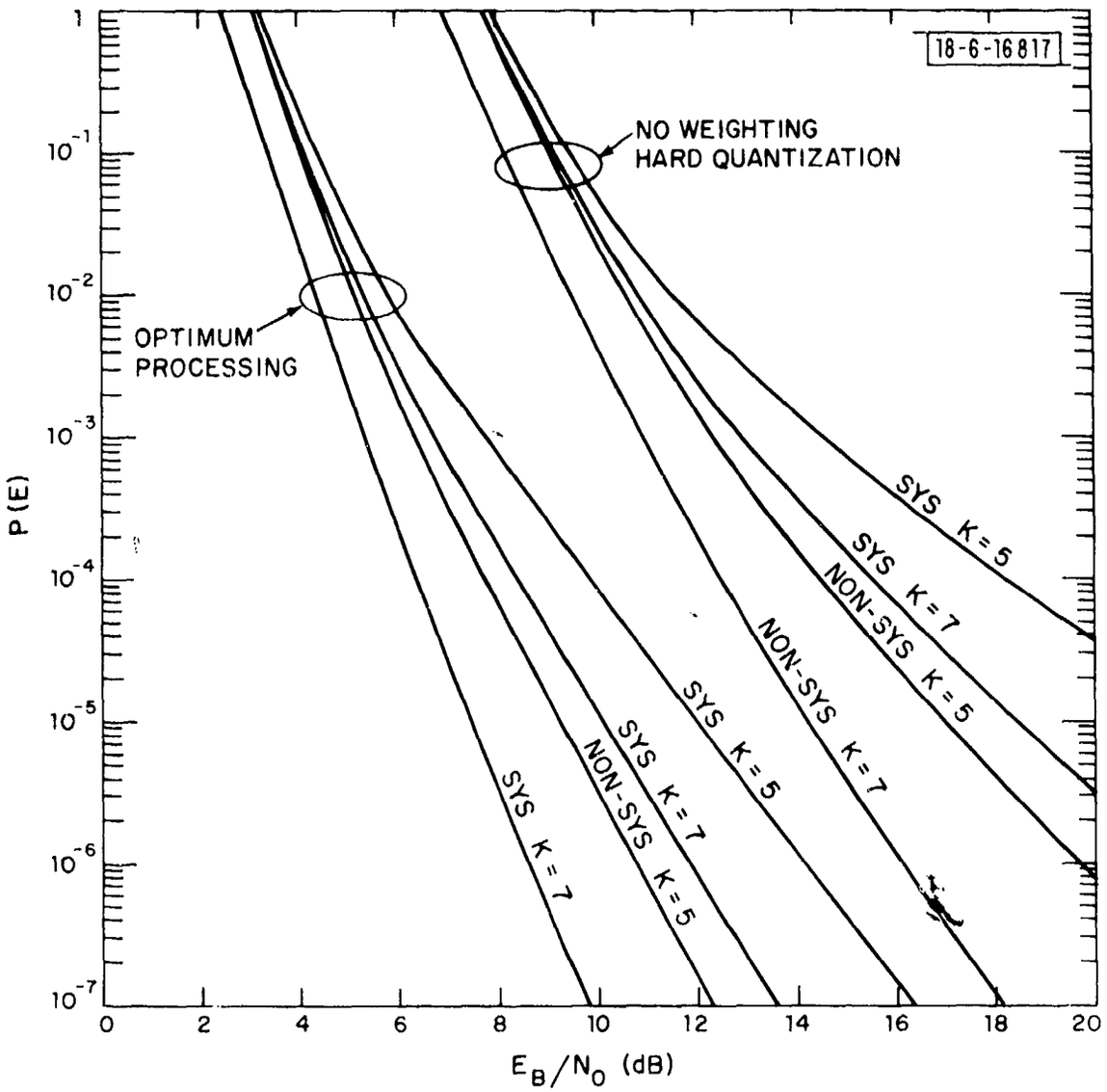

Fig. 4-8. Comparison of decoder performance with optimum processing and processing with neither weighting nor chip voltage levels for selected convolutional codes with Viterbi decoding and PSK modulation with statistically independent Rayleigh fading from chip-to-chip.

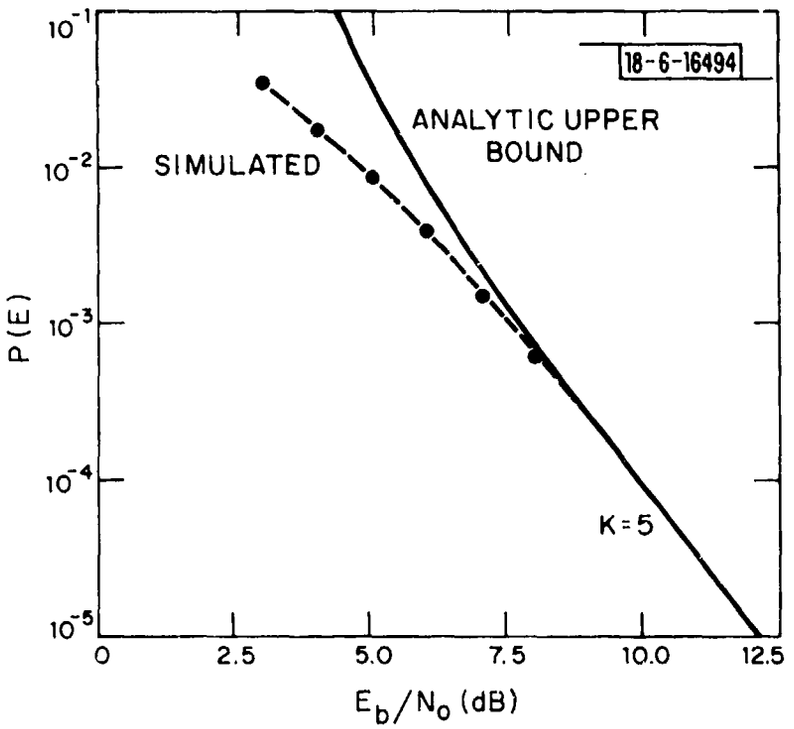

Fig. 4-9. Comparison of simulated and analytic upper bound bit error probability for K=5 systematic convolutional code with Viterbi decoding and PSK chip modulation with statistically independent Rayleigh fading from chip-to-chip.

compared with the error probability when the received chips were unquantized but no weights (no channel information other than chip signal levels) were used and when the chips were hard-quantized (0/1 decision) and unquantized weights were used. From Fig. 4-10 we may estimate that deletion of the weighting in the optimum receiver decreases performance by 1 dB in E_b/N_o while using the weighting with hard quantized received chips decreases performance 2 dB from that obtained with the optimum receiver. These two alternatives are ways of reducing receiver/decoder complexity by either deleting the channel estimator which produces the weights or by reducing the amount of storage required to store the received chips in the interleaver prior to decoding. For comparison, the simulated performance of a decoder using unweighted and hard-quantized chips is also shown in Fig. 4-10. The unweighted hard-quantized case is worse in two respects than any of the other cases in that both 1) the knee of the curve or the threshold is higher and, 2) the probability of error decreases less rapidly with increasing E_b/N_o than the other cases. Intuitively, the cause of this markedly worse performance for unweighted hard-quantized chips is that all information about when the channel was faded is lost while either weighting of hard quantized chips or combining unquantized chip signals still provides the decoder some means of discounting signals received during fades.

One method of assessing the effects of quantization in either received chip signals or receiver weights is to consider the effects of quantizing one of these two parameters when the fade depth information provided by the other is not present. With this approach, the effects of quantization in the weights would be measured with hard quantization of the received chips and the effects of various chip quantization strategies would be measured without receiver weighting. Figure 4-11 shows the simulated bit error probability for the K=5 systematic convolutional code with hard chip quantization and the decoder weights quantized to 8, 4 and 2 levels. The weight which is the normalized voltage gain $\sqrt{P_r(t)/\langle P_r \rangle}$ was linearly quantized with increments selected for best performance. The bit error probability as a function of quantization increment has a rather broad flat minimum; thus, selection of the precisely optimum quantization increment by simulation is very difficult because the differences are almost indistinguishable. This relative

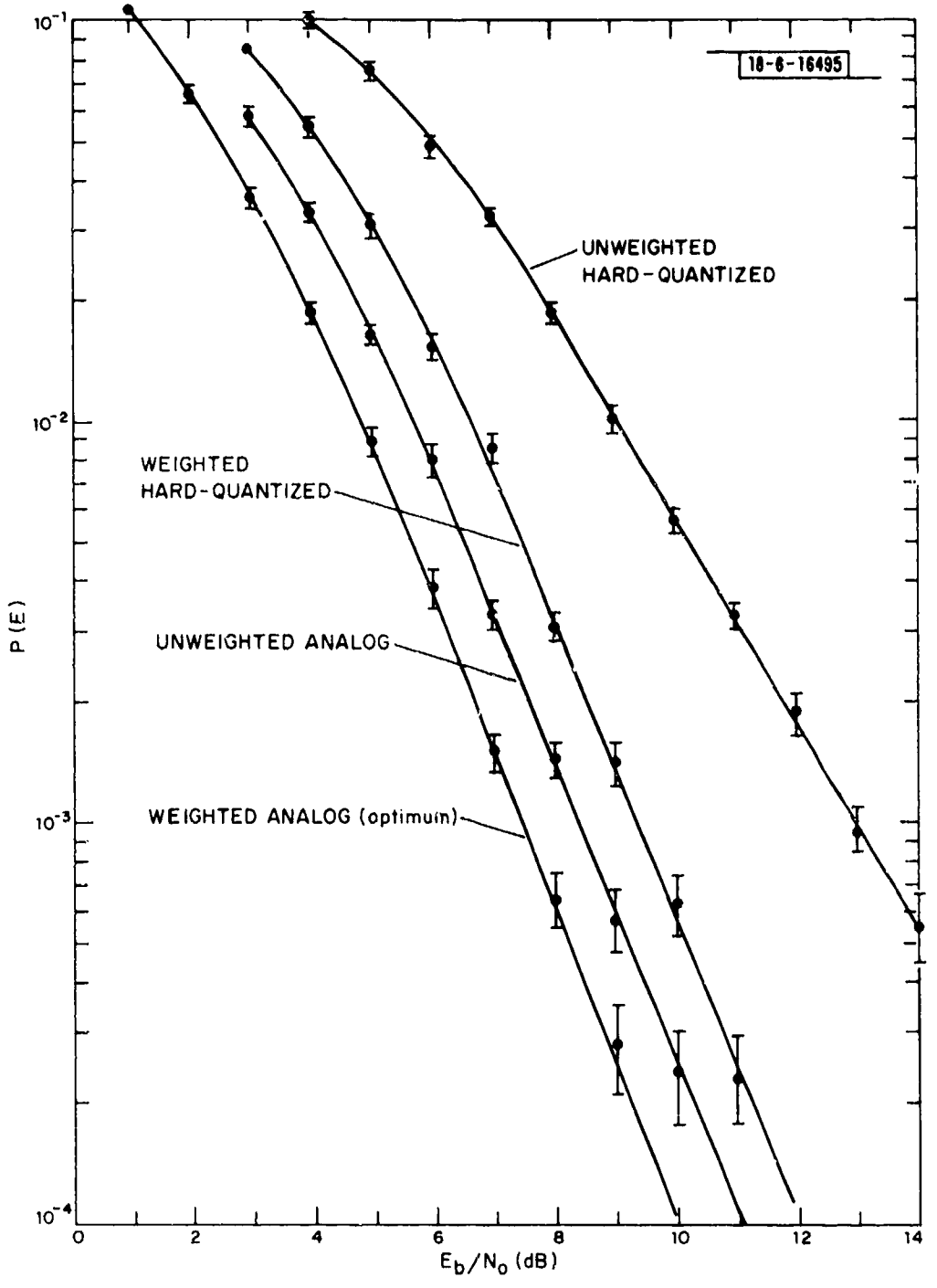

Fig. 4-10. Comparison of various sub-optimum receiver strategies for K=5 systematic convolutional code with Viterbi decoding with PSK chip modulation and statistically independent Rayleigh fading from chip-to-chip.

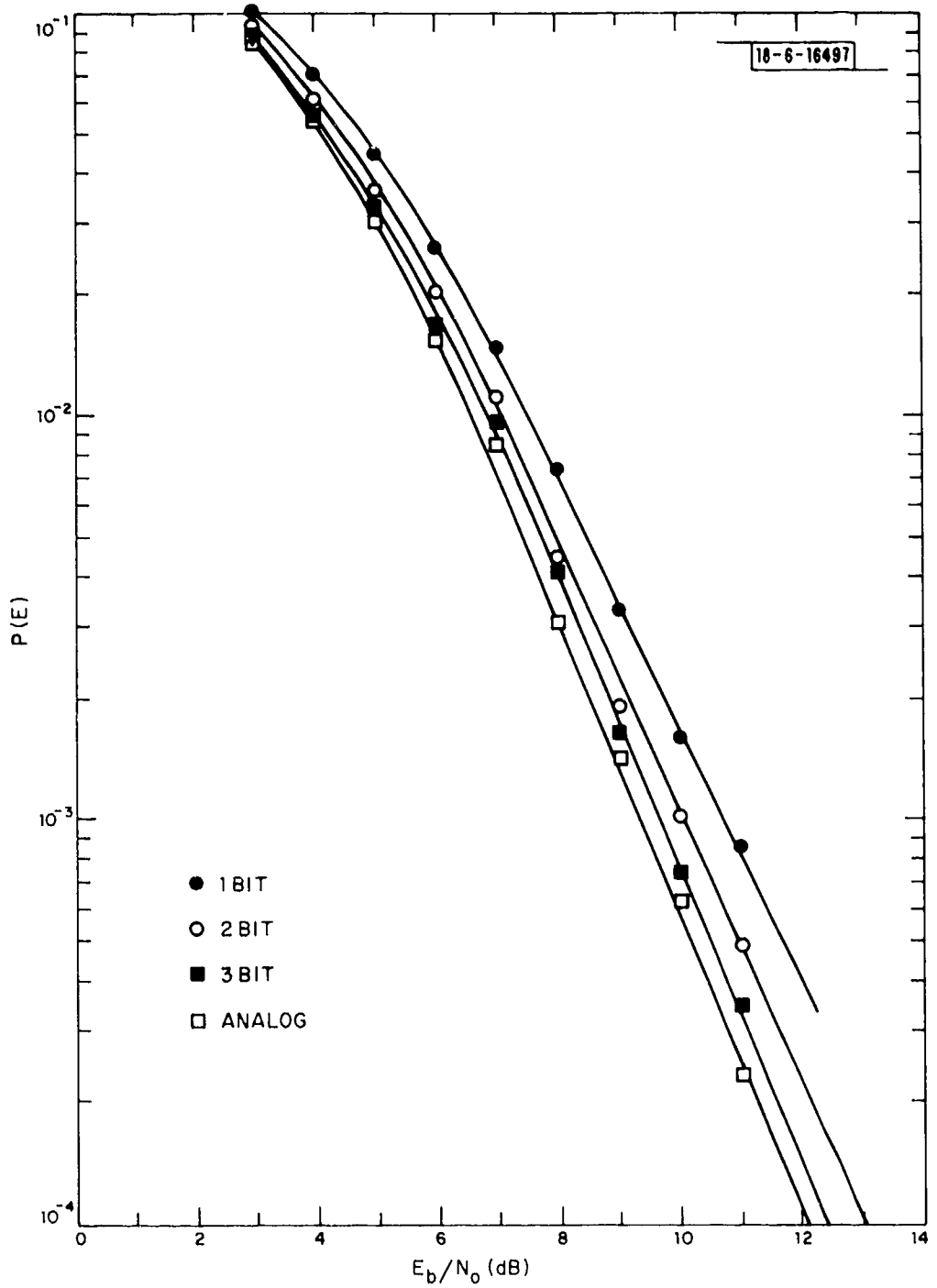

Fig. 4-11. Comparison of decoder performance with various weighting factor quantization strategies.

insensitivity to quantization increment is convenient in the practical sense of simplifying hardware design. The values of 0.175, 0.35 and .7 were chosen as the quantization increments for the 8, 4 and 2 level quantizations of the normalized weights ($\sqrt{P_r(t)/\langle P_r \rangle}$), respectively, and are all well within the minimal ranges. Figure 4-12 shows the performance of the same code except that no receiver weighting was used and the received PSK chips were quantized to 8 and 4 levels (-v to v). Here again there is no sharp minimum in error probability as a function of quantizer increment and the increments of 0.6 and 1.2 times the standard deviation of the gaussian noise in the matched filter output were selected as being part of the minimal range. Figure 4-11 shows that 3 bit (8 level) weighting factor quantization degrades performance approximately 0.3 dB from that possible with full analog precision weighting while 2 bit quantization degrades performance 0.7 dB and 1 bit quantization (accept/reject) degrades performance approximately 1.5 dB at 10^{-3} bit error rate. Figure 4-12 shows that 3 bit chip voltage quantization degrades performance approximately 0.4 dB while 2 bit chip voltage quantization degrades performance approximately 1.0 dB at 10^{-3} error rate. In Figs. 4-11 and 4-12 only weighting or soft quantized chip voltages were considered but not both. Figure 4-13 compares the combined effects of 3-bit chip voltage quantization and 2-bit weighting factor quantization with the optimum performance receiver which uses unquantized weights and chip voltages. The net effect of these two quantizations is to degrade performance by approximately 0.3 dB from optimum at 10^{-3} error rate. If the weight chip-voltage product calculated from these quantized terms is then quantized to 3-bits itself, the degradation increases to a total degradation of approximately 0.7 dB from optimum at 10^{-3} error rate.

For PSK format chip signals, the receiver must have a coherent phase reference and the shaping function f( ) is a simple linear transfer f(x)=x. For chips transmitted in DPSK format, the receiver may use either coherent detection with a phase reference or incoherent detection if a phase reference is unavailable. For coherent and incoherent detection of DPSK chips, the shaping function f( ) is the logarithm of a hyperbolic cosine and of an I_o Bessel function, respectively. Both of these functions are approximately linear for large arguments and approximately square-law for small arguments.

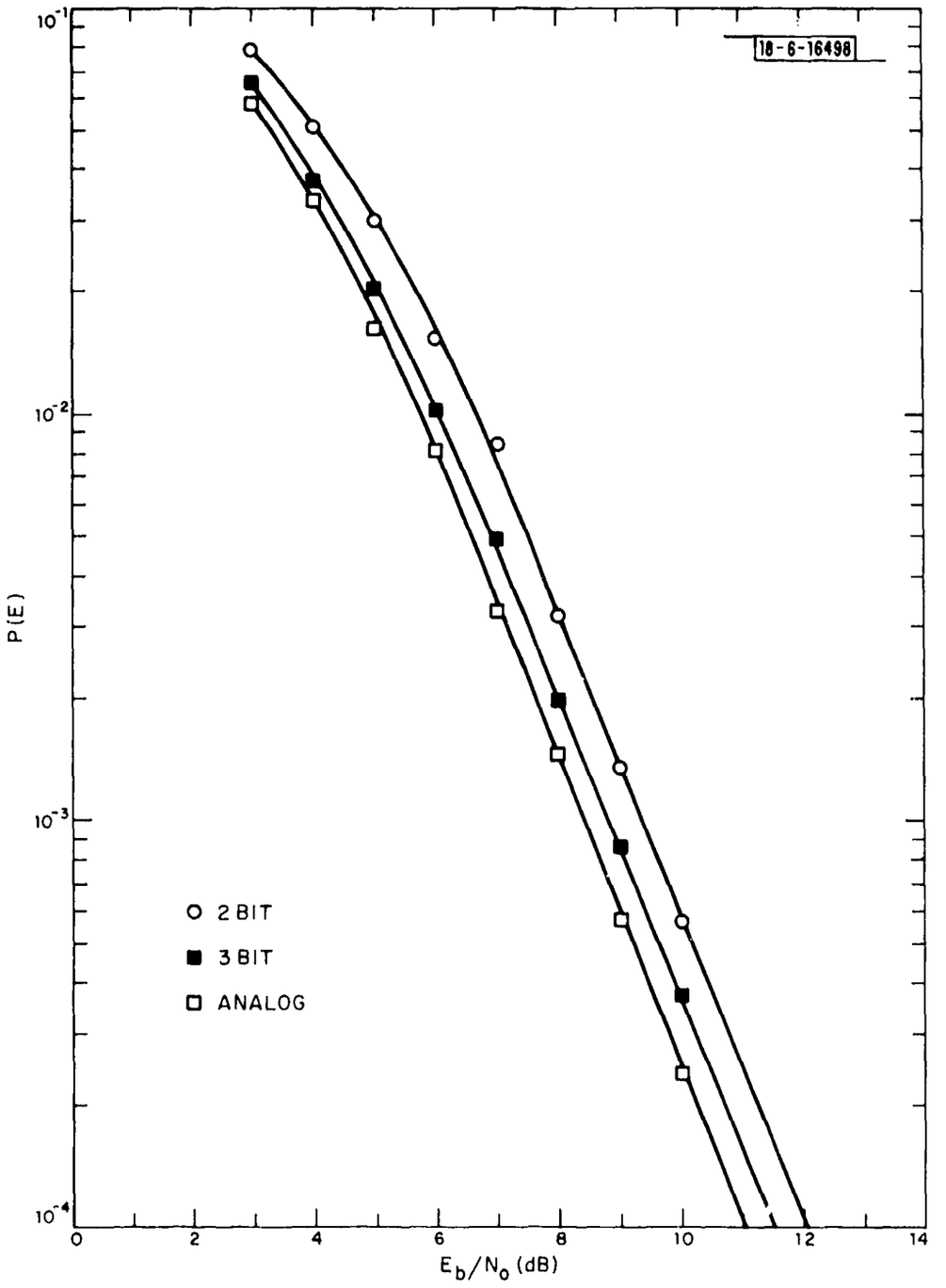

Fig. 4-12. Comparison of decoder performance with various chip-voltage quantization strategies.

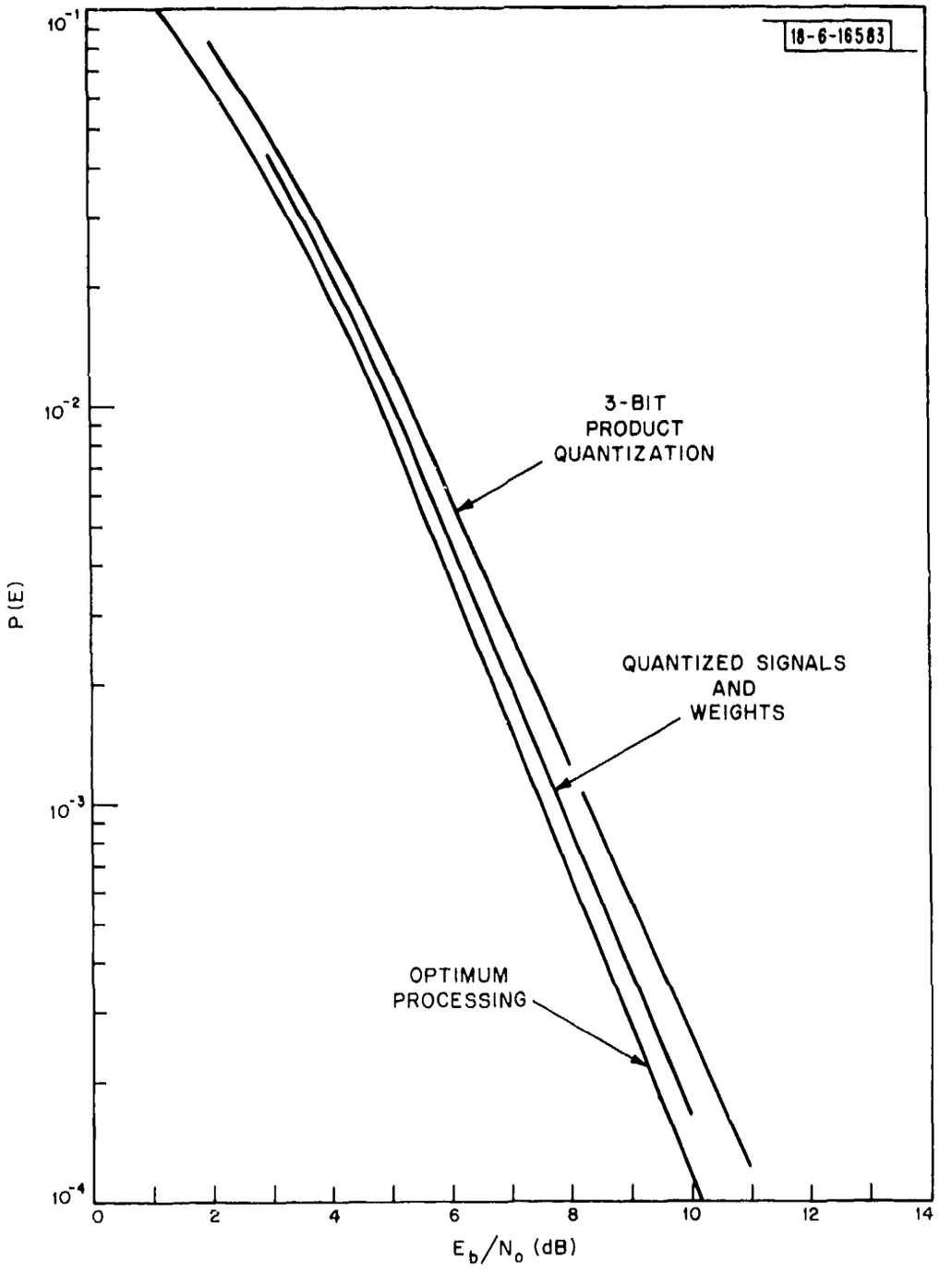

Fig. 4-13. Effects of quantization of the weighting-factor matched-filter output product.

Use of either a linear or square-law shaping function for DPSK format chips simplifies receiver implementation. For DPSK chips with coherent detection, a linear f(x)=x function performs slightly better than square-law shaping with the reverse true for DPSK chips with incoherent detection. Figure 4-14 compares the simulated performance of PSK, coherent DPSK and incoherent DPSK with receivers having full analog precision and using linear, linear and square-law shaping f( ) functions, respectively.

E. Interleavers

Interleaving may be used to arrange the receiver decoding in such a way that each decoder decision is based on a set of chips each of which was on the channel at widely separated times. For random slow fading, such as that induced by UHF scintillation, the fading affecting each chip in a specific decoder decision may be assumed independent if the separation produced by the linerleaver is long enough. Although bit error rate performance will not degrade if the interleaver separation is made wider, decoding delay and interleaver size and cost do increase with interleaver separation. Thus, the extent of the interleaving must be judiciously chosen in a compromise between error rate performance which increases with interleaver separation and cost which also increases with interleaver separation.

The effects of a shorter than ideal interleaving interval on a given digital decoding demodulation technique can be most easily determined by simulation of the channel, interleaver and decoder. Figure 4-15 shows the bit error probability as a function of E_b/N_o for the K=5 systematic convolutional code with Viterbi decoding when the successive chips used in a decoder decision are not statistically independent but have a correlation ρ. The correlation ρ is the power correlation function defined in Eq. (2-3). The normalized channel gains for the simulation were generated using a sampled data version of the filtered gaussian process technique described in Section II and sketched in Fig. 2-12 with the filter frequency and sampling interval chosen to provide the specified correlation between successively generated simulated normalized channel gains. Figure 4-15 shows little performance degradation for correlation values of up to approximately 0.5 with the degradation then increasing substantially as the successive chip fades become more correlated. Given the correlation

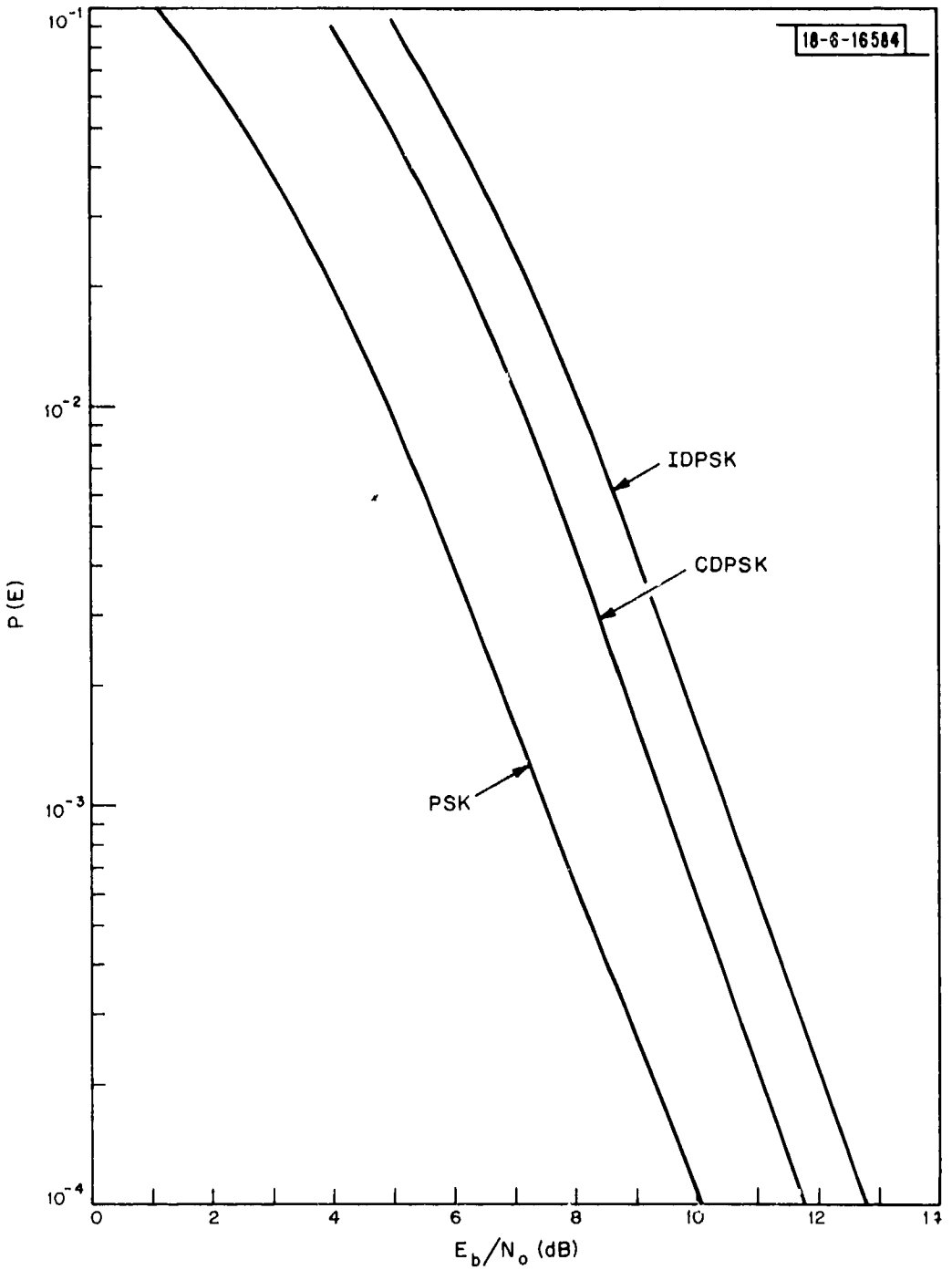

Fig. 4-14. Comparison of decoder performance with PSK, coherent DPSK and incoherent DPSK chip modulation for K=5 systematic convolutional code and Viterbi decoding with statistically independent Rayleigh fading from chip-to-chip.

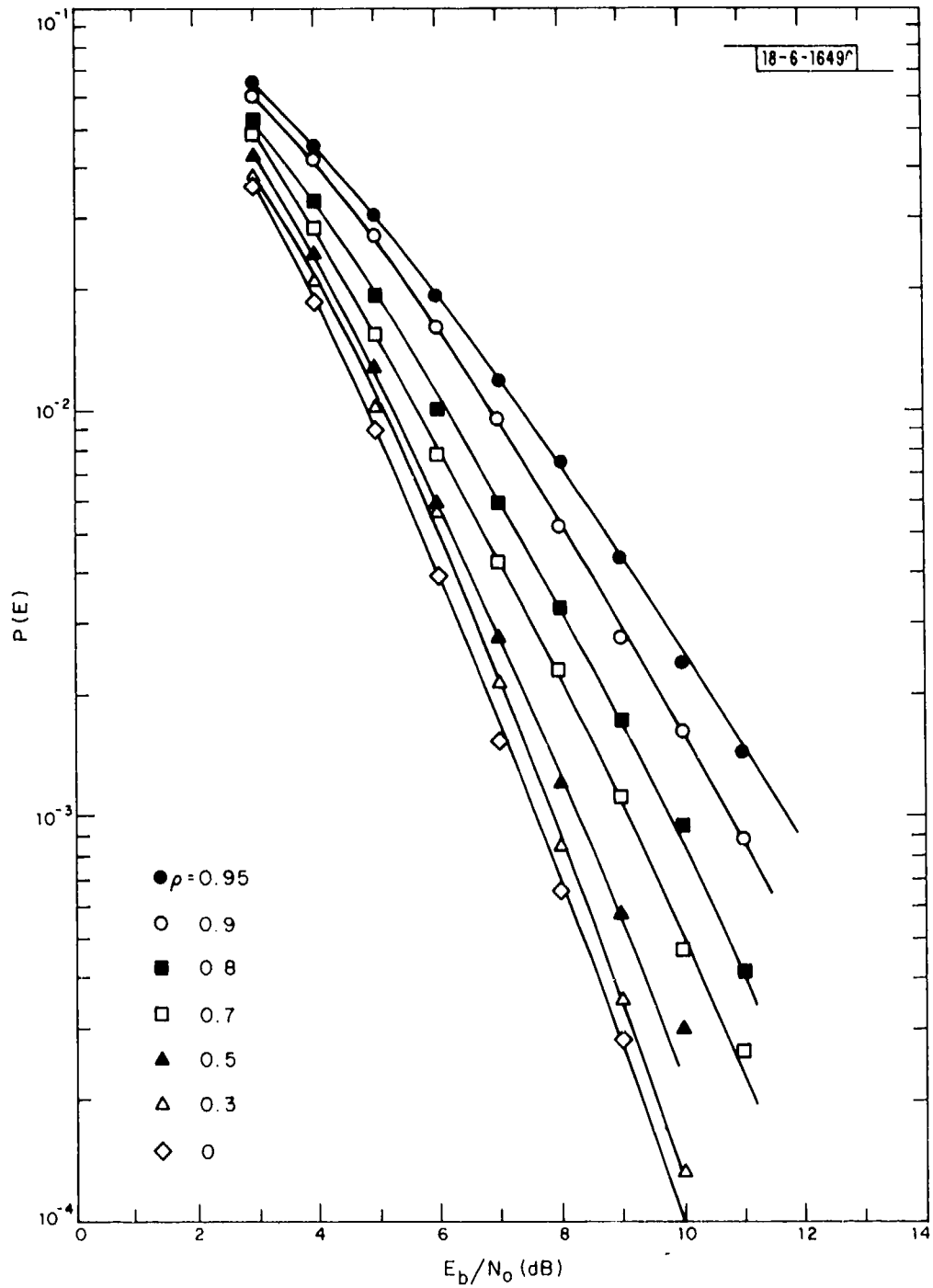

Fig. 4-15. Decoder performance for K=5 systematic convolutional code with Viterbi decoding of PSK chip signals with Rayleigh fading with correlation ρ between signal levels of consecutive chips used in decoder decisions.

function $\rho_s(\tau)$ for a given sample of the received power fluctuations of the fading channel, the value of ρ characterizing an interleaver spacing τ may be determined. Given this estimate of ρ, the error performance for that specific code and interleaver on that data segment can be estimated from Fig. 4-15 or its equivalent for the specific code of interest. This use of the correlation function of the data sample permits the estimation of the performance of a variety of interleaver spacings on a variety of fading samples with only one basic set of curves which are independent of the data samples .

There are many possible interleaver structures, one of the simplest is the convolutional interleaver proposed by Ramsey[4-5] which is also optimum in the sense of producing the largest separation in the interleaved output with a given delay. The implementation of a convolutional interleaver which uses a minimum of memory elements to achieve a specific interleaver is sketched in Fig. 4-16. A stack of s shift registers having various numbers of stages $\ell_1 \ldots \ell_s$ has commutators at both the input and output. Ramsey's design specifies that all the register lengths be a multiple of the basic separation plus some constant. The input and output commutators are always connected to the same register. When a data sample is received at the interleaver input, it is shifted into the shift register whose input stage is presently connected to the input commutator. When this register is shifted, the data sample in the output stage of the shift register is picked up by the output commutator and passed on as interleaved data. Before the next data sample is accepted, the commutators are moved to the next register in the stack. Only the register connected to the commutators is shifted when the data sample is accepted. When the commutators reach the bottom of the stack, they go to the top of the stack and work their way down again. The whole structure of the convolutional interleaver is specified by the number of stacks s and the lengths of the s shift registers $\ell_1 \ldots \ell_s$. The deinterleaver has the same basic structure as the interleaver except that the order of the register lengths is reversed. Synchronization of the interleaver and deinterleaver requires only synchronization of the two commutators.

The performance of convolutional interleavers and Viterbi decoding of convolutional codes in the presence of UHF scintillation was simulated

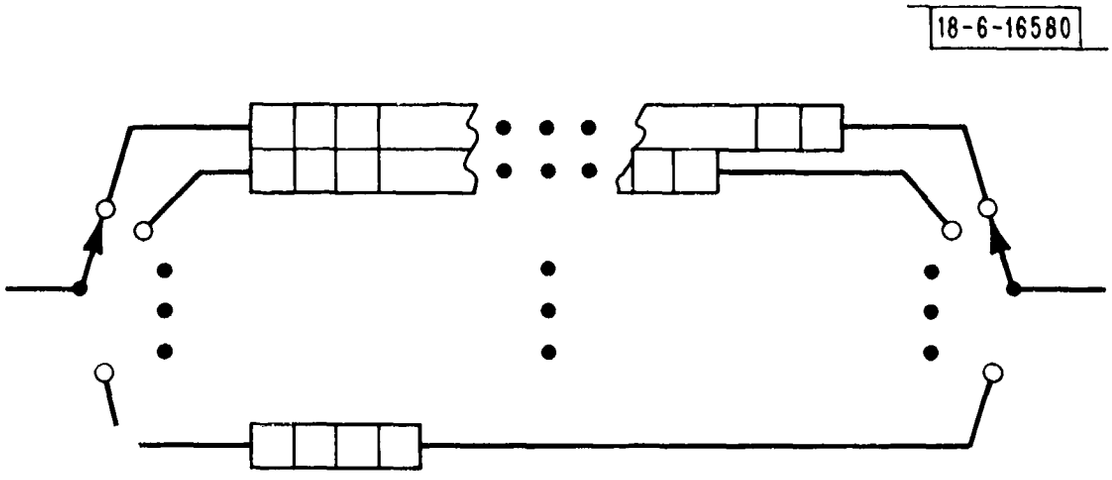

Fig. 4-16. Block diagram of a convolutional interleaver.

digitally. The scintillation induced fading was simulated using a digital version of the filtered gaussian process technique discussed in Section II. For the simulation, a chip rate of 150 chips/sec was assumed with a rate 1/2 systematic convolutional code with K=5. The net effective data rate of this modulation coding would be 75 bits/sec. The pole frequencies of the filter in the fading simulator were 0.06 Hz chosen to simulate some of the slowest intense scintillation fading observed during the 1972 experiments on Guam. With a 32 stack interleaver with register lengths 4, 8, 12,...,128 for the t_1-chips and register lengths 68, 72, 76,...,128, 4,8,...,64 for the t_2 chips, (see Fig. 4-4) the simulated bit error rates shown in Fig. 4-17 were observed. This set of interleaver lengths and stack heights resulted from a suggestion of a particularly simple implementation by David P. White. With this interleaver structure successive chips came out of the deinterleaver separated by 1.72 sec, for the fading simulator filter parameters chosen this separation produced a correlation coefficient $\rho \sim .69$ between consecutive interleaved chip fades. The simulated performance is compared with the $\rho = 0.7$ curve from Fig. 4-15; this close agreement of results indicates a method of estimating the effectiveness of various interleaver lengths in the face of various rates of UHF scintillation induced fading. The simulated performance with this set of convolutional interleaver register lengths was somewhat better than that obtained with the length sets 4, 8,...,128 for the t_1-chips and 128, 124,...,8,4 for the t_2-chips probably because the latter configuration gives slightly more clustering of the chips output from a deep fade. The performance of a randomly chosen block interleaver with the same total time delay as the convolutional interleaver was also simulated against the same fading and found to be inferior to the convolutional interleaver which can be implemented with approximately half the storage elements as the random block interleaver.

F. Extensions to Other Codes

The principal use of theoretical models is predicting the performance of various possible systems without having to build or simulate each one. The performance degradations imposed by various quantization and modulation format choices tend to be more or less constant for any code. However, the effects of different correlations between fade levels of consecutive chips in the decoder decision is dependent upon the partiuclar code and must be determined for each

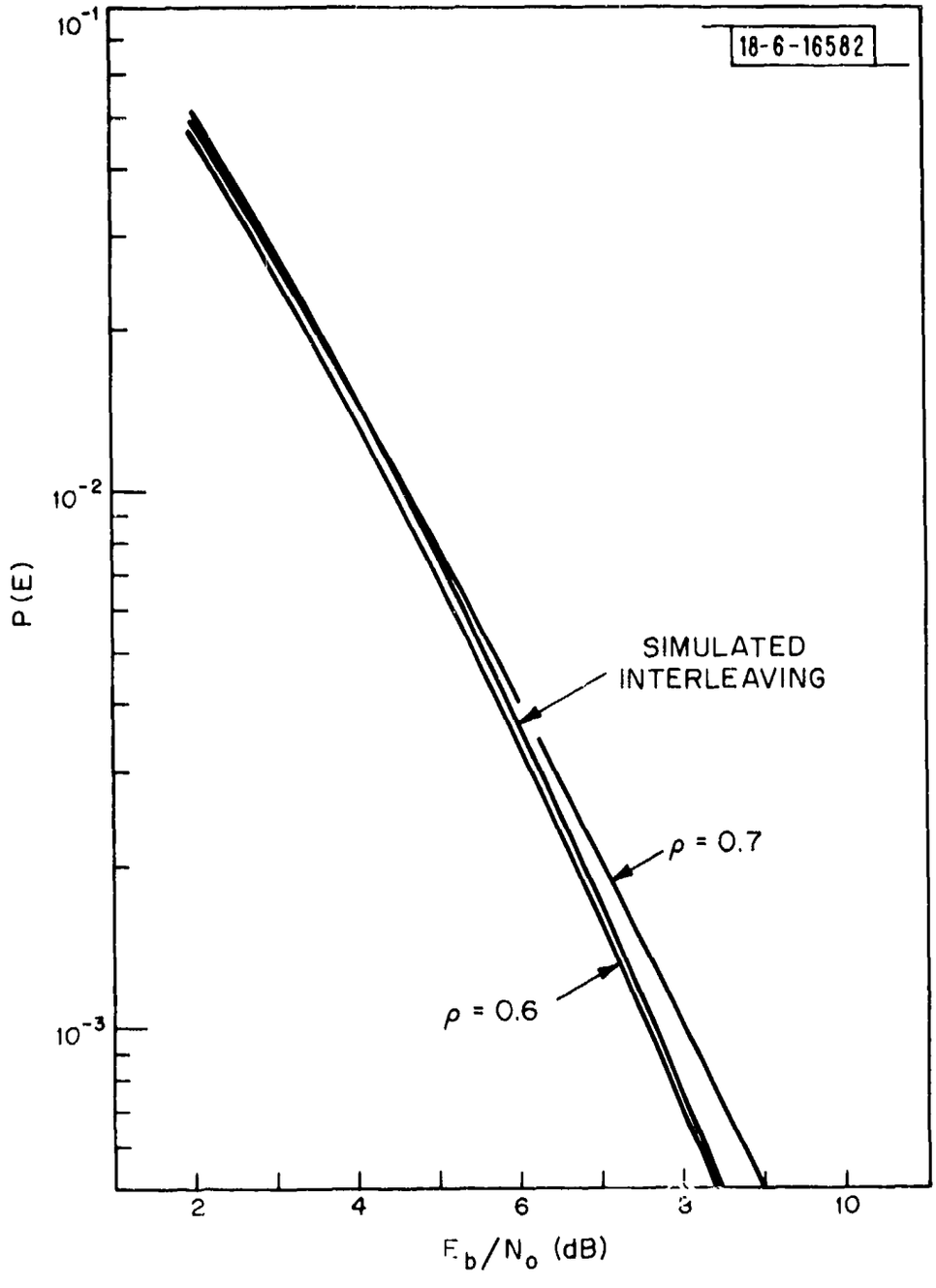

Fig. 4-17. Comparison of simulated decoder performance on simulated scintillation with convolutional interleaving and performance estimate using correlation function.

specific code considered. The performance possible with some convolutional interleaver design operating on a specific sample of real scintillation can be estimated by determining the maximum correlation coefficient between fade levels of successive chips involved in a decoder decision from the interleaver design and the correlation function of the fading sample. Using this extrapolation technique leads to predictions of the required E_b/N_o for 0.001 error probability for some real scintillation samples which are with 1 dB of the predicted values.

G. Comparison of Performance Between Fading and Non-fading Conditions

Figure 4-18 compares the error probability upper bounds for the rate 1/2 systematic and non-systematic convolutional codes with both a Rayleigh fading channel and a non-fading white gaussian noise channel with PSK chip modulation. For the stronger code, the non-systematic convolutional code, the extra E_b/N_o required to maintain a 10^{-5} bit error probability during Rayleigh fading is 3.4 dB. For the weaker code, the systematic convolutional code, the incremental E_b/N_o required to maintain a 10^{-5} bit error probability is 4.9 dB. With adequate interleaving, a channel model of statistically independent Rayleigh fading from chip to chip is a characterization of the worst possible fading induced by UHF scintillation. Thus, with the restriction of adequate interleaving, implementable techniques using Viterbi decoding of non-systematic K=7 convolutional codes offer a means of countering scintillation which require an increment of 3.4 dB in E_b/N_o. This incremental 3.4 dB to counter scintillation for time diversity modulation is close to the information theoretic limit of no increase in power required to counter Rayleigh fading and the simple no-rate-adjustment no-power-adjustment limit of 4.3 dB.

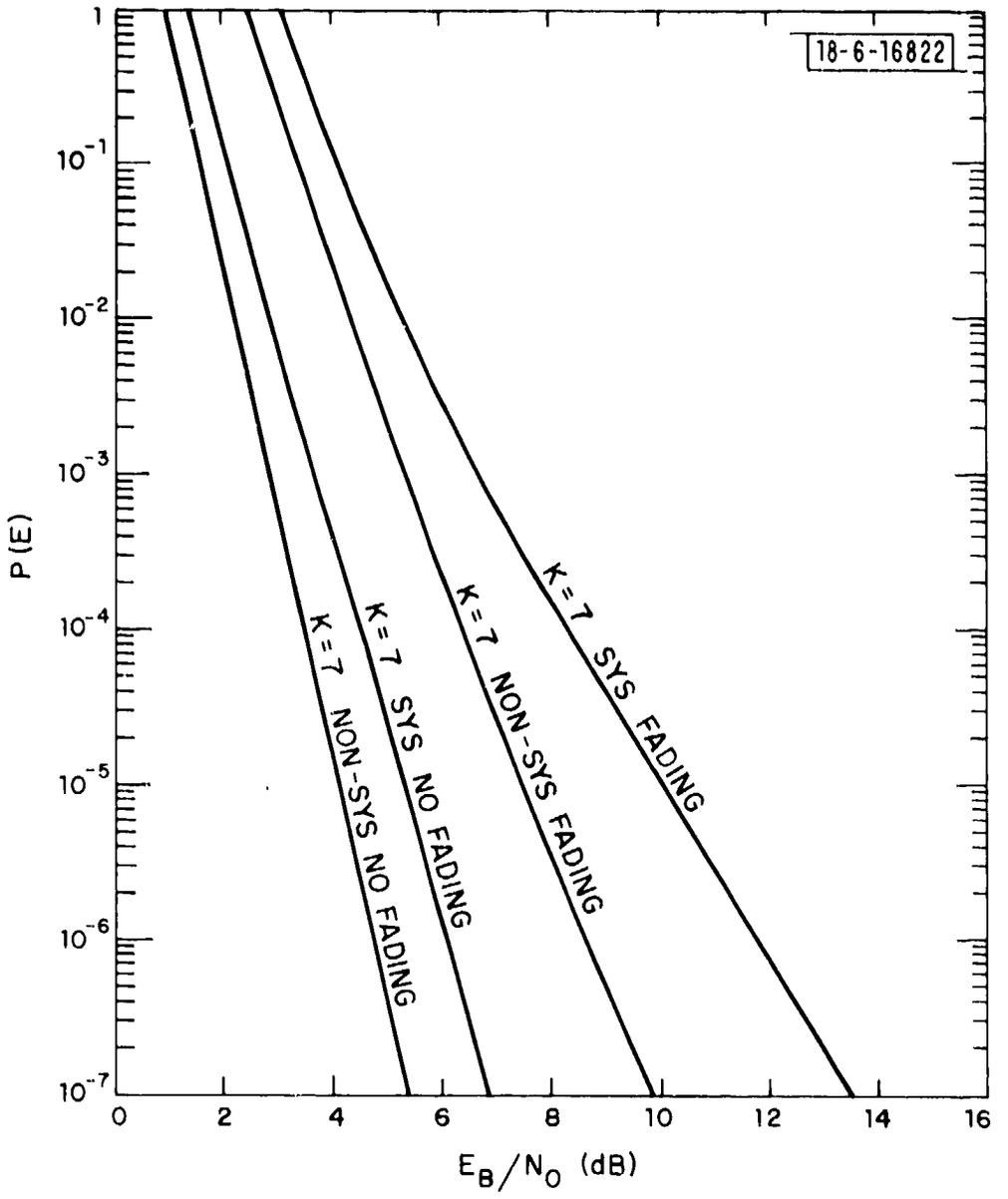

Fig. 4-18. Comparison of bit error probability upper-bounds for selected convolutional codes with and without statistically independent Rayleigh fading from chip-to-chip and PSK chip modulation.

V. EXPERIMENT INCORPORATING SCINTILLATION PROTECTION INTO AN EXISTING BROADCAST NETWORK

When adding UHF scintillation protection to a large broadcast network, a compatible system allowing simultaneous operation of receivers both with and without anti-scintillation processors may reduce cost and ease installation requirements. For example, a compatible system could reduce costs by reducing or eliminating the amount of modified or additional equipment required for receivers on platforms which operate outside regions where scintillation occurs. Furthermore, a compatible system could also reduce the logistic requirement of installing modifications simultaneously in a large dispersed network. If the basic signal structure multiplexes several individual information streams together, systematic convolutional codes discussed in Section IV can be implemented in such a compatible way by putting the basic message on one sub-channel and the parity or coding bits on other sub-channels. This multiplexing may be either frequency-division multiplexing or time-division multiplexing as used in the SSR-1 satellite broadcast receiver.

A systematic rate 1/2 convolutional code encodes one message stream into two character streams for transmission. One of these character streams is an unaltered copy of the message text and the other is a mathematically generated combination of message symbols which is useful to the decoder but not directly readable otherwise. Figure 5-1 sketches the information flow in a compatible system with a rate 1/2 systematic convolutional code, a Viterbi decoder and interleavers like the anti-scintillation system discussed in Section IV. The two transmission channels A and B are obtained by using two of the multiplexed sub-channels in the basic transmission stream. With an SSR-1 broadcast type receiver there are fifteen such sub-channels in the basic transmission format. The strange positioning of the interleavers in channels A and B is necessary in order both to allow natural order transmission for the unaltered message text and to permit interleaving to scatter the fades before decoding.

When appending an anti-scintillation processor decoder to an existing radio receiver system, there are several interfaces required between the existing receiver and the decoder. First, the received chips will have to be

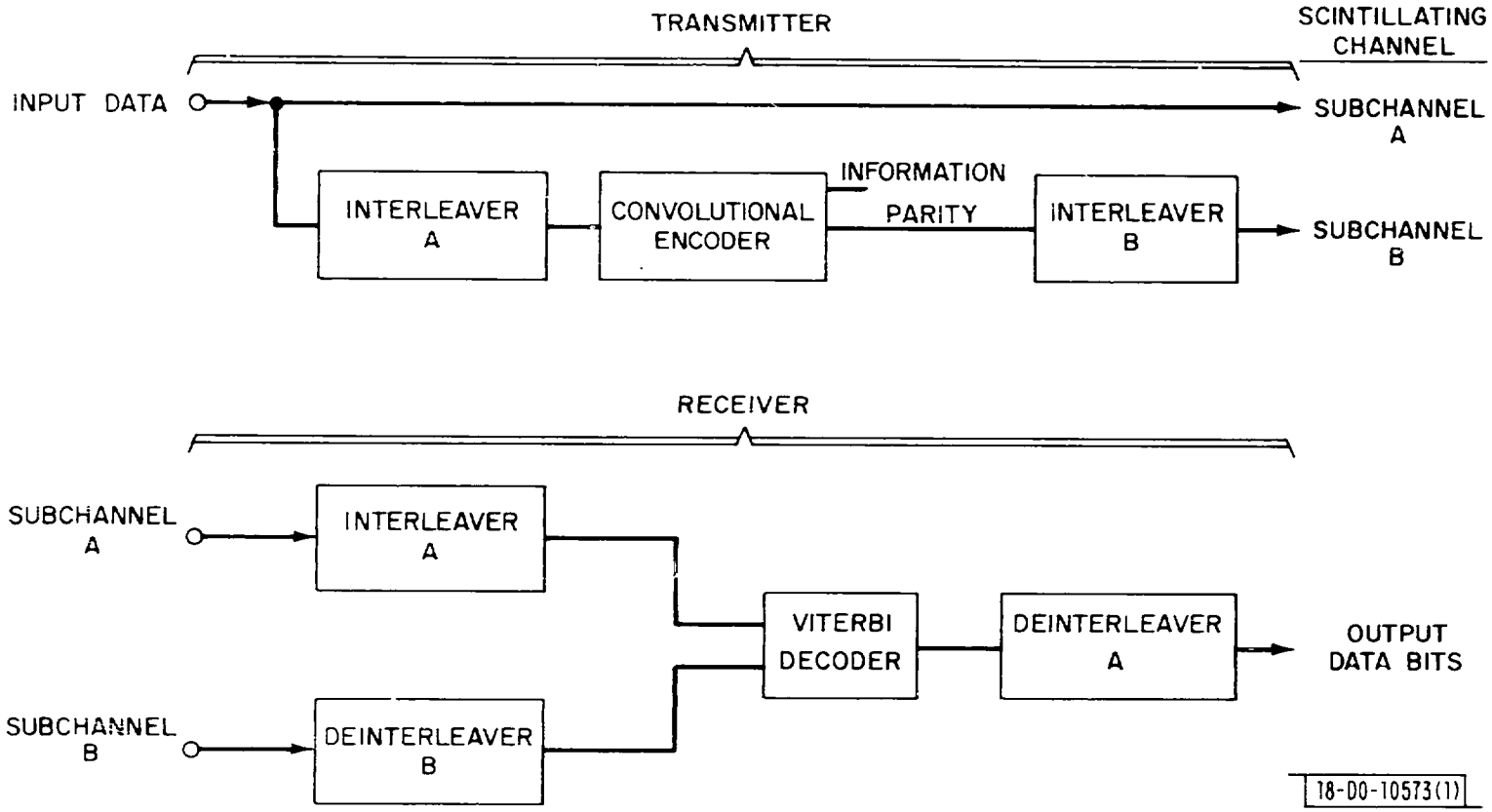

Fig. 5-1. Block diagram of system adding time diversity modulation to a broadcast system allowing unmodified receivers without decoders to recover the basic message if there is no scintillation and providing time diversity modulation to counter scintillation for those receivers with decoders.

transferred from the receiver to the decoder. Since the basic receiver makes hard quantized 0/1 bit decisions and the time diversity decoder operates much more efficiently with a few bits of resolution on the matched filter outputs, some internal modifications in the receiver will be necessary to provide the received chip voltages to the decoder. Second, the more efficient time diversity decoders also use a signal level estimate to further suppress unreliable chips. This signal level estimate can be obtained from the receiver and is available as the automatic gain control, AGC, loop control voltage in many receiver designs. Third, bit and chip timing must be obtained from the receiver.

Presently, there is no experimental data accurately indicating what received phase stability is anticipated during scintillation. Theoretical estimates indicate a Doppler spread on the order of 10 Hz. However, the dynamic performance of the phase lock loop combined with these received phase variations could substantially alter the effective receiver phase stability. Because of these uncertainties, the circuits of an experimental receiver must be designed with sufficient flexibility to permit incoherent detection without a phase reference if none can be established during scintillation and to gather data on phase stability for design of an operational version of the experimental receiver. One compromise is to use the DPSK chip modulation of the AN/SSR-1 receiver and to provide both for coherent detection with a phase reference and for incoherent detection without a phase reference if necessary. This dual approach is used in the experimental add-on scintillation decoder being built and interfaced with an AN/SSR-1 receiver by Lincoln Laboratory for a scintillation experiment using the Fleet Broadcast on a Navy UHF channel of the MARISAT satellite. This experiment will both test a particular design of a time diversity modulation system for countering scintillation induced fading and collect data on scintillation phase stability and receiver performance to permit the resolving of the present uncertainty between coherent and incoherent chip detection during scintillation. This experimental hardware will also test several higher rate convolutional codes which would allow a single sub-channel of parity information to protection two of three message sub-channels.

Some of these higher rate codes will be the more powerful non-systematic convolutional codes which offer increased error protection at the cost of giving up the compatibility feature. The details of the experimental hardware and the results of the experiments will be published separately.

ACKNOWLEDGEMENT

The author would like to acknowledge the assistance of several of his colleagues at M.I.T. Lincoln Laboratory. R. K. Crane's work on the basic physical phenomenology of ionospheric-induced scintillation greatly aided in formulating and characterizing its impact on UHF satellite communication. David P. White and Steven L. Bernstein helped raise some of the issues involved in a practical implementation of anti-scintillation processing. Christopher H. Moulton wrote the simulation and data-reduction programs.

The UHF scintillation data provided by R. U. F. Hopkins of the Naval Electronics Laboratory Center greatly facilitated the development of the description of UHF scintillation.

APPENDIX

This appendix derives $P_2(E)$ the probability of a receiver's making an error in determining which of two different sequences of chips was transmitted for the special case of PSK modulation with known statistically independent Rayleigh fading from chip to chip. Given the observables at the receiver, the decision rule which minimizes the probability of error for equally likely transmitted sequences is to choose the sequence s_i which maximizes the conditional probability

$$P(s_i/\text{observables});$$

that is, the best receiver strategy is to select the s_i which is most likely given the receiver's observables. For PSK modulation, the transmitted sequence is a series of chip signals with the same energy E_s and either + or - arithmetic sign modulated onto the carrier by a 180° phase reversal. At the receiver, the observed quantities are a matched filter output voltage y_i

$$y_i = s_i g_i \sqrt{\frac{2E_s}{N_o}} + n_i \qquad \text{(A-1)}$$

where n_i is unit variance gaussian noise and g_i is the normalized voltage gain $\sqrt{P_{ri}/P_{av}}$ where P_{ri} is the received signal power for the i^{th} chip and P_{av} is the average received power and s_i is +1 or -1 for + and - transmitted signal, respectively. It is assumed that the g_i are known at the receiver and statistically independent Rayleigh distributed random variables.

The decision between two transmitted sequences $\underline{s}_a$ and $\underline{s}_b$ can be made by the rule

$$\frac{P(\underline{s}_a/y_i\text{'s and } g_i\text{'s})}{P(\underline{s}_b/y_i\text{'s and } g_i\text{'s})} \begin{matrix} a \\ > \\ < \\ a \end{matrix} 1 \qquad \text{(A-2)}$$

where the decoded sequence number is the number nearest the true inequality. The decision expression A-2 may be made more tractable by using the definitions of conditional probability to rewrite the decisions as

$$\frac{P(\underline{s}_a,\ y_i's,\ g_i's)/P(y_i's,\ g_i's)}{P(\underline{s}_s,\ y_i's,\ g_i's)/P(y_i's,\ g_i's)} \begin{matrix} a \\ > \\ < \\ b \end{matrix} 1 \qquad \text{(A-3)}$$

Rewriting the joint probabilities and assuming that the fading is statistically independent of the sequence sent, the decision rule becomes

$$\frac{P(y_i's/\underline{s}_a \text{ and } g_i's)}{P(y_i's/\underline{s}_b \text{ and } g_i's)} \begin{matrix} a \\ > \\ < \\ b \end{matrix} 1 \qquad \text{(A-4)}$$

For statistically independent fading from chip to chip, the probability of a sequence of y_i's can be written as the product of the probabilities of the individual members of the sequence. Thus, the decision rule becomes

$$\prod_i \frac{P(y_i/s_{ai},\ g_i)}{P(y_i/s_{bi},\ g_i)} \begin{matrix} a \\ > \\ < \\ b \end{matrix} 1 \qquad \text{(A-5)}$$

where s_{ai} denotes the i^{th} symbol in the transmitted sequence s_a.

The conditional probability $P(y_i/s_{ai},\ g_i)$ for gaussian noise is

$$P(y_i/s_{ad}g_i) = \frac{1}{\sqrt{2\pi}} \exp\left[-(y_i - s_{ai}g_i\sqrt{2E_s/N_o})^2/2\right]$$

Since the logarithm is a monotonic function, the outcome of the decision rule in (A-5) is unchanged if the logarithm of both sides of (A-5) is used in the decision rule. Taking the logarithms of both sides of (A-5) and using (A-6), the decision rule becomes,

$$\sum_i (s_{ai}-s_{bi})y_i g_i\sqrt{\frac{2E_s}{N_o}} \begin{matrix} a \\ > \\ < \\ b \end{matrix} 0 \qquad \text{(A-7)}$$

This decision rule can be interpreted as "weight the received y_i's by the channel voltage gains g_i and then correlate the weighted received signal with

the hypothesized transmitted signal and select the hypothesis with the largest correlation". Once the received chip voltages y_i have been weighted, the receiver structure is identical to the receiver used for non-fading PSK modulation.

The outcome of the decision in (A-7) between whether hypotheses a or b is most likely depends only on those chips in the sequences $\underline{s}_a$ and $\underline{s}_b$ which differ. Thus, in evaluating the probability of error in a decision between only the true hypothesis a and one possible erroneous hypothesis b, the number of chips d in which the two signal sequences differ is crucial and $P_2(E)$ becomes a function of d represented as $P_2(E,d)$. Without loss of generality, we may assume that the transmitted sequence for a is all positive pulses and $s_{ai} = +1$ for all i. In this case, the only s_{bi} which really enter the decision must be -1 and there can be an error in the decision between a and b if, and only if,

$$\sum_{\substack{\text{i in which } s_{ai} \\ \text{and } s_{bi} \text{ differ}}} y_i g_i \frac{2E_s}{N_o} < 0 \qquad \text{(A-8)}$$

To determine $P_2(E,d)$, one must know the statistics of the composite decision quantity in the left-hand side of (A-8). Since this decision quantity is the sum of several random variables, we must work with the statistics of a sum of random variables. The probability density of a sum of random variables is perhaps most easily found by using the characteristic function or Fourier transform of the probability density rather than the density itself. The characteristic function of $\phi_{yi}(\nu)$ is the Fourier transform of the right-hand side of (A-6)

$$\phi_{yi}(\nu) = \exp[i\nu s_i g_i \sqrt{2E_s/N_o} - \nu^2/2] \qquad \text{(A-9)}$$

The effect of weighting each y_i by g_i to produce a weighted quantity z_i can be entered into the characteristic function by multiplying the Fourier transform variable ν by g_i. Thus, the $\phi_{zi}(\nu)$ characteristic function of z_i the

weighted received chip is given by

$$\phi_{zi}(\nu) = \exp[i\nu s_i g_i^2 \sqrt{2E_s/N_o} - \nu^2 g_i^2/2] \qquad \text{(A-10)}$$

For Rayleigh fading, the probability density of the normalized channel voltage gain g_i

$$p(g_i) = 2g_i e^{-g_i^2} \qquad \text{(A-11)}$$

Taking the expectation of $\phi_{zi}(\nu)$ over g_i to average the decision over all fading levels, we obtain $\phi_i(\nu)$ the characteristic function of one of the d terms in the decision between the two hypotheses.

$$\phi_i(\nu) = \frac{1}{1 - i\nu s_i \sqrt{\frac{2E_s}{N_o} + \frac{\nu^2}{2}}} \qquad \text{(A-12)}$$

For statistically independent random variables, the characteristic function of a sum of these random variables is the product of the characteristic functions of the individual random variables added. Thus, $\phi_{dec}(\nu)$, the characteristic function of the final decision quantity with the expectation taken over fading for the special case of all +1 signals is

$$\phi_{dec}(\nu) = \left[\frac{1}{1 - i\nu \sqrt{\frac{2E_s}{N_o} - \frac{\nu^2}{2}}}\right]^d \qquad \text{(A-13)}$$

Taking the inverse Fourier transfor of (A-13) produces the probability density function of the decision quantity which can then be integrated from $-\infty$ to 0 to find the error probability $P_2(E,d)$. The first step in finding the inverse Fourier transform is to factor the denominator and expand in a partial fraction expansion.

$$\phi_{dec}(\nu) = \frac{1}{\left(\frac{2E_s}{N_o}+2\right)^{d/2}} \sum_{j=o}^{d-1} \frac{\binom{d-1+j}{j}}{\left[2\sqrt{\frac{2E_s}{N_o}+2}\right]^j} \frac{1}{\left[\sqrt{\frac{2E_s}{N_o}+2} - \sqrt{\frac{2E_s}{N_o}} - i\nu\right]^{d-j}}$$

$$+ \frac{1}{\left[\sqrt{\frac{2E_s}{N_o}+2} + \sqrt{\frac{2E_s}{N_o}} + i\nu\right]^{d-j}} \qquad \text{(A-14)}$$

Taking the inverse transform term by term

$$p_{dec}(x) = \frac{1}{\left(\frac{2E_s}{N_o}+2\right)^{d/2}} \sum_{j=o}^{d-1} \binom{d-1+j}{j} \frac{|x|^{d-j-1} e^{-\left(\frac{2E_s}{N_o}+2+\frac{2E_s}{N_o}\right)|x|}}{(d-j-1)!\left[\sqrt{2\frac{2E_s}{N_o}+2}\right]^j}$$

for $x \leq 0$

$$\frac{1}{\left(\frac{2E_s}{N_o}+2\right)^{d/2}} \sum_{j=o}^{d-1-j} \binom{d-1-j}{j} \frac{x^{d-j-1} e^{-\left(\frac{2E_s}{N_o}+2-\frac{E_s}{N_o}\right)x}}{(d-j-1)!\left[\sqrt{2\frac{2E_s}{N_o}+2}\right]^j}$$

for $x \geq 0$ (A-15)

Integrating $p_{dec}(x)$ from $-\infty$ to 0, we find

$$P_2(E,d) = \frac{1}{\left(\frac{2E_s}{N_o}+2\right)^{d/2}} \sum_{j=o}^{d-1} \binom{d-1+j}{j} \frac{1}{\left[\sqrt{2\frac{2E_s}{N_o}+2}\right]^j \left[\sqrt{\frac{2E_s}{N_o}+2} + \sqrt{\frac{2E_s}{N_o}}\right]^{d-j}}$$

(A-16)

Rearranging terms

$$P_2(E,d) = \frac{1}{\left(\frac{2E_s}{N_o}+2\right)^d \left(1+\frac{\sqrt{E_s/N_o}}{\sqrt{E_s/N_o+1}}\right)^d} \sum_{j=o}^{d-1} \binom{d+j-1}{j} \left[\frac{1+\frac{E_s/N_o}{E_s/N_o+1}}{2}\right]^j \quad \text{(A-17)}$$

Let us now derive a simple upper bound to $P_2(E,d)$ which turns out to be quite tight. The j-summation may be viewed as a sum of d terms $T_o \cdots T_{d-1}$. The ratio of two successive terms

$$\frac{T_j}{T_{j-1}} = \frac{d+j-1}{j}\left[\frac{1+\sqrt{\frac{E_s/N_o}{E_s/N_o+1}}}{2}\right]$$

For all j in the range from 1 to d-1, the ratio (d+j-1)/j is greater than or equal to 2, thus

$$\frac{T_j}{T_{j-1}} \geq \left(1+\sqrt{\frac{E_s/N_o}{E_s/N_o+1}}\right)$$

and the j=d-1 term dominates the sum. Thus,

$$P_2(E,d) = \frac{1}{\left(\frac{2E_s}{N_o}+2\right)^d \left[1+\frac{\sqrt{E_s/N_o}}{\sqrt{E_s/N_o+1}}\right]^d} \binom{2(d-1)}{d-1} \left[\frac{1+\frac{\sqrt{E_s/N_o}}{\sqrt{E_s/N_o+1}}}{2}\right]^{d-1}$$

$$\times \sum_{j=o}^{d-1} \frac{T_{d-1-j}}{T_{d-1}} \quad \text{(A-18)}$$

$$\leq \frac{\binom{2(d-1)}{(d-1)}}{2^{2d-1}\left(\frac{E_s}{N_o}+1\right)^d \left(1+\frac{\sqrt{E_s/N_o}}{\sqrt{E_s/N_o+1}}\right)} \sum_{j=o}^{d-1} \frac{1}{\left(1+\frac{\sqrt{E_s/N_o}}{\sqrt{E_s/N_o+1}}\right)^j}$$

Raising the upper limit in the j sum to infinity and summing the geometric series

$$P_s(E,d) \leq \frac{\binom{2(d-1)}{(d-1)}}{2^{2d-1}\left(\frac{E_s}{N_o}+1\right)^d} \sqrt{\frac{E_s/N_o+1}{E_s/N_o}} \qquad \text{(A-19)}$$

Fano[A-1] gives an upper-bound for the binomial coefficient

$$\binom{2(d-1)}{(d-1)} \leq \sqrt{\pi(d-1)}\ \ 2^{2d-2} \qquad \text{(A-20)}$$

Hence,

$$P_2(E,d) \leq \frac{1}{2}\sqrt{\frac{E_s/N_o+1}{E_s/N_o}}\ \frac{1}{\sqrt{\pi(d-1)}}\ \ \frac{1}{\left(\frac{E_s}{N_o}+1\right)^d} \quad .$$

REFERENCES

2-1 R. K. Crane, "Morphology of Ionospheric Scintillation," Technical Note 1974-29, Lincoln Laboratory, M.I.T. (21 May 1974), DDC AD-780522/9.

2-2 M. R. Paulson and R. U. F. Hopkins, "Effects of Equatorial Scintillation Fading on Satcom Signals," Technical Report 1875, Naval Electronics Laboratory Center, San Diego, California (1973).

2-3 H. E. Whitney, J. Arrons, R. S. Allen, and D. R. Seemann, "Estimation of the Cumulative amplitude Probability Distribution Function of Ionospheric Scintillation," Radio Sci. 7 1085-1104 (1972).

2-4 B. H. Briggs and I. A. Parkin, "On the Variation of Radio Star and Satellite Scintillations with Zenith Angle," J. Atmos. Terr. Phys. 24 339-365 (1963).

2-5 J. M. Wozencraft and I. M. Jacobs, Principles of Communication Engineering, Sec. 7.4 (Wiley, New York, 1965).

2-6 B. E. Nichols, "UHF Fading from a Synchronous Satellite Observed at Kwajalein October 1970 Through June 1972," Technical Note 1974-19, Lincoln Laboratory, M.I.T. (22 March 1974), DDC AD-780174/9.

2-7 R. K. Crane, "Spectra of Ionospheric Scintillation," J. Geophys. Res. (to be published).

2-8 J. K. Cavers, "Variable-Rate Transmission for Rayleigh Fading Channels," IEEE Trans. Inf. Theory IT-20 15-23 (1972).

2-9 R. G. Gallager, Information Theory and Reliable Communication, Chapter 4 (Wiley, New York, 1968).

3-1 W. Feller, An Introduction to Probability Theory and Its Applications, Vol. 1, 2nd Edition, Chapters 15-17 (Wiley, New York, 1957).

3-2 D. R. Cox and H. D. Miller, The Theory of Stocastic Processes, Chapters 3-5 (Wiley, New York, 1965).

3-3 J. G. Kemeny and J. L. Snell, Finite Markov Chains (Van Nostrand, Princeton, 1960).

3-4 W. W. Peterson and E. J. Weldon, Jr., Error Correcting Codes, Edit. II (M.I.T. Press, Cambridge, Massachusetts, 1972).

3-5 E. R. Berlekamp, Algebraic Coding Theory (McGraw-Hill, New York, 1968).

4-1 J. M. Wozencraft and I. M. Jacobs, Principles of Communication Engineering, Sec. 7.4 (Wiley, New York, 1965).

4-2 A. J. Viterbi, "Convolutional Codes and Their Performance in Communication Systems," IEEE. Trans. Commun. COM-19, 305-310 (1974).

4-3 E. A. Bucher and J. A. Heller, "Error Probability Bounds for Systematic Convolutional Codes," IEEE Trans. Inf. Theory IT-16, 219-224 (1970).

4-4 I. M. Jacobs, "Practical Applications of Coding," IEEE Trans. Inf. Theory IT-20, 305-310 (1974).

4-5 J. L. Ramsey, "Realization of Optimum Interleavers," IEEE Trans. Inf. Theory IT-16, 338-345 (1970).

A-1 R. M. Fano, Transmission of Information, Sec. 7 (M.I.T. Press, Cambridge, Massachusetts, 1961).